Manipulation of peripheral donor and acceptor substituents in emitter-layer materials toward highly efficient and stable OLEDs

アマンダークーン アーラッチゲ バギャ マドゥシャーニ

2024

Doctor thesis

Manipulation of peripheral donor and acceptor substituents in emitter-layer materials toward highly efficient and stable OLEDs

A. A. Bhagya Madushani

Department Applied Chemistry
Graduate School of Engineering
Kyushu University

Table of Contents

Chapter I. Introduction

1.1. Introduction

Because of their distinctive qualities, including high contrast ratios, wide viewing angles, high color purity, low power consumption, and rich and vibrant colors, organic light-emitting diodes (OLEDs) are in high demand among other technologies[1]. Compared to liquid crystal display (LCD) technology, which often uses a backlight, OLED technology is easier for small and flexible screens, as each pixel of an OLED emits light independently[2]. In addition, the remarkable resistance of OLED technology to even the harshest mechanical conditions makes it suitable for wearables, robotics, biomedical applications, and other applications. Tang et al. at Eastman Kodak established the first effective, low-voltage OLED in 1987[3]. They are now the focus of in-depth research and development for display and lighting technologies.

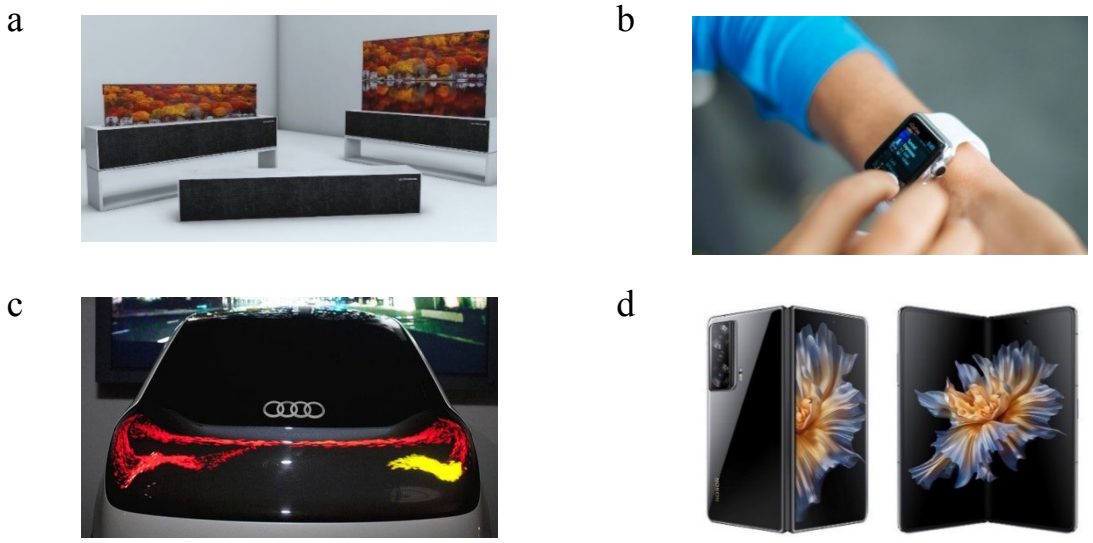

Figure 1.1: Representative applications of OLED technology. (a) LG rollable OLED TV, (b) smartwatch, (c) OLED taillights, and (d) foldable smartphone display[4,5,6,7].

1.2. Luminosity of organic semiconductors

The building blocks of organic semiconductors are unsaturated organic molecules containing sp2-hybridized carbon atoms that form a conjugated π-electron system through their orbitals. The π-bonding is far weaker than the σ-bonds, constituting the molecules' backbone. Conjugated organic molecules undergo the least energetic electron excitation through π-π* type transitions from the highest occupied molecular orbital (HOMO) to the lowest unoccupied molecular orbital (LUMO) energy levels, resulting in an excited state for

the molecule. The energy bandgap in organic semiconductors, typically between 1.5 and 3 eV, is the energy gap between the LUMO and HOMO, and it directly impacts both optical and charge transport properties[8]. The molecular design of organic semiconductors enables control of the energy gap and fine-tuning optoelectronic properties. According to Koopmans' theorem, the ionization potential (IP) and the electron affinity (EA) of a molecular system are equal to the HOMO and LUMO energies, respectively[9].

Based on their total spin, organic molecules in excited states can be classified as either an excited singlet state or an excited triplet state in terms of their electronic state. When two electrons have opposite spins and their combined spin value is zero (S=0), there is only one way to achieve this configuration. This state is called the excited singlet state. However, if the two electrons have the same spin and the combined spin value is one (S=1), there are three possible states of equal energy, which is called the excited triplet state. Because of the electron-electron repulsion, a triplet state will always have a lower energy than its related singlet state. As per the selection rule, the difference in spin state causes the transition from singlet to triplet (or vice versa) to be less likely than the singlet-to-singlet transition. This can be attributed to the fact that the transition mentioned above involves a change in the spin state, which is energetically less favorable than the transition that maintains the same spin state. Therefore, singlet-to-singlet transitions are more probable than the ones involving a change in spin state. Electrical excitation creates both singlet and triplet states, unlike optical excitation which only creates singlet states[10].

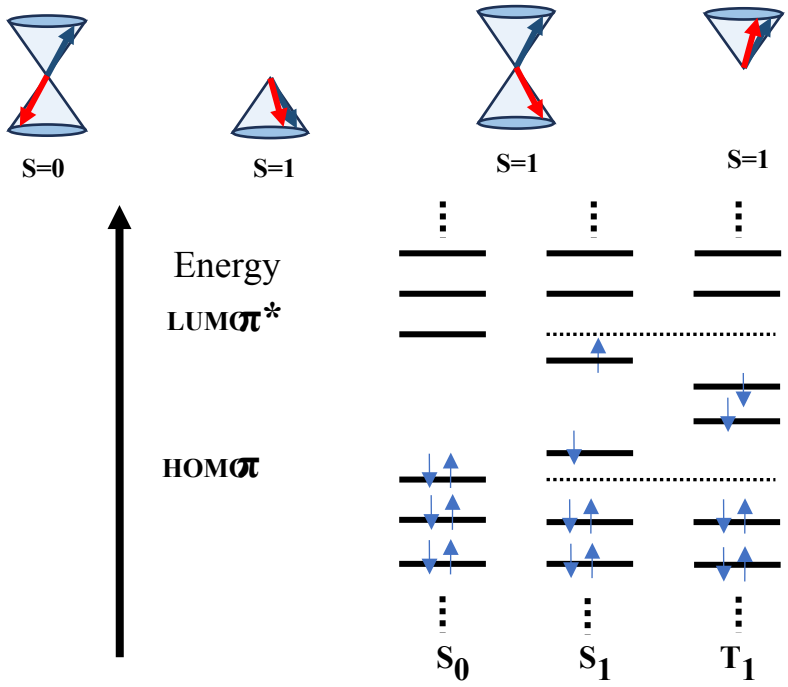

Figure 1.2: The distinction between the spin of ground (S_0), lowest singlet excited (S_1), and lowest triplet excited states (T_1).

1.3. Organic Light-Emitting Diodes (OLEDs)

OLEDs have attracted significant attention since Tang and VanSlyke's 1987 report because of their numerous uses in solid-state lighting sources and full-color flat-panel displays[3,11]. A thin layer of π conjugated materials is sandwiched between two electrodes to form an OLED. In a typical OLED, holes are injected via the anode and electrons are pumped through the cathode. Subsequently, the charges travel within the organic material, usually by hopping processes, before recombining to generate excitons. The recombination zone of an OLED depends on the charge injection barriers and the mobilities.

After we applied an electric field to the electrodes, electrons, and holes started to hop through the organic layers. Electrons cross multiple interfaces before recombining at the emissive layer (EML). Here, charges must cross these layers' energy barrier to move to the next layer. These energy barriers increase the driving voltage and create charge-accumulation regions close to the EML by forming nonradiative recombination paths which reduce device efficiencies[12,13,14]. A hole-electron pair, or exciton, is created in the EML by recombining the holes and electrons created from each electrode.

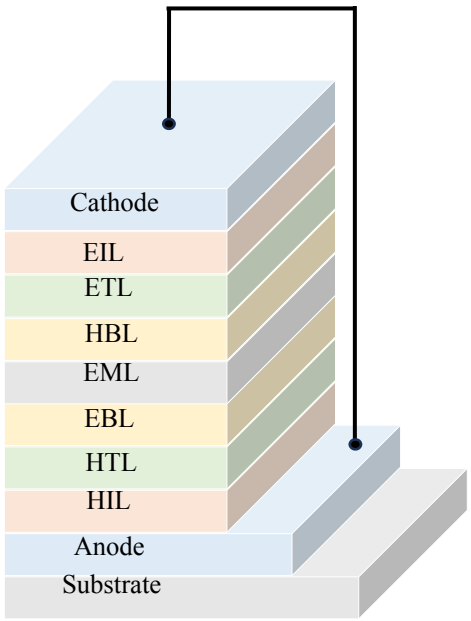

Figure 1.3: Schematic illustration of an OLED structure.

1.4. Emitter Materials Development

Organic light-emitting materials are divided into three main categories: fluorescent, phosphorescent, and TADF materials. These classifications are based on the nature of excitons and the luminescence process.

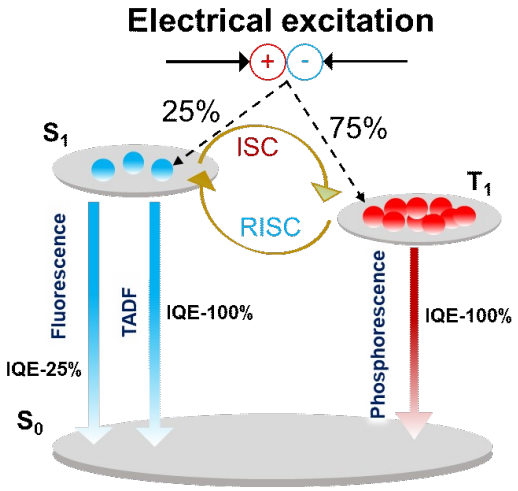

Figure 1.4: Light-emission mechanism of fluorescence, phosphorescence, and thermally activated delayed fluorescence emitters.

1.4.1. Fluorescent emitters

In 1987, Tang et al. established fluorescent OLEDs, which are considered the first generation of OLEDs[3]. These emitters have nanosecond emission lifetimes and emit in the singlet state. According to the selection rule, the transition between S_1 and S_0 is only possible and radiative. Because, under electrical excitation, 25% of excitons are singlets and 75% are triplets, the 25% of the excitons only contribute to the emission. This is the reason for the low performance of the fluorescent emitters. However, due to their better device stability and low cost, fluorescent emitters are still used for blue emission in OLED applications[15].

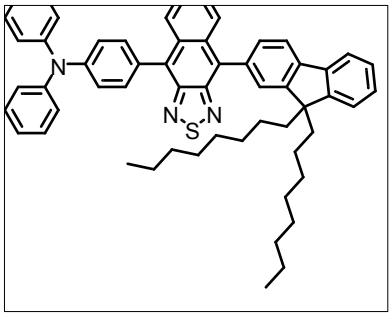

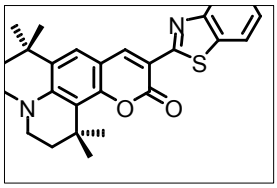

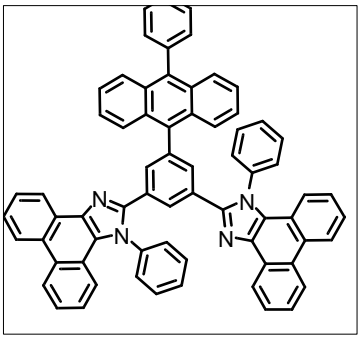

Figure 1.5: Structures of typical fluorescent (red, green, and blue) emitters with the maximum EQEs[16,17,18].

1.4.2. Phosphorescent emitters

In the second generation, the remaining 75% of excitons are utilized using heavy metal complexes. In 1998, Baldo et al. presented the first platinum complex with an internal quantum efficiency (IQE) of 23%[19]. After that, in 2001, Adachi et al. introduced the first heavy-metal phosphorescence emitters by achieving approximately 100% IQE[20]. The rare earth metals such as iridium and platinum could facilitate the spin-orbit coupling by transferring singlet excitons to triplet excitons through inter-system crossing (ISC)[19,20]. Commercial OLED displays nowadays rely on iridium complexes that generate red and green light due to their great stability and performance[21]. However, the high cost and toxicity of rare earth materials limit the applications of phosphorescence materials in the industry, regardless of their high efficiency.

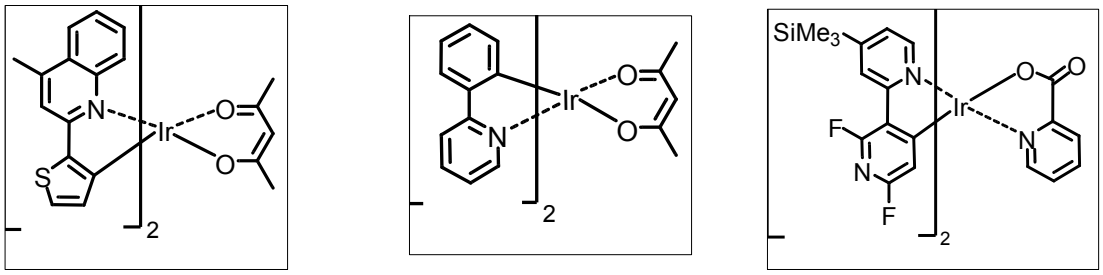

$(tmq)_2Ir(acac)$ $Ir(ppy)_2(acac)$ Ir-2

EQE_{max}= 25.9% EQE_{max}= 29.1% EQE_{max}= 31.9%

Figure 1.6: Structures of typical phosphorescence (red, green, and blue) emitters with the maximum EQEs[22,23,24].

1.4.3. TADF emitters

In TADF emitters, the triplet excitons are converted into singlets through the reverse inter-system crossing, and all singlets can emit prompt fluorescence or delayed fluorescence[25,26]. One significant benefit of TADF emitters is their ability to be entirely organic, which eliminates the issues related to using organometallic complexes based on

heavy metals[27]. The characteristic feature of these molecules is their dependence on a small singlet-triplet energy gap (ΔE_{ST}) typically less than 0.1 eV between the S_1 and T_1 states.

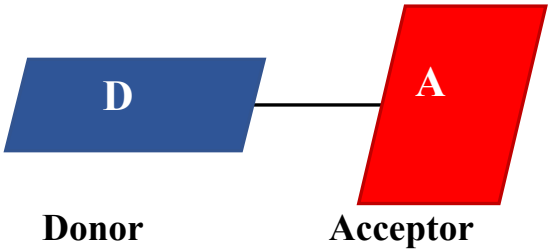

Figure 1.7: Molecular design of highly twisted structure for TADF emitters.

As previously indicated, TADF depends on ΔE_{ST}, which controls the exciton harvesting by reverse intersystem crossing (k_{RISC}) based on the Boltzmann distribution shown below[28].

$$k_{RISC} \exp(-) \quad (1)$$

where k_b is the Boltzmann constant and T is the temperature.

Thus, a smaller ΔE_{ST} will result in a higher k_{RISC}, and the singlet and triplet excitons will be collected more efficiently.

Theoretically, ΔE_{ST} can be expressed as,

$$\Delta E_{ST} = 2_{HOMO}(1)\ _{LUMO}(2)\ \ _{HOMO}(2)\ _{LUMO}(1)\ d\tau_1\tau_2 \quad (2)$$

where Φ_{HOMO} and Φ_{LUMO} are the wavefunctions of the HOMO and LUMO, respectively, and r_{12} is the distance between the electrons 1 and 2[25].

According to the equation, HOMO and LUMO overlap increases the ΔE_{ST}. Therefore, reducing a molecule's HOMO-LUMO overlap by molecular structural engineering is essential to creating effective TADF emitters. The LUMO and HOMO of molecules can be separated to get the small ΔE_{ST}. Localizing the HOMO and LUMO electron densities on the donor (D) and acceptor (A) units, respectively, is an effective strategy to reduce the overlap between the wave functions. As a result, TADF molecules often have twisted D A molecular structures. Adachi's group developed and applied the essential molecular architecture for a productive TADF process to OLEDs[25,29]. Goushi et al. published the first report on TADF-based OLEDs

(TADF-OLEDs) with exciplex emission using m-MTDATA molecule as D and 3TPYMB molecule as A[30]. However, in exciplex emission, the photoluminescence quantum yield (PLQY) is poor due to the limited overlap of HOMO and LUMO. While the smaller ΔE_{ST} is the outcome of the decreased overlap between the HOMO and LUMO, the oscillator strength (f) is also reduced.

In intramolecular TADF emitters, the D and A units are in the same molecule, forming a charge transfer (CT) excited state. The CT state is more polar than the locally excited state (LE). Because of that, the triplet energy of D and A units is higher than that of the CT state. In these molecules, the HOMO-LUMO separation is obtained by the large dihedral angle between the D and A units. The control of the dihedral angle can reduce the ΔE_{ST} [31,32].

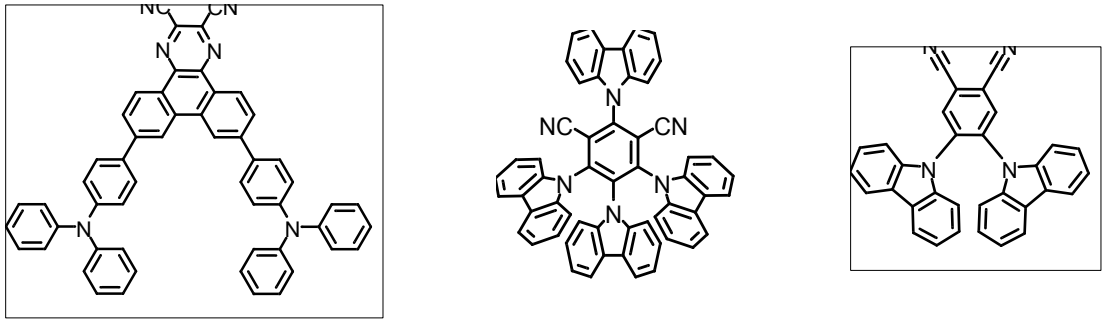

TPA-DCPP

EQE_{max}= 10.8%

4CzIPN

EQE_{max}= 29.6%

2CzPN

EQE_{max}= 38.4%

Figure 1.8: Structures of typical TADF (red, green, and blue) emitters with the maximum EQEs[33,34,35].

1.5. HOST materials

To create a host-guest system that facilitates effective energy transfer, guest emitters are often inserted in conductive hosts to prevent undesirable quenching[36]. For determining the overall performance of a device, host materials are just as crucial as emitters. Effective host materials must meet some standard requirements. At first, for effective energy transmission, the hosts' singlet and triplet energies need to be greater than the emitters. Furthermore, the hosts must possess strong charge-balancing characteristics to confine triplet excitons inside the emitting layer. Thirdly, to lower the interface energy barrier, the hosts' HOMO and

LUMO values should match those of the next layer. Finally, for effective energy transfer from the host to the emitter, there must be a significant overlap between the host's emission spectra and the emitter's absorption spectrum. Additional advantages of host materials include great morphological and thermal stability[37]. The hosts can be divided into four groups based on the behavior of the carriers: (1) hole transporting (HT), (2) bipolar, (3) nonpolar, and (4) electron transporting (ET)[38]. Most of the host materials are based on either carbazole or phosphine oxide groups since the high triplet energy needed limits the range of functional groups. These materials can be made at a reasonable cost in large quantities.

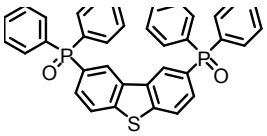

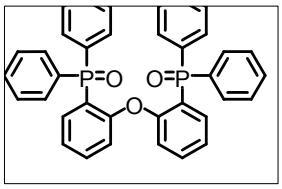

DPEPO PPT mCP mCBP

Figure 1.9: Molecular structures of the most commonly used host materials employed in TADF OLEDs.

Compared to red and green emitters, the design of host materials for blue emitters is more challenging since the host material needs to have a higher triplet energy than the emitter. DPEPO is a widely used host material that has a high triplet energy of 3.0 eV[39,40,41]. However, because it is a phosphine-based host, the stability is limited[42,43]. Also, DPEPO has unbalanced carrier transport properties due to the strong electron-withdrawing nature of the oxide groups, which increases the monopolar behavior of the DPEPO. Similarly, PPT is also a phosphine-based host material, which has a high triplet energy of 3.0 eV[37,44]. Except for this group, most hosts are based on the carbazole groups. Because of its strong hole-transporting capabilities, high triplet energy (3.02 eV), and outstanding thermal stability, carbazole is the most frequently used electron-donating moiety in OLED materials. Since its derivatives have more rigid structures and a sp3-hybridized nitrogen atom at the 9-position, they produce molecules with high thermal stability with improved film morphology[45]. The high triplet energy of 2.9 eV of mCP has made it a popular choice for blue TADF OLEDs[46]. On the other hand, it has limited morphological stability (T_g = 65°C) and monopolar characteristics (hole conducting

material)[47]. Also, another method for providing charge balance is to use two monopolar hosts[48].

In recent years, several molecular types have been used to address the limited applications of host materials for blue TADF emitters. To give bipolar characteristics, the most effective method is to mix donor and acceptor pairs with high triplet energy (**Fig. 1.10**). Hosts can transport electrons and holes equally in this manner. Because of the balanced charge density and wide recombination zone in the emitting layer, bipolar transport hosts often have higher device performances than p-type and n-type hosts[49].

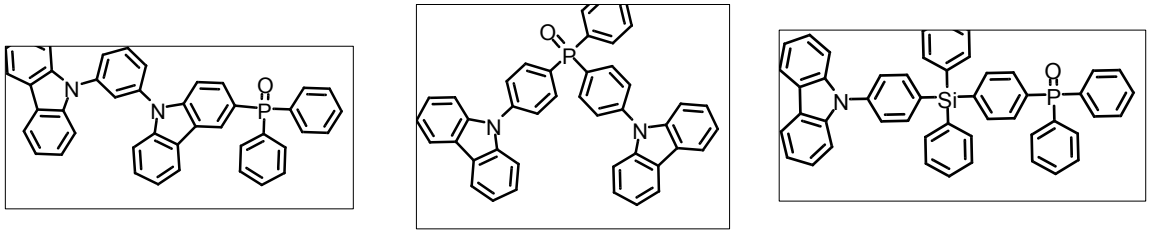

mCPPO1 BCPO CSPO

Figure 1.10: Molecular structures of bipolar host materials.

1.6. Efficiency of OLEDs

The efficiency of an OLED is determined mainly by external quantum efficiency (EQE, η_{ext}). The EQE explains the ratio of extracted photons to injected electrons and charge carriers:

$$\eta_{ext} = \eta_{int} \times \eta_{out} = (\gamma \times \eta_{ST} \times \Phi_{PL}) \times \eta_{out} \quad (3)$$

where η_{int} is the internal quantum efficiency, η_{out} is the light-outcoupling efficiency, γ is the proportion of holes and electrons that recombine to produce excitons in the emitting layer, η_{ST} is the exciton generation efficiency determines the radiative transition-based on spin selection principles, and Φ_{PL} is the PL quantum efficiency for the exciton radiative decay. η_{out} is the percentage of photons that the device emits into the air. Advanced device structures and molecules with a controlled non-radiative activity can achieve up to 100% γ and Φ_{PL}, respectively. γ can be changed by the type of emission mechanisms (fluorescence =

~25% and phosphorescence). If we consider the η_{out} is 20%, for fluorescence-based OLEDs, η_{ext} is limited to 5%, and for phosphorescence-based OLEDs, η_{out} is as high as 20%[50]. Compared to fluorescence and phosphorescence emitters, in TADF emitters, the T_1 is converted to S_1 through RISC. The following equation can obtain the theoretical maximum η_{int} of TADF OLEDs,

$$\eta_{int} = \eta_S \times \Phi_p + \eta_s \times \Phi_d + \eta_T \times \Phi_P \times \Phi_d/\Phi_{ISC} \quad (4)$$

where η_S and η_T are the singlet and triplet exciton generation rates (25% and 75%), and Φ_d is the ISC efficiency ($1-\Phi_p$). According to that, the theoretical maximum of the TADF OLEDs is about 20% (η_{out}= 20%).

1.6.1. Efficiency Rolloff in OLEDs

To design highly efficient OLEDs, efficiency rolloff is a main issue. With the increase in current density, the EL efficiency of OLEDs decreases by exciton quenching. This is one of the critical problems in displays and lighting applications[51,52]. Even though phosphorescence and TADF-based OLEDs achieved more than 20% efficiency, the current density at 90% rolloff is as low as 1−30 mA cm^{-2}. However, fluorescence-based OLEDs show a nearly constant η_{ext} of 5% with a negligible rolloff behavior[53]. This low rolloff behavior is mainly due to the short lifetime of fluorescence compared to the phosphorescence. The reason for the efficiency rolloff is not only due to the annihilation but also due to the unbalanced electron and hole transport and injection. These imbalanced losses result from poor charge carrier mobilities of the component materials and energy barriers, which cause a substantially larger efficiency rolloff. Devices featuring materials with strong charge-carrier mobility, such as doped charge-transport layers, can reduce such resistive losses.

1.6.2. Outcoupling efficiency

Significant improvements have been achieved in utilizing both singlet and triplet states for a high IQE of 100%. However, due to internal reflection and optical confinement caused by the different refractive indices of the adjacent layers, most of the emitted photons cannot escape from the device[54,55]. According to Snell's law based on ray optics, the light extracted into the air can be calculated as a fraction.

Snell's law, $\eta_{out}=$ (5)

where *n* is the refractive index of the organic layer relative to the air.

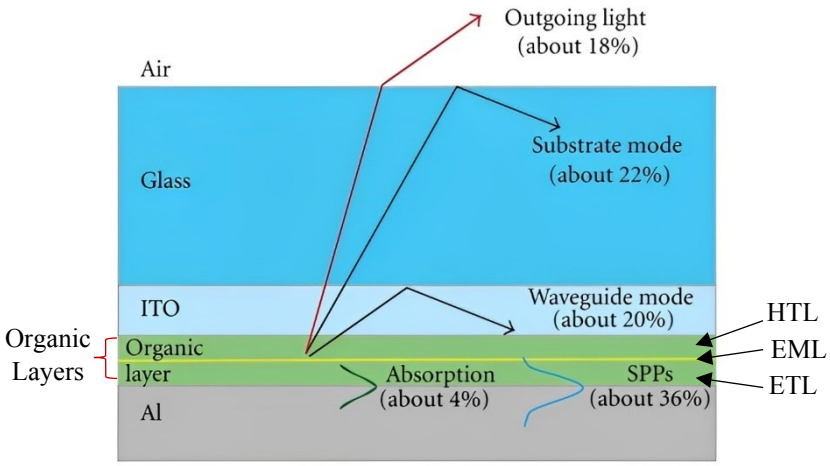

Figure 1.11: Schematic representation of multilayer OLED structure with optical ray diagram of light transmission via different modes. **(**This figure was cited from Q. Yue *et al.*, *Adv. Mater. Sci. Eng.* **2012**, 2 (2012)[56]).

A significant portion of emitted photons is trapped within the substrate (substrate mode, ~22%), confined within the organic layers, and anode (waveguide mode, ~20%), dissipates at the interface between the organic and cathode (SPPs and absorption, ~ 40%). Hence, only about 18% of the energy flow is emitted as usable light outside the device. Because of the low outcoupling efficiency, the performance of the OLEDs is limited. As a result, several sophisticated light out-coupling techniques have been investigated in recent years to recover lost photons for useful lighting and display applications[57,58,59].

1.7. Angle dependent photoluminescence

To examine the orientation of the guest molecules in the guest-host-doped films, it is essential to have a technique that is reliable and simple. Although ellipsometry can provide information on the orientation of a molecule and its transition dipole moment, it is not sensitive enough to identify the smallest amounts of dopant emitters embedded in a host matrix. To solve this problem, a method was developed that uses the far-field angular-dependent PL emission spectrum of the organic layer and the numerical simulation fittings[59-62].

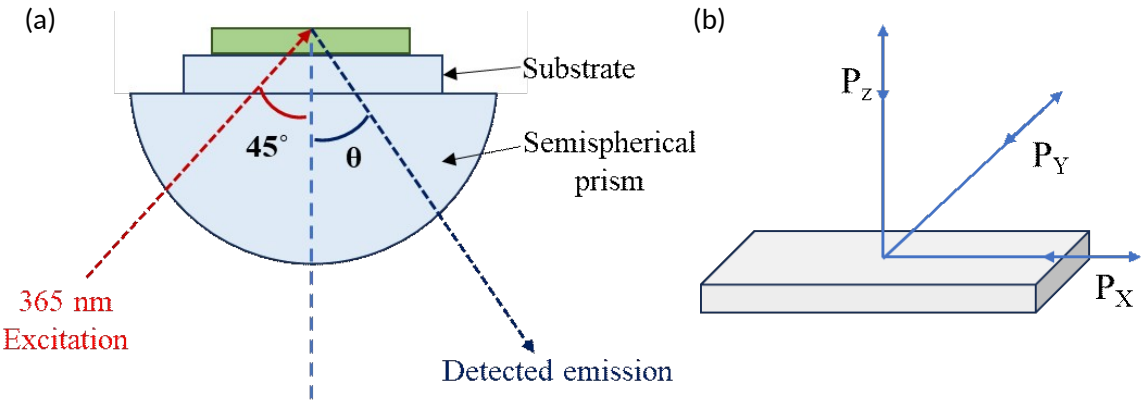

Figure 1.12: (a) Measurement setup for angular-dependent PL measurements and cross-sectional schematic view of the layer structure. (b) Definition of dipole orientations.

Figure 1.12 shows the coordinate system and the specification of the emission angle used in the analysis. Px, Py, and Pz dipoles can be superposed, with one-third of each, to form an organic thin film made up of molecules displaying random transition dipole orientation. The only emission taken into consideration is the x-z plane since no in-plane optical anisotropy is seen, and this is done without losing generality. Therefore, the P_X and P_Z dipoles emit P-polarized emission, but the P_Y dipoles exclusively generate S-polarized light. The sample is positioned on a computer-controlled rotation stage and is stimulated by a laser diode that emits light at a 45° incidence angle and a wavelength of 365 nm. To maintain a constant excitation state during the experiments, both the excitation beam and the sample were rotated simultaneously. To distinguish between S and P-polarized emissions, the angle-dependent PL spectrum was obtained from 0° to 90° using a fiber optic spectrometer and a polarizer. By

comparing the angle spectra obtained by the experimental and simulated results with an optical simulator (Setfos), the order parameters (S) of the emitting molecules were calculated. The following equation gives the S,

$$S = \tfrac{1}{2} < \cos^2\theta > \quad (6)$$

The angle θ represents the separation between the substrate normal and the transition dipole. Transition dipole orientation: The ratio between horizontally oriented dipoles and total dipoles is determined by

$$\Theta_h = (p_x + p_y)/(p_x + p_y + p_z) \quad (7)$$

where the p_x and p_y are the existence probability of a dipole parallel to the substrate, and the p_z is the existence probability of a dipole orthogonal to the substrate. It is possible to compute the orientational order parameter as

$$S = (p_z^2 - p_x^2)/(p_z^2 + 2p_x^2) \quad (8)$$

where the S is defined as a parameter ranging from −0.5 to 1. The complete horizontal orientation relative to the plane of the film surface marks Θ_h = 100% and S = −0.5, the randomly orientated dyes show Θ_h = 67% and S = 0, and vertical orientation indicates Θ_h = 0% and S = 1.

1.8. Motivation and purpose of this thesis

1.8.1. Molecular design

TADF materials are often available in many variants. Here, we can categorize two major structures: one is linear/single donor-acceptor and the other one is a multi-donor/ hetero-donor condensed structure. In comparison to linear/single donor-acceptor designs, the multi-donor/hetero-donor design improves k_{RISC} and device stability because of the delocalization effect, intramolecular π-π interactions, and modification of the strength of D-A contacts[25,63].

(a)

(b)

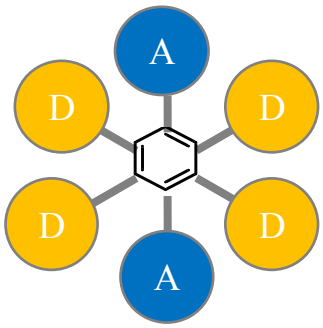

Figure 1.13: a) Linear/single donor-acceptor design, and b) Multi-donor/Hetero-donor design.

Multiple D–A type compounds are a promising group of TADF materials, known for their promising stability and efficiency. The properties of the multi-donor/hetero-donor design depend on, 1) the number of donors and acceptors in TADF molecules, and 2) the substitution positions of the donors and acceptors.

In this molecular series (**Fig. 1.14**), the well-known TADF molecule 4CzIPN has been introduced[25]. 4CzIPN is still one of the best molecules because it is known to be very stable and has a condensed structure. The donor unit in 4CzIPN is carbazole (Cz), and the acceptor unit is cyanide (CN). The D, A combination in this molecule is a weak donor and strong acceptor.

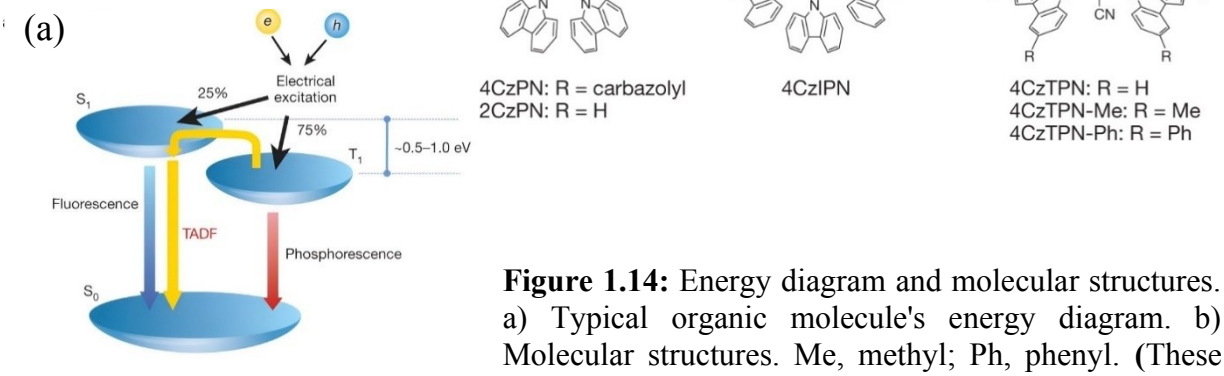

Figure 1.14: Energy diagram and molecular structures. a) Typical organic molecule's energy diagram. b) Molecular structures. Me, methyl; Ph, phenyl. **(**These figures were cited from H. Uoyama *et al.*, *Nature* **492**, 234 (2012)[25]).

H. Noda et al. introduced a series of hetero-donor type molecules consisting of two types of D units[63]. All these D units consist of Cz-based donors. According to the results, the hetero-donor strategy improves the $k_{RISC,}$ and also the carrier transport properties can be enhanced by the bulky D units[63].

The first equation defines the external quantum efficiency (EQE) of an OLED, where IQE denotes the internal quantum efficiency, and η_{out} represents the outcoupling efficiency. The IQE of an OLED is expressed by the second equation, where β is the exciton generation factor, γ is the carrier balance ratio, and Φ_{PL} is the photoluminescent quantum yield.

$$\eta_{EQE} = IQE \times \eta_{out}$$

$$IQE = \beta \times \gamma \times \Phi_{PL}$$

(9)

(10)

The IQE has improved significantly thus far, with almost 100% efficiency achieved by harvesting both singlet and triplet excitons for light emission. Still, there has been a significant issue with improving outcoupling efficiency. Moreover, the orientation of the emitting dipoles affects the outcoupling efficiency, in addition to the device structure itself. The horizontally oriented emitter molecules improve the optical characteristics of the OLEDs since the horizontally oriented transition dipole moment (TDM) increases the outcoupling efficiency of OLEDs. Because molecules emit light mostly in the direction perpendicular to their TDM, the horizontal molecular orientation is preferred over the vertical orientation for high light outcoupling efficiency in OLEDs (**Fig. 1.15**).

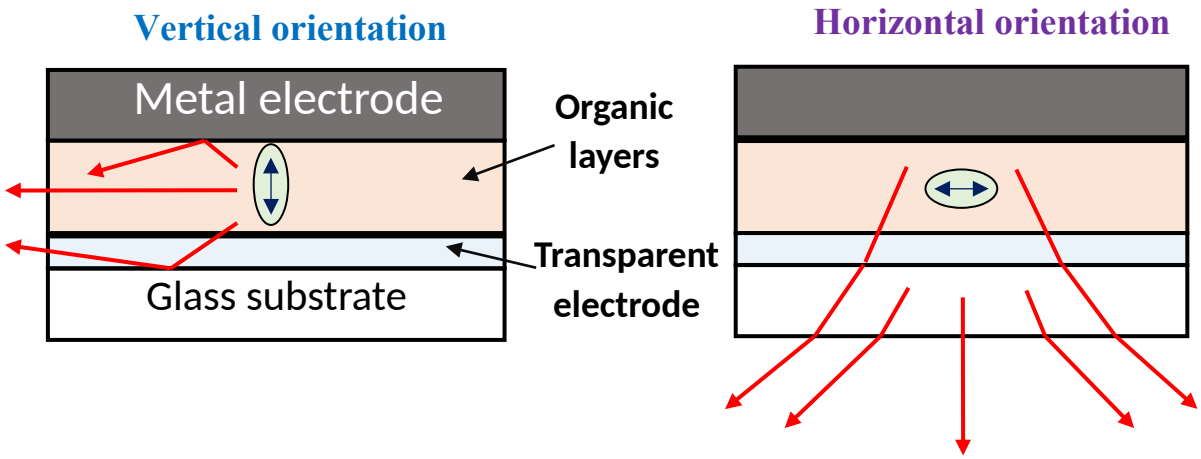

Figure 1.15: The effect of the guest molecule orientation on OLED emission.

However, in the research field of OLEDs, most researchers focused on the PL properties of the films, the performance of the OLEDs, and single molecular characteristics, and sufficient experiments were not considered to examine the molecular orientation and its alignment in the films. Since Tang and VanSlyke began exploring OLEDs in 1987, it has been presumed that molecular orientation in OLEDs is random and isotropic for approximately 20 years[3]. It's known as the "0th approximation".

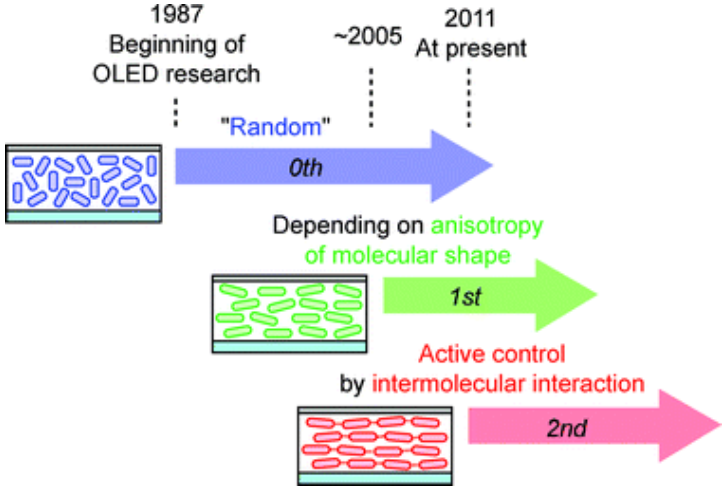

Figure 1.16: The molecular orientation approximations from the beginning of OLED research. **(**This figure was cited from D. Yokoyama, *J. Mater. Chem.* **21**, 19188 (2011)[64]).

Subsequently, it has been discovered that anisotropy of the molecular shape and substrate heating during vacuum deposition might affect the orientation of the molecules; this approximation is referred to as the "1st approximation."

Thus, owing to the orientations of their long molecular axes on substrates, it is generally recognized that molecules with a linear structure predominantly display TDM orientation. According to the "2nd approximation," the molecular orientation can be controlled by intermolecular interactions such as hydrogen bonds and the electrical properties of the OLEDs could be improved by the stacking of the molecules during vacuum deposition[64].

Tanaka et al. discovered in 2020 that host materials with high glass transition temperatures (*T*g) enhanced the horizontal orientation of the emitter, and the horizontal orientation could be influenced by the polarity of the host and guest. He used several emitters with different polarity[65]. Here, the polar host with a polar emitter shows a high horizontal orientation. However, there are not enough studies regarding the effect of the host properties on the guest's molecular orientation.

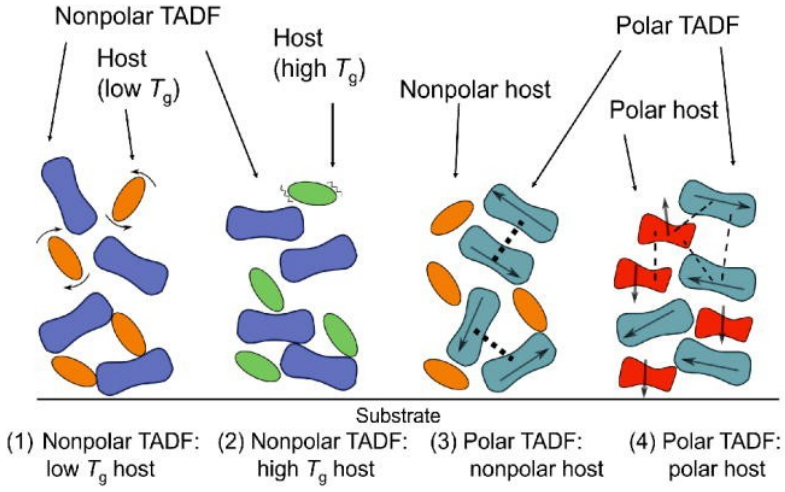

Figure 1.17: The orientation of the polar and non-polar TADF emitters with the T_g of the host materials. **(**This figure was cited from M. Tanaka *et al.*, *Appl. Phys. Lett.* **116**, 023302 (2020)[65]).

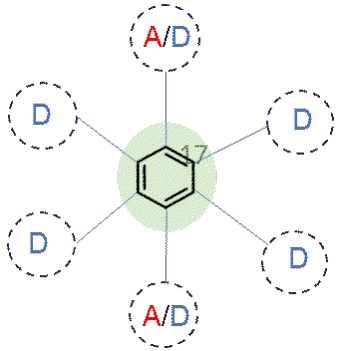

Figure 1.18: Molecular design in this work.

This study features symmetric molecules with bulky donor units connected through a phenyl ring. Also, I investigate the correlation between molecular structures and photophysical properties, such as the k_{RISC} and device durability. By comparing the stabilities of various TADF molecules, I can unleash the potential for developing innovative TADF materials. Generally, all muli-donor/hetero-donor TADF molecules are based on carbazole-based donor units[25,63]. Additionally, I introduce acridine (DMAC) as a donor in a hetero-donor-designed emitter. DMAC is a donor that has a strong donor strength; it has a crowded structure that provides the steric effect, and the highly twisted DMAC could offer a small $\Delta E_{ST.}$ Furthermore, although the IQE of OLEDs can reach 100% by utilizing singlets and triplets in TADF OLEDs, the outcoupling efficiency reduces the EQE to 20-30%. It is well known that the host molecule plays a key role in achieving better molecular orientation of the guest molecule in the emissive layer (EML)[65]. Here, we present a host material with high thermal stability and triplet energy, which results in improved orientation of various guest materials.

In Chapter 2, I developed a novel TADF compound that features multiple D-A type architectures with a hetero-donor design utilizing two distinct donor units, namely 9,10-dihydro-9,9-dimethylacridine (DMAC) and carbazole. The newly designed emitter presented a high photoluminescence quantum yield (PLQY) under several types of circumstances, including polar media and high concentrations. The EQE of OLEDs was reasonably high. Furthermore, we discovered that multiple D-A-type molecules showed better photostability than single D-A-type molecules. However, various other factors may also have an impact on the OLEDs' operating stability.

In Chapter 3, I introduce a new molecule, 6CzPh, as a host molecule. Compared to traditional host materials, 6CzPh, an unexplored carbazole derivative in OLEDs, exhibits

remarkable properties as a host material. Our findings highlight that 6CzPh is a promising candidate for OLED applications. Several approaches have been used to enhance OLED performance, such as triplets in TADF and phosphorescence emitters to maximize the internal quantum efficiency and control the molecule orientation to increase the outcoupling efficiency. The high triplet energy and rigid structure of the novel host contribute to the high EQE and device stability. In addition to their inherent properties, the host material can enhance the horizontal molecular orientation of various guest emitters.

This thesis is summarized and potential directions for the future are discussed in Chapter 4.

1.9. References

1. Wong, M. Y. & Zysman-Colman, E. Purely Organic Thermally Activated Delayed Fluorescence Materials for Organic Light-Emitting Diodes. *Adv. Mater*. **29,** 1605444–1605497 (2017).
2. Zhang, D., Huang, T. & Duan, L. Emerging Self-Emissive Technologies for Flexible Displays. *Adv. Mater.* **32,** 1902391 (2020).
3. Tang, C. W. & VanSlyke, S. A. Organic electroluminescent diodes. *Appl. Phys. Lett.* **51**, 913-915 (1987).
4. Safy, (2019, September, 09). *LG Rollable OLED TV 65 inch.* TurboSquid. https://www.turbosquid.com/3d-models/lg-rollable-oled-tv-model-1445657
5. *4 Current Applications for OLED Devices.* avantama. (2019, January 28). https://avantama.com/current-applications-oled-devices/
6. *Audi Lights Up With OLED light bulbs.* SimplyLED. (2023). https://blog.simplyled.co.uk/audi-lights-up-with-oleds/
7. Mertens, R. (2023, July, 22). *The Honor Magic V2 smartphone is highly popular in China, according to JD.com.* OLED-info. https://www.oled-info.com/honor-magic-v2-smartphone-highly-popular-china-according-jdcom
8. Brütting, W (ed.). Physics of organic semiconductors. *Wiley-VCH*. **2**, 1866–1876 (2005).

9. Koopmans, T. On the assignment of wave functions and eigenvalues to the individual electrons of an atom. *Physica* **1**, 104 (1934).
10. Köhler, A. & Bässler, H. Triplet states in organic semiconductors. *Mater. Sci. Eng. R Rep.* **66**, 71–109 (2009).
11. Reineke, S., Lindner, F., Schwartz, G., Seidler, N., Walzer, K., Lüssem, B. & Leo, K. White Organic Light-Emitting Diodes with Fluorescent Tube Efficiency. *Nature* **459**, 234–238 (2009).
12. Kampen, T. U. Electronic structure of organic interfaces – a case study on perylene derivatives. *Appl. Phys. A* **82**, 457–470 (2006).
13. Hughes, G. & Bryce, M. R. Electron-transporting materials for organic electroluminescent and electro phosphorescent devices. *J. Mater. Chem*. **15**, 94–107 (2005).
14. Scott, J. C. Metal–organic interface and charge injection in organic electronic devices. *J. Mater. Chem.* **21,** 521–531 (2003).
15. Xu, Z., Tang, B. Z., Wang, Y. & Ma, D. Recent advances in high performance blue organic light-emitting diodes based on fluorescence emitters. *J. Mater. Chem. C* **8**, 2614–2642 (2020).
16. Kongsabay, S., Funchien, P., Chasing, P., Sudyodsuk, T. & Promarak, V. An efficient solution-processable hybridized local and charge-transfer (HLCT)-based deep-red fluorescent emitter for simple structured non-doped OLED. *J. Lumin.* **248**, 118921 (2022).
17. Zhao, X., & Mi, X., Efficient Green Fluorescent Organic Light-Emitting Devices with Stepwise Energy Levels. *J. Phys.: Conf. Ser.* **1739**, 012049 (2021).
18. Pachariyangkun, A., Senapak, W., Sudyoadsuk, T., Namuangruk, S. & Promarak, V. Efficient deep-blue fluorescent emitters from imidazole functionalized anthracenes for simple structure deep-blue electroluminescent devices. *Electron.* **85***,* 105897 (2020).
19. Baldo, M. A., O'Brien, D. F., You, Y., Shoustikov, A., Sibley, S., Thompson, M. E. & Forrest, S. R. Highly efficient phosphorescent emission from organic electroluminescent devices. *Nature* **395**, 151–154 (1998).
20. Adachi, C., Baldo, M. A., Forrest, S. R., Lamansky, S., Thompson, M. E. & Kwong, R. C. High-efficiency red electrophosphorescence devices. *Appl. Phys. Lett*. **78**, 1622–1624 (2001).

21. Xu, H., Chen, R., Sun, Q., Lai, W., Su, Q., Huang, W. & Liu, X. Recent progress in metal-organic complexes for optoelectronic applications. *Chem. Soc. Rev*. **43**, 3259–3302 (2014).
22. Fan, C. H., Sun, P., Su, T. H. & Cheng, C. H. Host and Dopant Materials for Idealized Deep-Red Organic Electrophosphorescence Devices. *Adv. Mater*. **23**, 2981–2985 (2011).
23. Park, Y. S., Lee, S., Kim, K. H., Kim, S. Y., Lee, J. H. & Kim J. J. Exciplex-Forming Co-host for Organic Light-Emitting Diodes with Ultimate Efficiency. *Adv. Funct. Mater*. **23**, 4914–4920 (2013).
24. Shin, H., Ha, Y. H., Kim, H. G., Kim, R., Kwon, S. K., Kim, Y. H. & Kim, J. J. Controlling Horizontal Dipole Orientation and Emission Spectrum of Ir Complexes by Chemical Design of Ancillary Ligands for Efficient Deep-Blue Organic Light-Emitting Diodes. *Adv. Mater*. **31**, 1808102–1898107 (2019).
25. Uoyama, H., Goushi, K., Shizu, K., Nomura, H. & Adachi, C. Highly efficient organic light-emitting diodes from delayed fluorescence. *Nature* **492**, 234–238 (2012).
26. Zhang, Q., Li, B., Huang, S., Nomura, H., Tanaka, H. & Adachi, C. Efficient blue organic light-emitting diodes employing thermally activated delayed fluorescence. *Nat. Photon.* **8**, 326–332 (2014).
27. Endo, A., Sato, K., Yoshimura, K., Kai, T., Kawada, A., Miyazaki, H. & Adachi, C. Efficient up-conversion of triplet excitons into a singlet state and its application for organic light emitting diodes. *Appl. Phys. Lett.* **98**, 083302 (2011).
28. Palmeira, T. & Berberan-Santos, M. N. Kinetic Criteria for Optimal Thermally Activated Delayed Fluorescence in Photoluminescence and in Electroluminescence. *J. Phys. Chem. C* **121**, 701–708 (2017).
29. Endo, A., Ogasawara, M., Takahashi, A., Yokoyama, D., Kato, Y. & Adachi, C. Thermally Activated Delayed Fluorescence from Sn^{4+}–Porphyrin Complexes and Their Application to Organic Light Emitting Diodes - A Novel Mechanism for Electroluminescence. *Adv. Mater.* **21**, 4802–4806 (2009).
30. Goushi, K., Yoshida, K., Sato, K. & Adachi, C. Organic light-emitting diodes employing efficient reverse intersystem crossing for triplet-to-singlet state conversion. *Nat. Photon*. **6**, 253–258 (2012).
31. Shizu, K., Noda, H., Tanaka, H., Taneda, M., Uejima, M., Sato, T., Tanaka, K., Kaji, H. & Adachi, C. Highly Efficient Blue Electroluminescence Using Delayed-Fluorescence

Emitters with Large Overlap Density between Luminescent and Ground States. *J. Phys. Chem. C* **119**, 26283–26289 (2015).

32. Kaji, H., Suzuki, H., Fukushima, T., Shizu, K., Suzuki, K., Kubo, S., Komino, T., Oiwa, H., Suzuki, F., Wakamiya, A., Murata, Y. & Adachi, C. Purely organic electroluminescent material realizing 100% conversion from electricity to light. *Nat. Commun*. **6**, 8476 (2015).
33. Yamanaka, T., Nakanotani, H., Hara, S., Hirohata, T. & Adachi, C. Near-infrared organic light-emitting diodes for biosensing with high operating stability. *Appl. Phys. Express* 10, 074101 (2017).
34. Sun, J. W., Lee, J. -H., Moon, C.-K., Kim, K. -H., Shin, H. & Kim, J. -J. A Fluorescent Organic Light-Emitting Diode with 30% External Quantum Efficiency. *Adv. Mater*. 26, 5684-5688 (2014).
35. Zhang, D., Duan, L., Li, Y., Zhang, D. & Qiu, Y. Highly efficient and color-stable hybrid warm white organic light-emitting diodes using a blue material with thermally activated delayed fluorescence. *J. Mater. Chem*. C 2, 8191–8197 (2014).
36. Tao, Y., Yang, C. & Qin. J. Organic host materials for phosphorescent organic light-emitting diodes. *Chem. Soc. Rev.* **40**, 2943 (2011).
37. Nishimoto, T., Yasuda, T., Lee, S. Y., Kondo, R. & Adachi, C. A six-carbazole-decorated cyclophosphazene as a host with high triplet energy to realize efficient delayed-fluorescence OLEDs. *Mater. Horiz.* **1**, 264–269 (2014).
38. Duan, L., Qiao, J., Sun, Y. & Qiu, Y. Strategies to Design Bipolar Small Molecules for OLEDs: Donor-Acceptor Structure and Non-Donor-Acceptor Structure. *Adv. Mater.* **23**, 1137 (2011).
39. Zhang, Q., Li, J., Shizu, K., Huang, S., Hirata, S., Miyazaki, H. & Adachi, C. Design of efficient thermally activated delayed fluorescence materials for pure blue organic light emitting diodes. *J. Am. Chem. Soc*. **134**, 14706–14709 (2012).
40. Lee, S. Y., Yasuda, T., Yang, Y. S., Zhang, Q. & Adachi, C. Luminous butterflies: efficient exciton harvesting by benzophenone derivatives for full-color delayed fluorescence OLEDs. *Angew. Chem.* **53**, 6402–6406 (2014).
41. Han, C., Zhao, Y., Xu, H., Chen, J., Deng, Z., Ma, D., Li, Q. & Yan, P. A simple phosphine-oxide host with a multi-insulating structure: high triplet energy level for efficient blue electrophosphorescence. *Chem. Eur. J.* **17,** 5800–5803 (2011).

42. Hirata, S., Sakai, Y., Masui, K., Tanaka, H., Lee, S. Y., Nomura, H., Nakamura, N., Yasumatsu, M., Nakanotani, H., Zhang, Q., Shizu, K., Miyazaki, H. & Adachi, C. Highly efficient blue electroluminescence based on thermally activated delayed fluorescence. *Nat*. *Mater*. **14**, 330–336 (2015).
43. Kim, M., Jeon, S. K., Hwang, S. H. & Lee, J. Y. Stable blue thermally activated delayed fluorescent organic light-emitting diodes with three times longer lifetime than phosphorescent organic light-emitting diodes. *Adv. Mater*. **27**, 2515–2520 (2015).
44. Tsai, Y. S., Hong, L. A., Juang, F. S. & Chen, C.Y. Blue and white phosphorescent organic light emitting diode performance improvement by confining electrons and holes inside double emitting layers. *J. Lumin.* **153**, 312–316 (2014).
45. Godumala, M., Choi, S., Cho, M. J. & Choi, D. H. Thermally activated delayed fluorescence blue dopants and hosts: from the design strategy to organic light-emitting diode applications. *J. Mater. Chem. C* **4**, 11355–11381 (2016).
46. Dong, S. C., Zhang, L., Liang, J., Cui, L. S., Li, Q., Jiang, Z. Q. & Liao, L. S. Rational Design of Dibenzothiophene-Based Host Materials for PHOLEDs. *J. Phys. Chem. C* **118**, 2375–2384 (2014).
47. Naqvi, B. A., Schmid, M., Crovini, E., Sahay, P., Naujoks, T., Rodella, F., Zhang, Z., Strohriegl, P., Bräse, S., Zysman-Colman, E. & Brütting, W. What Controls the Orientation of TADF Emitters? *Front. Chem*. **8**, 750 (2020).
48. Wang, Q., Tian, Q. S., Zhang, Y. L., Tang, X. & Liao, L. S. High-efficiency organic light-emitting diodes with exciplex hosts. *J. Mater. Chem. C* **7**, 11329–11360 (2019).
49. Wang, Y., Yun, J. H., Wang, L. & Lee, J. Y. High Triplet Energy Hosts for Blue Organic Light-Emitting Diodes. *Adv. Funct. Mater.* **31**, 2008332 (2021).
50. Dias, F. B. Kinetics of thermal-assisted delayed fluorescence in blue organic emitters with large singlet–triplet energy gap. *Philos. Trans. R. Soc. A Math. Phys. Eng. Sci.* **373**, 20140447 (2015).
51. Murawski, C., Leo, K. & Gather, M. C. Efficiency Roll-Off in Organic Light-Emitting Diodes. *Adv. Mater.* **25**, 6801–6827 (2013).
52. a) Baldo, M. A., Adachi, C. & Forrest, S. R. Transient analysis of organic electrophosphorescence. II. Transient analysis of triplet-triplet annihilation. *Phys. Rev. B* **62**, 10967–10977 (2000) b) Lee, K. H., Kang, L. K., Lee, J. Y., Kang, S., Jeon, S. O., Yook, K. S., Lee, J. Y. & Yoon, S. S. Molecular engineering of blue fluorescent molecules based on silicon end-capped diphenylaminofluorene derivatives for efficient

organic light-emitting materials. *Adv. Funct. Mater.* **20**, 1345–1358 (2010) c) Gather, M. C., Köhnen, A. & Meerholz, K. White Organic Light-Emitting Diodes. *Adv. Mater.* **23**, 233–248 (2011).

53. Reineke, S., Thomschke, M., Lüssem, B. & Leo, K. White organic light-emitting diodes: Status and perspective. *Rev. Mod. Phys*. **85**, 1245–1293 (2013).
54. Gu, G., Garbuzov, D. Z., Burrows, P. E., Venkatesh, S., Forrest S. R. & Thompson, M. E. High-external-quantum-efficiency organic light-emitting devices. *Opt. Lett*. **22**, 396–398 (1997).
55. Greenham, N. C., Friend R. H. & Bradley, D. D. C. Angular dependence of the emission from a conjugated polymer light-emitting diode: implications for efficiency calculations. *Adv. Mater*. **6**, 491–494 (1994).
56. Yue, Q., Li, W., Kong, F. & Li, K. Enhancing the Out-Coupling Efficiency of Organic Light-Emitting Diodes Using Two-Dimensional Periodic Nanostructures, *Adv. Mater. Sci. Eng*. **2012**, 1–9 (2012).
57. Hauss, J., Bocksrocker, T., Riedel, B., Lemmer, U. & Gerken, M. On the interplay of waveguide modes and leaky modes in corrugated OLEDs. *Opt. Exp.* **19**, A851–A858 (2011).
58. Smith, L. H., Wasey, J. A. E., Samuel I. D. W. & Barnes. W. L. Light out-coupling efficiencies of organic light-emitting diode structures and the effect of photoluminescence quantum yield. *Adv. Funct. Mater*. **15**, 1839–1844 (2005).
59. Nowy, S., Krummacher, B. C., Frischeisen, J., Reinke N. A., & Bru¨tting, W. Light extraction and optical loss mechanisms in organic light-emitting diodes: Influence of the emitter quantum efficiency. *J. Appl. Phys*. **104**, 123109 (2008).
60. Frischeisen, J., Yokoyama, D., Adachi, C. & Brütting, W. Determination of molecular dipole orientation in doped fluorescent organic thin films by photoluminescence measurements. *Appl. Phys. Lett*. **96**, 073302 (2010).
61. Frischeisen, J., Yokoyama, D., Endo, A., Adachi, C. & Brütting, W. Increased light outcoupling efficiency in dye-doped small molecule organic light-emitting diodes with horizontally oriented emitters. *Org. Electron*. **12**, 809–817 (2011).
62. Komino, T., Tanaka, H. & Adachi, C. Selectively Controlled Orientational Order in Linear-Shaped Thermally Activated Delayed Fluorescent Dopants. *Chem. Mater*. **26**, 3665−3671 (2014).

63. Noda, H., Nakanotani, H. & Adachi, C. Excited state engineering for efficient reverse intersystem crossing. *Sci. Adv.* **4**, eaao6910 (2018).
64. Yokoyama, D. Molecular orientation in small-molecule organic light-emitting diodes. *J. Mater. Chem*. **21**, 19187–19202 (2011).
65. Tanaka, M., Noda, H., Nakanotani, H. & Adachi, C. Molecular orientation of disk-shaped small molecules exhibiting thermally activated delayed fluorescence in host-guest films. *Appl. Phys. Lett.* **116**, 023302 (2020).

Chapter II. Multiple donor-acceptor design for highly luminescent and stable thermally activated delayed fluorescence emitters

2.1. Introduction

Thermally activated delayed fluorescence (TADF) emitters have recently received considerable attention since they can provide 100% internal quantum efficiency (IQE) in organic light-emitting diodes (OLEDs)[1]. TADF emitters have a special chemical structure that is built on different kinds of donor (D) and acceptor (A) units[2-5]. There has been a recent interest in the TADF research field in controlling the rate constants, such as enhancing the RISC rate (k_{RISC})[6-14]. Long-lived triplet excitons can be minimized via fast k_{RISC}, which will contribute to reducing exciton losses and efficiency rolloff[15,16]. However, 4CzIPN, which contains carbazole donors and benzonitrile acceptors, received high stability despite the relatively high k_{RISC}[1,17]. The multiple donor-acceptor design allows different D-A interactions, intermolecular interactions, CT strength, and specifically, the delocalization effect, which may be related to the high stability[18].

Furthermore, the hetero-donor design, which consists of different donor units may improve the stabilities further with better photophysical characteristics[19,20]. Although the key requirement for use in practical applications is the stable operation of the devices, the relationship between molecular structures and device durability has not been fully understood. In addition, it is not clear how the excited state dynamics, including the k_{RISC}, affect the stabilities. Therefore, the direct comparison of the stabilities of some TADF molecules will contribute to advancing molecular designs of TADF materials.

Among the various structural types of TADF molecules, the molecular structures with multiple donor-acceptor (D-A) units are promising candidates for developing highly stable materials[1,17]. However, these compounds are always incorporated with carbazole-based donors[21-25]. Therefore, I developed a new molecule, named 2Cz2DMAC2BN, with two distinct donor units, 9,10-dihydro-9,9-dimethylacridine (DMAC) and carbazole (Cz), with a hetero-donor design (**Fig. 2.1**). The combination with the weak acceptor benzonitrile (BN) leads to a relatively high singlet excited state energy (S_1) with sky blue to green emission. The performance of the emitter is investigated with n-type host PPT and p-type hosts CCP and mCBP. Further, the device optimization is done by changing the doping concentration. Also, I compared the photophysical properties of the new molecule with a few TADF molecules which have the same range of S_1 energy and k_{RISC}, because these parameters significantly affect stabilities.

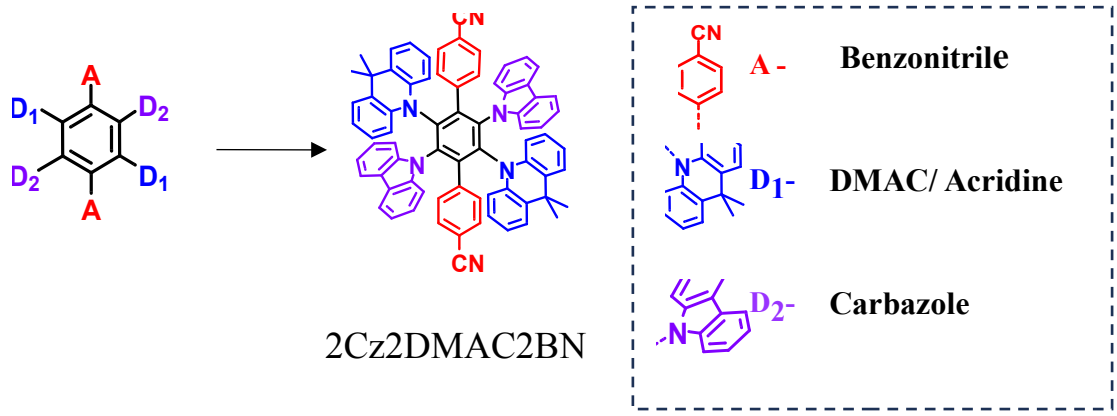

Figure 2.1: The molecular structure of 2Cz2DMAC2BN with the D and A groups.

Because DMAC is a strong donor relative to Cz, the emitters based on DMAC exhibit strong CT and a more twisted structure. Here, I discovered small ΔE_{ST} and high PLQY, demonstrating the effectiveness of 2Cz2DMAC2BN as a TADF molecule.

2.2. Experimental

2.2.1. Synthesis of 2Cz2DMAC2BN

To a dispersion of sodium hydride (60% in mineral oil, 0.38 g, 9.5 mmol) in dry DMF (15 ml) was added 9,10-dihydro-9,9-dimethylacridine (1.89 g, 9.1 mmol) in DMF (15 ml) at 0 °C under Ar. After stirring for 30 min, **4F2BN** (0.88 g, 2.5 mmol) was added as a solid. After stirring for 30 min, the reaction mixture was stirred at 80 °C overnight. After cooling, H_2O was added, and the precipitates were filtered and washed with H_2O and methanol. The crude product was purified by sublimation at 300 °C under vacuum, then column chromatography on a silica gel using DCM (R_f = 0.61), and recrystallization from DCM layered with MeOH to give the pure compound as a yellow solid **2F2DMAC2BN** (1.10 g, 60%). To a dispersion of sodium hydride (60% in mineral oil, 0.53 g, 13.4 mmol) in dry DMF (15 ml) was added carbazole (2.20 g, 13.2 mmol) in DMF (15 ml) at 0 °C under Ar. After stirring for 30 min, **2F2DMAC2BN** (1.20 g, 1.6 mmol) was added as a solid. After stirring for 30 min, the reaction mixture was stirred at 80 °C overnight. After cooling, H_2O was added, and the precipitates were filtered and washed with H_2O and methanol. The crude product was purified by sublimation at 380 °C under vacuum to remove carbazole, then column chromatography

on a silica gel using the hexane/DCM (1:2) mixture as eluent (R_f = 0.32), recrystallization from DCM layered with MeOH, and sublimation at 380 °C to give the pure compound as a yellow solid (1.40 g, 83%).

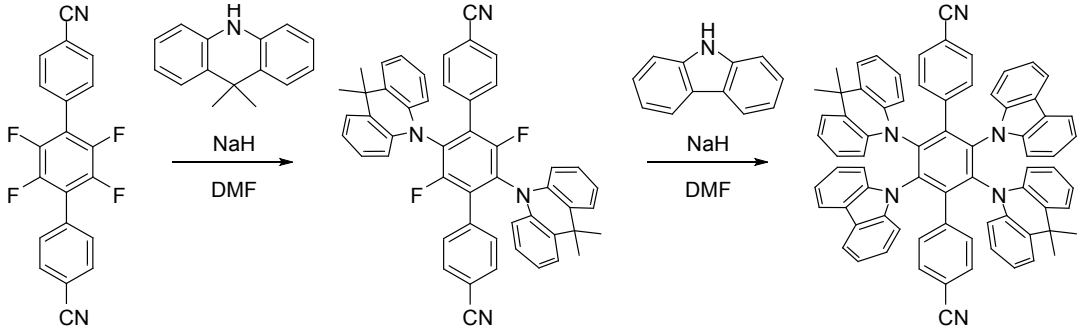

4F2BN **2F2DMAC2BN** **2Cz2DMAC2BN**

Scheme 2-1: Synthetic route to **2Cz2DMAC2B.** 2',3',5',6'-tetrafluoro-[1,1':4',1"-terphenyl]-4,4"-dicarbonitrile (**4F2BN**) was synthesized by modifying the literature[25].

a)

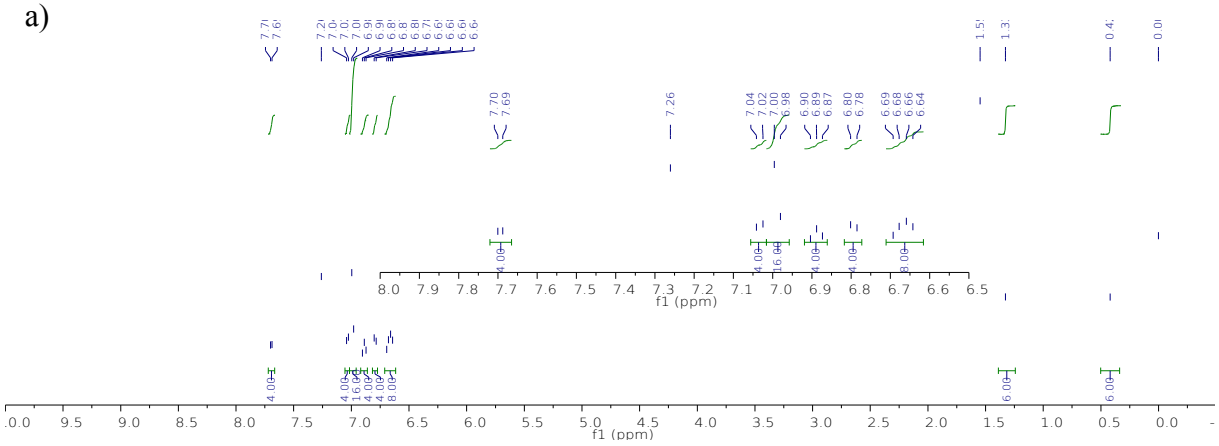

b)

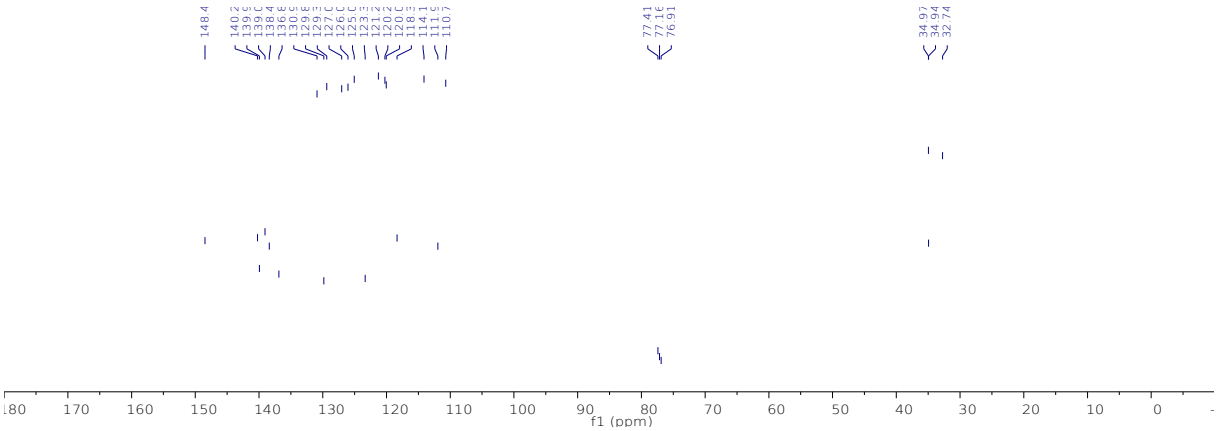

Figure 2.2: NMR spectra of 2Cz2DMAC2BN compound. a) ^{1}H-NMR spectrum (500 MHz, $CDCl_3$, 300 K), and b) ^{13}C-NMR-APT spectra (125 MHz, $CDCl_3$, 300 K).

2.2.2. Materials

The materials of tris-PCz, T2T, BPy-TP2, mCBP, PPT, HATCN, 4CzIPN, ACRXTN, Liq, and CCP were synthesized in-house.

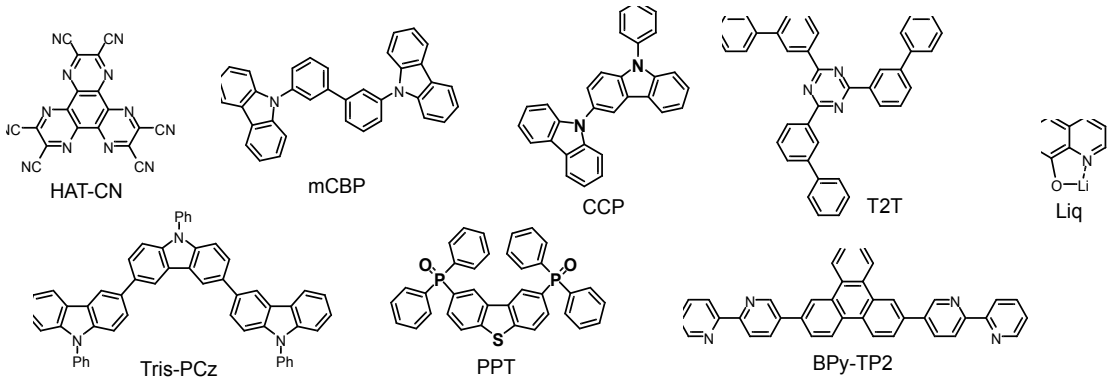

Figure 2.3: Chemical structures of the materials used in this study.

2.2.3. Sample preparation for device fabrication

Thermal evaporation was used for fabricating organic films with a thickness of 100 nm for photoluminescence studies on quartz substrates. Under vacuum, at pressures less than 5 x 10^{-5} Pa, the organic deposition was carried out. The anode was created using glass substrates with a thickness of 100 nm and a pre-patterned coating of tin-doped indium oxide (ITO).

The device structures: ITO (100 nm)/HAT-CN (10 nm)/Tris-PCz (30 nm)/electron blocking layer (EBL) (5 nm)/x-wt%-2Cz2DMAC2BN: host (30 nm)/hole blocking layer/(HBL) (10 nm)/BPy-TP2 (40 nm)/Liq (2 nm)/Al (100 nm). The devices were fabricated and then quickly sealed with glass lids using epoxy glue in a glove box filled with nitrogen (about 0.1 ppm of O_2 and 0.1 ppm of H_2O).

2.2.4. Preparation of organic films for photophysical measurements

Clean quartz and Si substrates were used to fabricate organic thin films for optical measurements by thermal evaporation at a pressure lower than 1×10^{-4} Pa. The substrates

were cleaned with acetone and isopropanol and then treated with UV/ozone to remove adsorbed organic species before deposition.

2.2.5. Optical characterization of organic thin films

The absorption spectra were measured by UV-vis spectrometer. The steady-state visible photoluminescence spectra and intensities were measured using a multichannel spectrophotometer (PMA-12, Hamamatsu Photonics). Photoluminescence quantum efficiency was measured using an absolute photoluminescence quantum yield measurement system (Quantaurus-QY Plus, Hamamatsu Photonics) under the flow of argon gas. Using the Quantaurus-Tau fluorescence lifetime measuring system (Quantaurants-Tau, Hamamatsu Photonics), the transient PL decay features were captured.

2.2.6. Characterization of OLEDs

The current-density–voltage–luminance (*J–V–L*) characteristics of the OLEDs were evaluated using a source meter (Keysight B2911A, Keysight Technologies) and a luminance meter (CS-2000, Konica Minolta, Japan) at a constant DC current at room temperature. The reproducibility of the device performance of the presented devices was confirmed by measuring at least four different samples. For the device lifetime tests, the luminance and electroluminescence spectra of the driving devices in the normal direction were measured using a luminance meter (SR-3AR, TOPCON, Japan) under constant current density driving conditions with an initial luminance of 100 cd m^{-2}.

2.2.7. Photostability measurement of emissive molecules

The photostability of TADF materials was measured by irradiating continuous-wave laser light at 355 nm (excitation power of 2.7 W cm^{-2}).

2.2.8. Angular-dependent PL measurement of emissive molecules

Radiation patterns of the *p*-polarized light of the doped films were obtained by the angular-dependent PL measurement system (Hamamatsu Photonics C14234-01). The optical

simulation was performed using simulation software (Setfos 4.6, Fluxim). The n and k values for each layer were measured by variable angle spectroscopic ellipsometry.

2.3. Result and Discussion

The molecular structure was confirmed by X-ray single crystal analysis. The crystal contains two independent molecules with an inversion center, where the dihedral angles between DMAC and center phenyl (Ph) rings are varied from 77° to 90° (**Fig. 2.4)**.

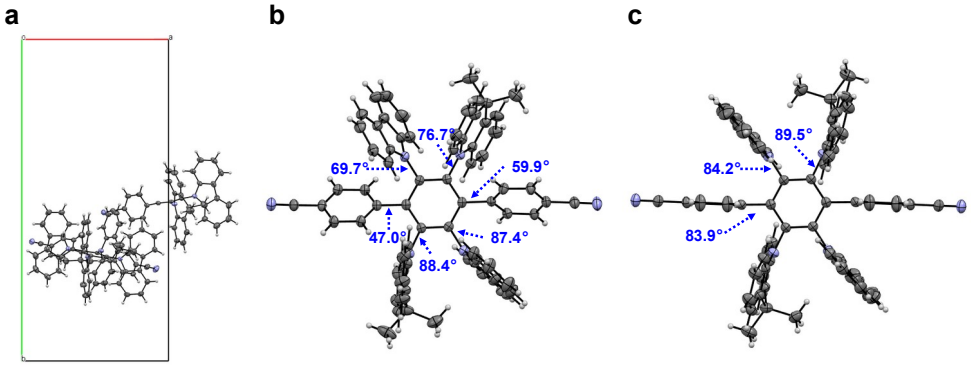

Figure 2.4: X-ray single crystal analysis. (a) The molecular structure in the asymmetric unit. (b) The dihedral angles for molecule 1. (c) The dihedral angles for molecule.

Since the calculated angle is 79°, the packing effect might cause the highly twisted structures (**Fig. 2.5)**. This result suggests some degree of freedom for the rotation of substituted rings. Since the DMAC-Ph bond is highly twisted close to 90° in the excited states because of the CT, the molecule should easily form stable geometries in the excited states[26].

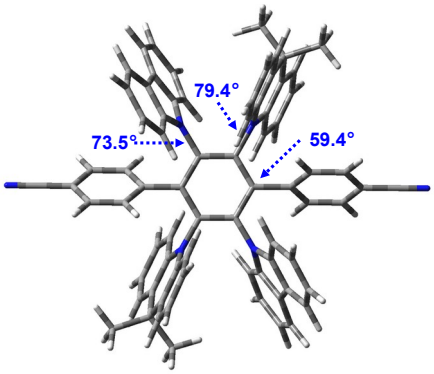

Figure 2.5: Calculated molecular geometries at the B3LYP/6-31+G(d,p).

The photophysical characteristics of 2Cz2DMAC2BN were fully characterized in solution and solid states. A high PLQY of 91% was obtained in toluene, where the small ΔE_{ST} of 0.01 eV and fast delayed lifetime (τ_d) of 3.8 μs were also achieved (**Table 2.1**), indicating efficient TADF properties. These properties are comparable to those of 4CzIPN, one of the best green TADF molecules[1].

Generally, 4CzIPN is a polar emitter that has a high dipole moment of 3.95 D. However, from the DFT calculations, I observed the dipole moment of 2Cz2DMAC2BN is 0.23 D which is a negligible dipole moment[27]. The molecular geometry, the polarity of the substituents, and the relative orientation of the moieties determine the overall dipole moment of a molecule. 4CzIPN consists of nitrile groups (-CN) which provide high polarity, contributing significantly to the dipole moment of the molecule, and also the molecular geometry is not symmetrical. On the other hand, the new molecule has a highly symmetrical molecular geometry (**Fig. 2.1**).

In polar solvents, the excited state of the TADF molecules stabilized and reduced its energy. The emission spectra of TADF emitters exhibit a bathochromic shift in polar solvents due to the polar CT state of TADF molecules. To examine TADF characteristic behavior, we examined the solution state properties of the two molecules in five different solvents. The solvents are cyclohexane (0 D), toluene (0.31 D), dichloromethane (DCM) (1.14 D), ethyl acetate (1.88 D), and acetone (2.69 D). Interestingly, 2Cz2DMAC2BN showed constantly high PLQY even in polar solvents such as acetone, which is a clear difference from 4CzIPN (**Fig. 2.6** and **Table 2.1).** The reason behind this behavior is the low polarity of the 2Cz2DMAC2BN and its high steric hindrance. Also, according to the TD-DFT calculations, the T_1 of 2Cz2DMAC2BN is LE dominant and 4CzIPN has CT dominant T_1 states. In acetone, we observed a short delay lifetime and zero $\Delta E_{ST.}$ Even though we did not check the k_{RISC}, we can predict it would be higher compared to that of 4CzIPN. This feature suggests a great potential to maintain high PLQY in high doping concentrations, including neat conditions, where the TADF molecules having D–A structures may reduce PLQY as the polar media.

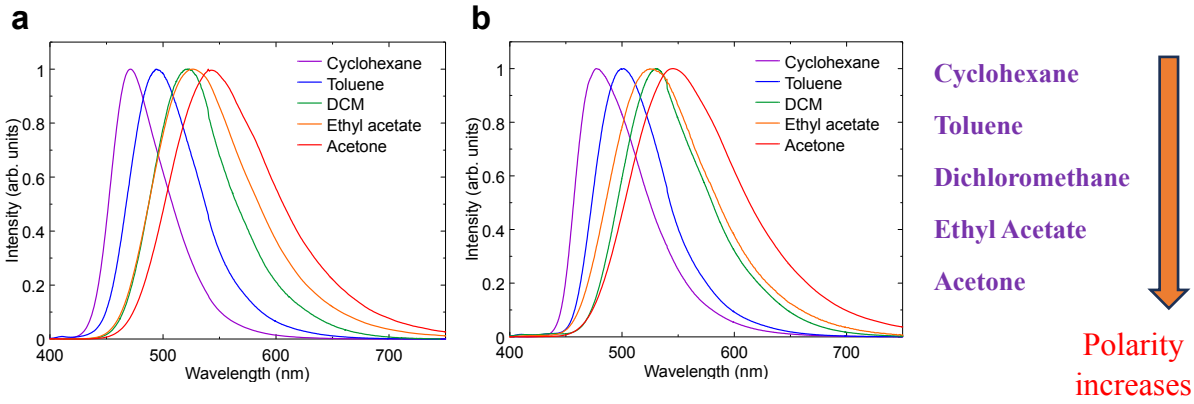

Figure 2.6: PL spectra in various solvents for (a) 2Cz2DMAC2BN and (b) 4CzIPN.

Table 2.1. Photophysical characteristics in various solvents for (a) 2Cz2DMAC2BN and (b) 4CzIPN.

Compound	Solvents	λ_{PL} [nm]	S_1 [eV]	T_1 [eV]	ΔE_{ST} [eV]	Φ_{PL} [-][a)]	τ_d [μs][a)]
2Cz2DMAC2BN	In cyclohexane	472	2.85	2.80	0.05	0.51	5.4
	In toluene	495	2.79	2.78	0.01	0.91	3.8
	In dichloromethane	522	2.71	2.70	0.01	0.73	4.4
	In ethyl acetate	526	2.73	2.73	0	0.70	4.2
	In acetone	544	2.66	2.66	0	0.68	1.2
4CzIPN	In cyclohexane	478	2.78	2.63	0.15	0.90	4.8
	In toluene	501	2.71	2.67	0.04	0.81	4.7
	In dichloromethane	530	2.66	2.64	0.02	0.59	4.4
	In ethyl acetate	526	2.69	2.66	0.03	0.59	4.2
	In acetone	546	2.65	2.63	0.02	0.41	3.6

[a)]Measured under N_2 in solution.

The phosphorescence spectrum in toluene at 77 K showed shoulder peaks, indicating that the T_1 state has a locally excited state (LE) character (**Fig. 2.7 a**). The triplet LE (^{3}LE) of Cz and DMAC are relatively high at > 3.0 eV[28]. Although the ^{3}LE of BN-Ph-BN was reported to be 2.9 eV, the highly twisted DMAC might offer the space to planarize BN-Ph-BN rings, resulting in the decrease of ^{3}LE[25]. The blend films of 2Cz2DMAC2BN and mCBP (3,3′-di(9*H*-carbazol-9-yl)-1,1′-biphenyl) kept near-unity PLQY in 6–50 wt% doping concentrations (**Fig. 2.7 b** and **Table 2.2.**). The emission wavelengths also showed small redshifts. These are advantageous to optimize the OLED because the doping concentrations in the emissive layer (EML) significantly affect charge transport ability. The ΔE_{ST} and τ_d are comparably good with those in the solution. The temperature dependence of the transient PL decay clearly showed the typical behavior of TADF with the increase of delayed fluorescence (**Fig. 2.7 c).**

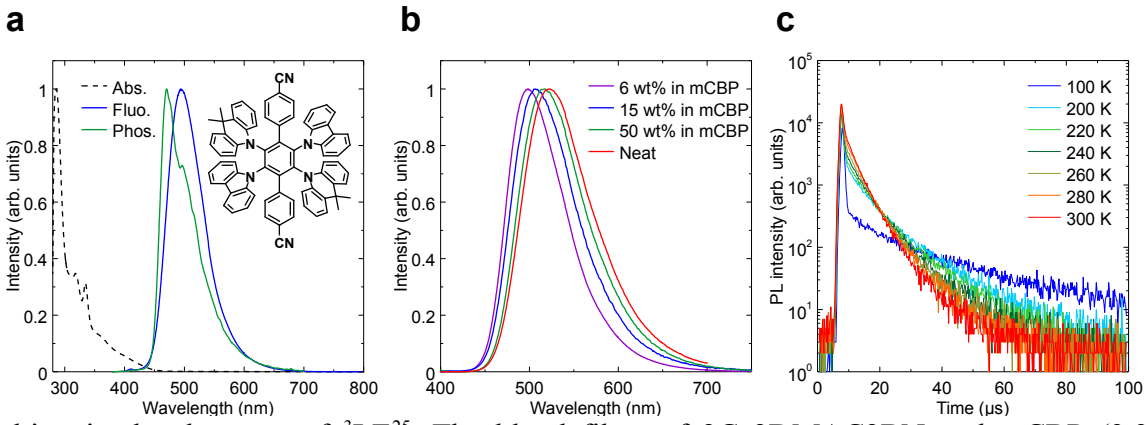

Figure 2.7: (a) Absorption and fluorescence spectra at room temperature and phosphorescence spectrum at 77 K for 2Cz2DMAC2BN in toluene. Inset: Chemical structures of 2Cz2DMAC2BN. (b) PL spectra for 2Cz2DMAC2BN doped films of mCBP and neat 2Cz2DMAC2BN film. (c) Temperature dependence of transient PL decay for 6-wt%-2Cz2DMAC2BN doped film of mCBP.

Table 2.2. Photophysical characteristics of 2Cz2DMAC2BN in toluene, blend films with mCBP, and neat film.

Condition	λ_{PL} [nm]	S_1 [eV]	T_1 [eV][a)]	ΔE_{ST} [eV]	Φ_{PL} [-][b)]	Φ_p/Φ_d [-][b)]	τ_p [ns][b)]	τ_d [μs][b)]	k_r [10^6 s^{-1}]	k_{ISC} [10^7 s^{-1}]	k_{RISC} [10^5 s^{-1}]
In toluene	496	2.79	2.78	0.01	0.91	0.20/0.71	46	3.8	4.3	1.7	11.7
In 6 wt% film[c)]	498	2.75	2.73	0.02	0.95	0.28/0.67	34	3.6	8.2	2.1	9.2
In 20 wt% film[c)]	507	2.75	2.72	0.03	1.0	0.35/0.65	47	3.8	7.5	1.4	7.5

In 50 wt% film[c)]	517	2.70	2.64	0.06	1.0	0.42/0.58	55	3.5	7.6	1.1	6.8
In Neat film	522	2.67	2.60	0.07	0.76	0.38/0.38	62	2.0	6.1	1.0	8.1

[a)]Measured at 77 K; [b)]Measured under N_2 in solution or Ar in films; [c)]Doped in mCBP.

The optical properties in other hosts such as CCP (9-phenyl-9*H*-3,9′-bicarbazole) and in PPT (2,8-bis(diphenyl-phosphoryl)-dibenzo[*b,d*]thiophene) are also excellent although the polarity of PPT is relatively higher than mCBP (**Fig. 2.8 and Table 2.3.**)[29]. The calculated k_{RISC} is close to 10^6 s^{-1}, which is similar to that of 4CzIPN. The neat film also exhibited good emission properties with a PLQY of 76%, indicating the suppression of the concentration quenching. The emission maximum in the neat film is only 24 nm redshifted from that in a 6 wt%-doped film of mCBP (**Fig. 2.7 b**). These results adequately demonstrate the efficient emission properties of 2Cz2DAMC2BN

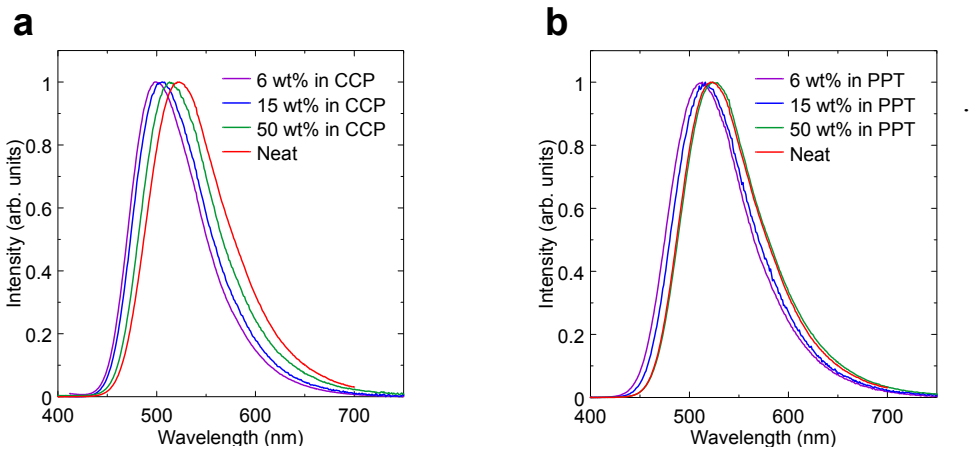

Figure 2.8: PL spectra in CCP and PPT hosts for 2Cz2DMAC2BN.

Condition	λ_{PL} [nm]	S_1 [eV]	T_1 [eV]	ΔE_{ST} [eV]	Φ_{PL} [-][a)]	Φ_p/Φ_d [-][a)]	τ_p [ns][a)]	τ_d [μs][a)]	k_r [10^6 s^{-1}]	k_{ISC} [10^7 s^{-1}]	k_{RISC} [10^5 s^{-1}]
In 6 wt% film of CCP	500	2.77	2.76	0.01	0.89	0.29/0.60	39	3.8	7.4	1.8	7.7
In 20 wt% film of CCP	505	2.75	2.73	0.02	0.91	0.28/0.63	49	3.3	5.7	1.5	9.5
In 50 wt% film of CCP	514	2.67	2.66	0.01	0.96	0.36/0.60	53	3.1	6.8	1.2	8.4
In 6 wt% film of PPT	511	2.75	2.73	0.02	0.89	0.38/0.51	58	2.4	6.5	1.1	9.0
In 20 wt% film of PPT	516	2.72	2.70	0.02	0.99	0.43/0.56	67	2.6	6.4	0.85	8.8
In 50 wt% film of PPT	525	2.66	2.62	0.04	0.90	0.47/0.43	58	3.5	8.1	0.91	4.9

Table 2.3. Photophysical characteristics in CCP and PPT hosts for 2Cz2DMAC2BN.

[a)]Measured under Ar.

To demonstrate the efficient TADF properties of 2Cz2DMAC2BN, the OLEDs were fabricated according to the report for 4CzIPN[17]. The device structures are ITO (100 nm)/HAT-CN (10 nm)/ Tris-PCz (30 nm)/electron blocking layer (EBL) (5 nm)/x-wt%-2Cz2DMAC2BN: host (30 nm)/hole blocking layer (HBL) (10 nm)/BPy-TP_2 (40 nm)/Liq (2 nm)/Al (100 nm), where HAT-CN is dipyrazino[2,3-*f*:2′,3′-*h*]quinoxaline-2,3,6,7,10,11-hexacarbonitrile, Tris-PCz is 9,9′,9″-triphenyl-9*H*,9′*H*,9″*H*-3,3′:6′,3″tercarbazole, BPy-TP_2 is 2,7-bis(2,2′-bipyridine-5-yl)triphenylene, and Liq is 8-hydroxyquinolinolato-lithium.

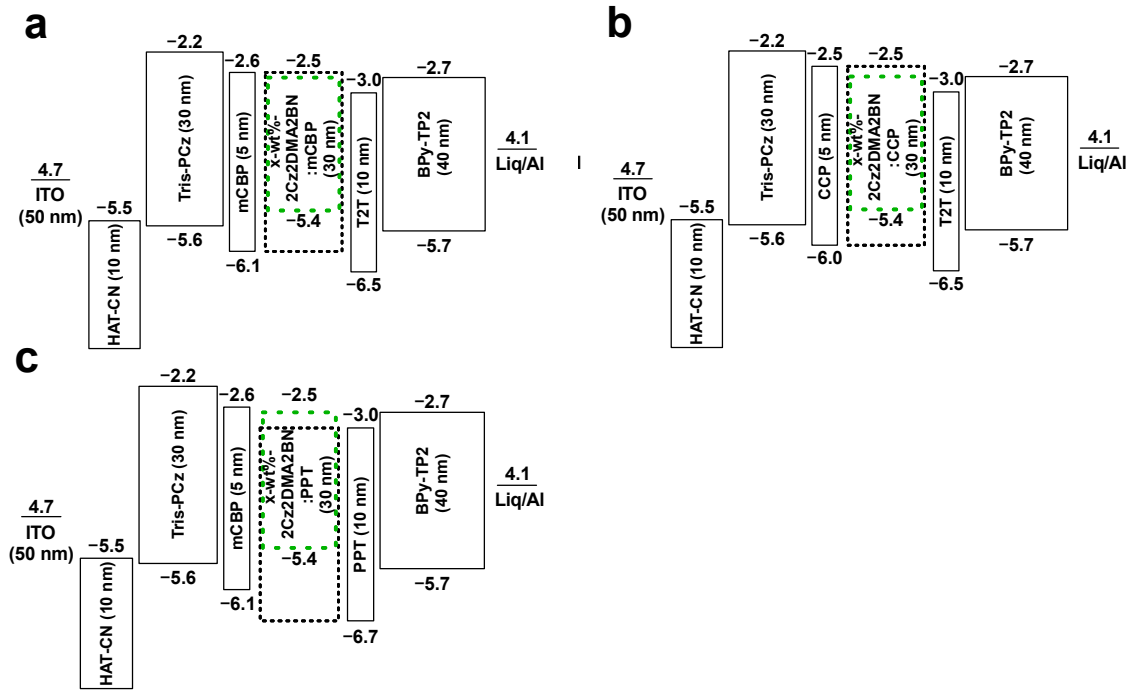

Figure 2.9: Energy diagram of the fabricated devices. (a) mCBP host. (b) CCP host. (c) PPT host.

The devices with mCBP and CCP hosts have the EBL of the neat layer of each host material and the HBL of T2T (2,4,6-tris(biphenyl-3-yl)-1,3,5-triazine). The devices with a PPT host have the EBL of mCBP and the HBL of PPT. The HOMO–LUMO energy levels of 2Cz2DMAC2BN were estimated to be −5.4 and −2.5 eV from the electrochemical measurements, where the redox processes were found to be stable (**Fig. 2.10**). The HOMO–LUMO

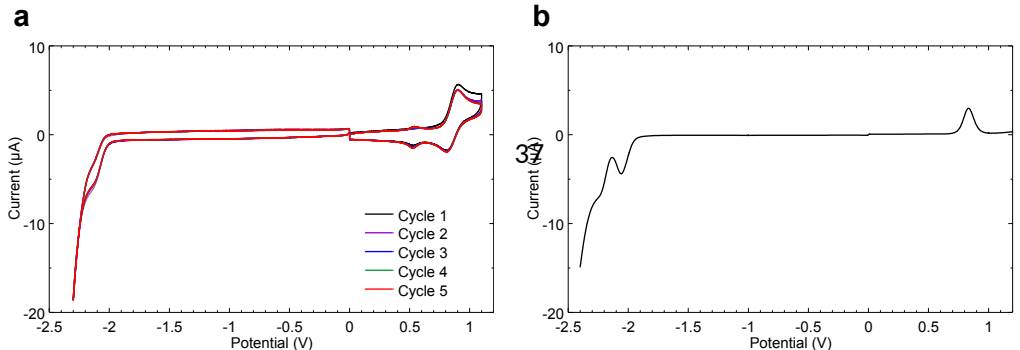

energies in the neat film measured by the photoelectron yield spectroscopy and optical energy gap were −5.75 and −3.15 eV.

Figure 2.10: Electrochemical measurements in dichloromethane. (a) Cyclic voltammograms (CV) (vs Ag/Ag^+). (b) Differential pulse voltammograms (DPV) (vs Ag/Ag^+).

The host materials of mCBP and CCP consisting of Ph and Cz rings are p-type while the PPT host with phosphine oxide is n-type. However, the charge carrier transport properties in the EML would be changed depending on the doping concentrations of 6, 15, and 50 wt% of bipolar 2Cz2DMAC2BN.

The 6 wt%-2Cz2DMAC2BN doped mCBP device showed a reasonably high EQE of 19%, although the efficiency rolloff is slightly large (**Fig. 2.11 and Table 2.4.**). The theoretical EQE is calculated to be 20% from the estimated 100% carrier balance and exciton utilization efficiency, experimental PLQY of 95%, and simulated outcoupling efficiency of 21%, which is consistent with the experimental result. The current density (*J*)-voltage (*V*) and rolloff characteristics were improved with the increase of the doping concentrations since the recombination zone shifted to the center by enhancing the electron transport in the EML as observed in the devices of 4CzIPN[17].

Although the PLQY values were nearly the same for 6–50 wt% doped mCBP films, the maximum EQE values were slightly decreased because of some quenching processes. The *J*–*V* characteristics of the devices using CCP hosts are independent of the doping concentrations (**Fig. 2.11**), indicating that the recombination always happened at the EML/HBL interface. This is due to the markedly higher hole mobility of CCP-host film as confirmed by hole-only and electron-only devices (HOD and EOD) (**Fig. 2.12**). However, the EQE characteristics for the CCP devices are strongly dependent on the doping concentrations. The 50 wt%-doped CCP device also suggested the existence of the exciton quenching in the high doping concentration, probably because the increase of the radical anion state of 2Cz2DMAC2BN

caused the annihilation. On the other hand, the electron transport in the guest 2Cz2DMAC2BN might be small in the devices using an n-type PPT host. Although the low doping concentration of 6 wt% showed a relatively large rolloff because of poor hole mobility, the 15 wt%-doped PPT device showed better rolloff characteristics and overall EQE than the p-type devices.

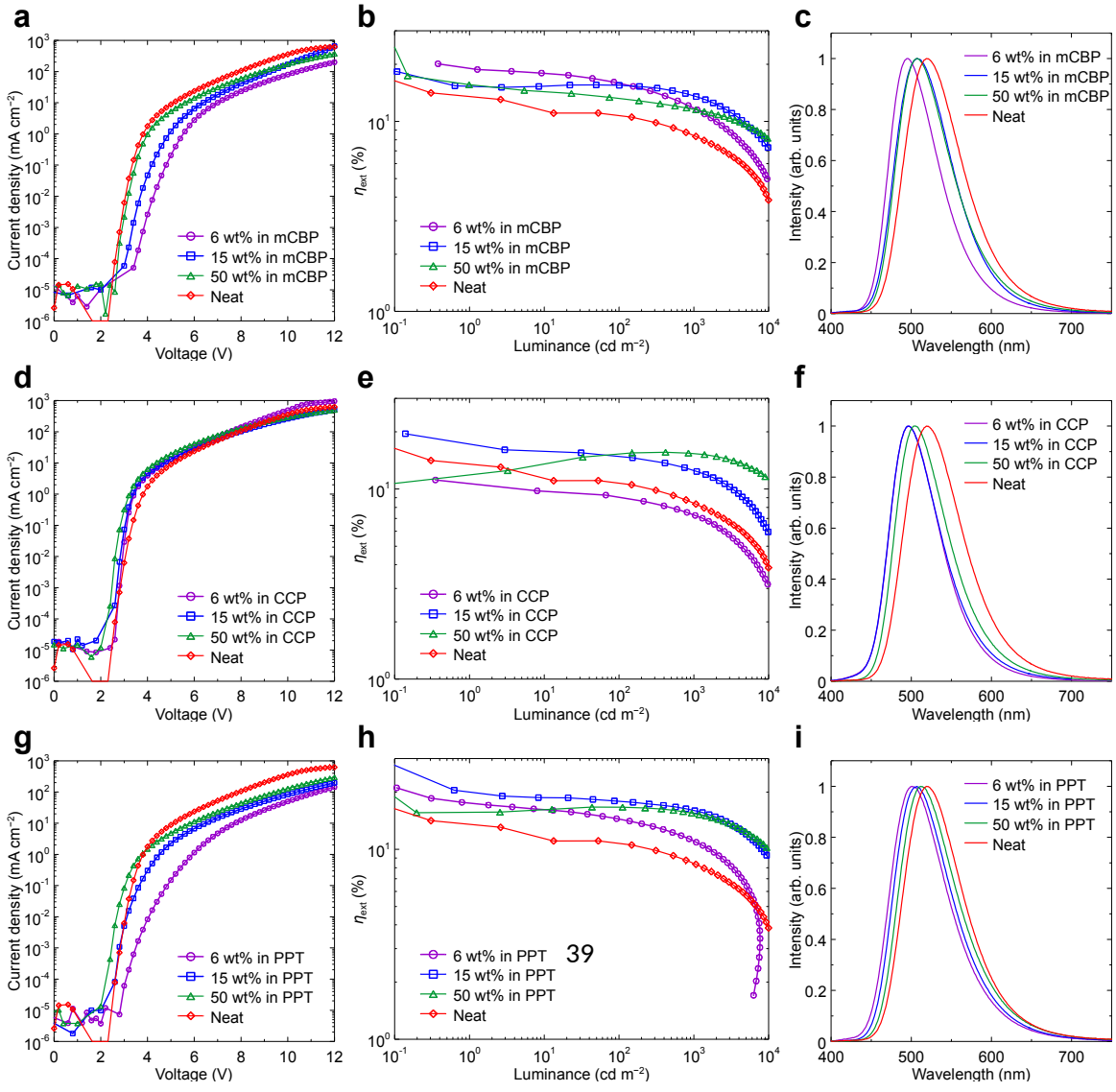

Figure 2.11: OLED performances for 2Cz2DMAC2BN-based devices. (a), (b), (c) The devices with mCBP host. (d), (e), (f) The devices with CCP host. (g), (h), (i) The devices with PPT host.

Host	Doping conc. [wt%]	Voltage [V][a)]	EQE [%][b)]	CE [cd A^{-1}][c)]	PE [lm W^{-1}][d)]	*L*max [cd m^{-2}][e)]	$\lambda_{EL}/\lambda_{FWHM}$ [nm][f)]
mCBP	6	4.0/5.1/6.0	19.0/15.9/11.7	38.5/29.0	38.4/14.6	12690	495/83
mCBP	15	3.5/4.4/5.4	15.5/15.5/13.5	46.1/39.5	32.9/22.9	19562	508/82
mCBP	50	3.0/3.7/4.6	15.6/13.2/11.5	44.8/33.7	46.9/23.0	20657	508/81
CCP	6	2.9/3.3/4.2	10.7/9.0/7.3	30.3/19.8	34.0/14.8	13340	497/72
CCP	15	2.7/3.1/3.8	17.3/14.8/12.4	44.2/32.8	49.6/27.1	15123	497/73
CCP	50	2.6/3.0/3.5	15.6/15.3/15.3	46.2/44.5	45.3/38.9	25641	505/77
PPT	6	3.7/5.2/6.8	17.5/14.4/11.0	53.2/29.1	52.3/13.4	7690	501/83
PPT	15	2.9/3.9/5.0	20.2/17.9/16.0	58.0/45.6	65.0/28.6	16108	506/82
PPT	50	2.5/3.2/4.3	16.7/16.7/15.5	51.3/47.4	50.4/35.5	20543	513/84
-	100 (Neat)	2.9/3.5/4.4	13.5/10.7/8.3	41.8/27.0	43.8/19.3	12302	520/85

Table 2.4. OLED performances of 2Cz2DMAC2BN-based devices.

[a)]Voltage at 1 (turn-on voltage, V_{on}), 100, and 1000 cd m^{-2}, respectively. [b)]EQE for maximum, and at 100, and 1000 cd m^{-2}, respectively. [c)]Current Efficiency for maximum, and at 1000 cd m^{-2}. [d)]Power Efficiency for maximum, and at 1000 cd m^{-2}. [e)]Maximum luminance. [f)]λ_{EL}: EL emission maximum, and λ_{FWHM}: full-width at half-maximum.

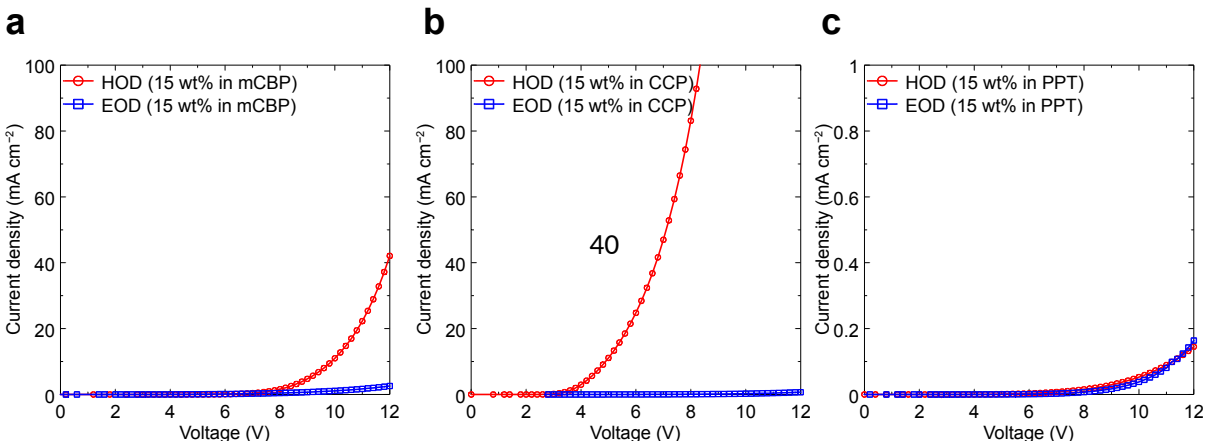

Figure 2.12: Current density-voltage characteristics for HODs and EODs. The devices with the EML of 15 wt%-2Cz2DMAC2BN-doped (a) mCBP, (b) CCP, and (c) PPT.

Interestingly, the device operational lifetime of the PPT device is better than those of mCBP and CCP devices (**Fig. 2.13**) even though the stabilities of phosphine oxide-based compounds are known to be much lower than carbazole-based compounds[30]. Thus, the stability for the radical anion of 2Cz2DMAC2BN might be dominant, which can be explained by the small bond dissociation energy of the C–N bond in the radical anion state[31].

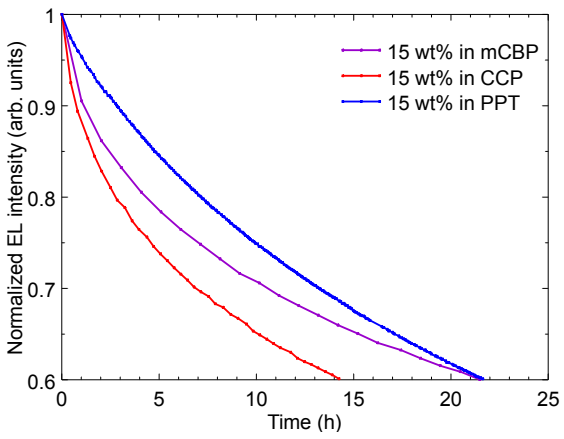

Figure 2.13: Luminance change versus operational time for 2Cz2DMAC2BN devices at an initial luminance of 100 cd m^{-2}.

To obtain a better understanding of the stability issues, we compared four different TADF materials, 2Cz2DMAC2BN, 4CzIPN[1], ACRXTN[32], and DACT-II[33], focusing on the types of donor structures (**Fig. 2.14**). Although 2Cz2DMAC2BN has two types of donors of Cz and DMAC, DMAC moieties provide the HOMO level of the molecule because of the stronger donor nature of DMAC compared to Cz moieties. Thus, the HOMO of 2Cz2DMAC2BN was shallower than that of 4CzIPN (ca. −5.4 eV vs. ca. −5.8 eV), although both molecules have four multiple donor units. ACRXTN having a single DMAC donor has a slightly deeper HOMO energy (ca. −5.7 eV) to 2Cz2DMAC2BN[34]. DACT-II can also have a single donor unit based on the Cz ring. However, the HOMO energy (−5.5 eV) is slightly

shallower owing to substituents of diphenyl amines at 3,6-positions of carbazole. The photophysical properties of these materials in the neat films are summarized in **Table 2.5.** These compounds showed green emission with similar S_1 energies. In addition, these materials also have similar τ_d values of 1–2 μs and k_{RISC} values of 8–10 × 10^5 s^{-1}, which is considered an important parameter related to the stability of TADF molecules. However, the excited state stabilities estimated from the PL intensity changes as a function of the irradiation time are largely different for these compounds.

The half-life times of the emission intensities are three times longer in 4CzIPN than 2Cz2DMAC2BN and DACT-II, and four times longer compared to ACRXTN. This result cannot be explained by only photophysical parameters such as HOMO–LUMO levels, PLQY, ΔE_{ST}, and k_{RISC} of the materials. Thus, we assume that the stability is strongly affected by the chemical structures of the compounds. Here, we classified two distinct features, that is, multiple donor-based D–A molecules (2Cz2DMAC2BN and 4CzIPN) vs. linearly linked single D–A molecules (ACRXTN and DACT-II), and donor structure types of DMAC-based (2Cz2DMAC2BN and ACRXTN) vs. Cz-based (4CzIPN and DACT-II) molecules. For the same class of donor units, the multiple donor-based D–A molecules showed better stabilities compared to the single linear D–A molecules. This is attributed to the crowded substituents with intramolecular π–π stacking. The photodegraded samples of carbazole derivatives showed products via dissociation of the C–N bond, e.g., carbazole and dicarbazole isophthalonitrile from 4CzIPN[35]. Thus, the delocalization and stabilization of the CT state in the excited state through the donor–donor interactions might suppress the dissociation of the donor units. This may also be related to the results that Cz-based TADF molecules showed better stability than DMAC-based ones. The larger dihedral angles between DMAC and Ph rings should not only weaken the bond strength but also localize the D–A in the CT. Note that the photostability for the doped films also showed a similar tendency (**Fig. 2.15 and Table 2.6.**).

I further compared the operational lifetime for the devices based on these four TADF emitters (**Fig. 2.14**), where the device structure was ITO (100 nm)/HAT-CN (10 nm)/Tris-PCz (30 nm)/mCBP (EBL) (5 nm)/15-wt%- emitters:mCBP (30 nm)/T2T (10 nm)/BPy-TP2 (40 nm)/Liq (2 nm)/Al (100 nm). Only 4CzIPN showed stable operation and the lifetime is several hundred times longer than those for other materials. Although the triplet formation is huge in the electrical excitation, the k_{RISC} of these materials are of the same order of

magnitude. Thus, the large difference with the excited state stability suggests that the dominant degradation path in the devices is related to the charged species. Although

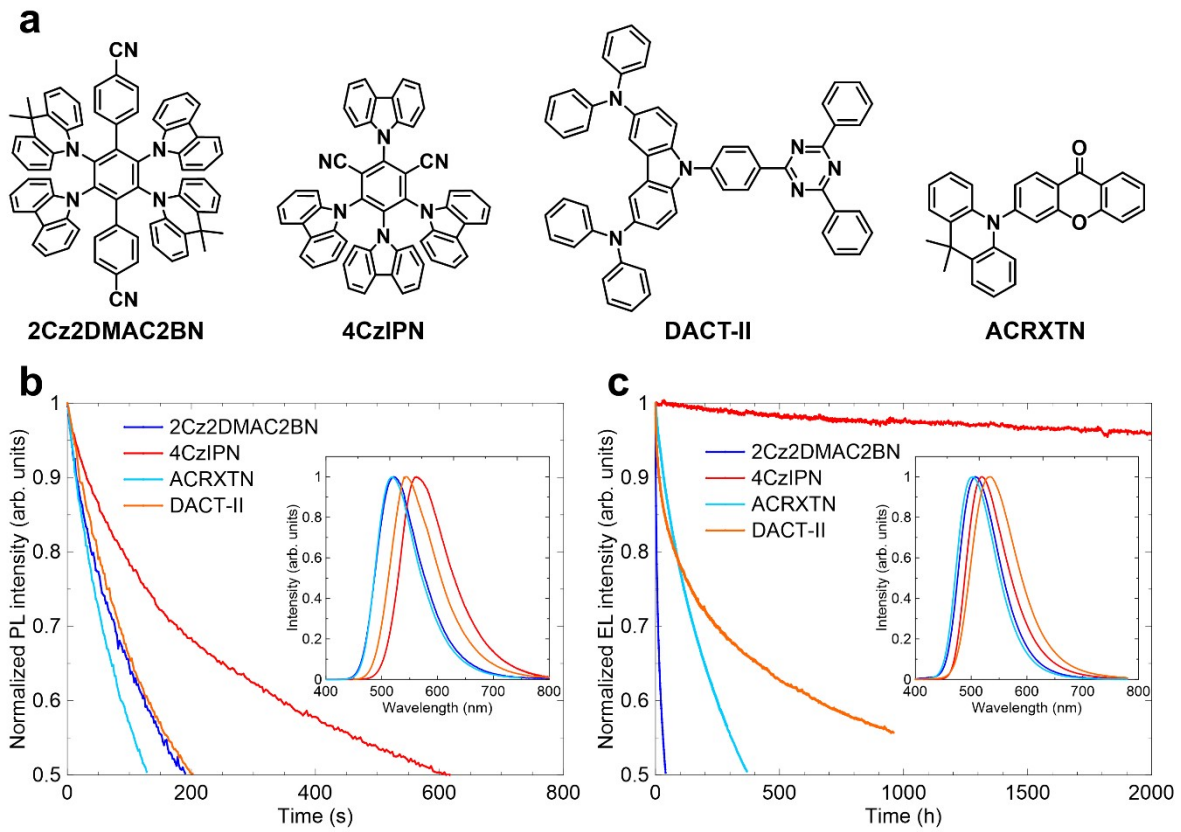

ACRXTN showed a slightly longer lifetime than 2Cz2DMAC2BN, DMAC moiety seems to essentially cause the lower stability. As mentioned above, the stability of the radical anion state might have a larger impact on the devices of 2Cz2DMAC2BN, and the C–N single bond is known to be vulnerable in the radical anion. Thus, the highly twisted C–N bond between DMAC and Ph rings by the steric hindrance might decrease the stability of 2Cz2DMAC2BN. In the blend films of TADF emitters and commonly used p-type hosts such as mCBP, TADF molecules play a key role in electron injection and transport[36]. Here, for realizing green emissions, 2Cz2DMAC2BN, ACRXTN, and DACT-II have relatively strong donors and weak acceptors, while 4CzIPN has relatively weak donors and strong acceptors. These differences indicate that 4CzIPN is advantageous to the balanced charge carrier injection and transport by taking into account the host properties. Thus, the choice of donor and acceptor units should primarily be important and carefully considered.

Figure 2.14: (a) Chemical structures of TADF materials under investigation. (b) Photostability of TADF materials in the neat films. PL intensity change versus excitation time irradiated by continuous-wave laser light at 355 nm (excitation power of 2.5 W cm^{-2}). Inset: PL spectra for the neat films. (c) Device operational stability for the OLED having EML of 15

wt%-TADF doped mCBP. Luminance change versus operational time at an initial luminance of 100 cd m^{-2}. Inset: EL spectra for the devices.

Table 2.5. Photophysical characteristics of the neat films of 2Cz2DAMC2BN, 4CzIPN, ACRXTN, and DACT-II.

Compound	λ_{PL} [nm]	S_1 [eV]	T_1 [eV]	ΔE_{ST} [eV]	Φ_{PL} [-][a)]	τ_p [ns][a)]	τ_d [μs][a)]	k_r [10^6 s^{-1}]	k_{ISC} [10^7 s^{-1}]	k_{RISC} [10^5 s^{-1}]	E_g^{opt} [eV]
2Cz2DMAC2BN	522	2.67	2.60	0.07	0.76	62	2.0	6.1	1.0	8.1	2.6
4CzIPN	563	2.45	2.40	0.05	0.43	22	1.3	11	3.5	8.1	2.4
ACRXTN	519	2.67	2.61	0.06	0.91	46	1.9	9.8	1.2	9.8	2.7
DACT-II	544	2.54	2.43	0.11	0.44	62	2.0	3.2	1.3	7.8	2.6

[a)]Measured under Ar

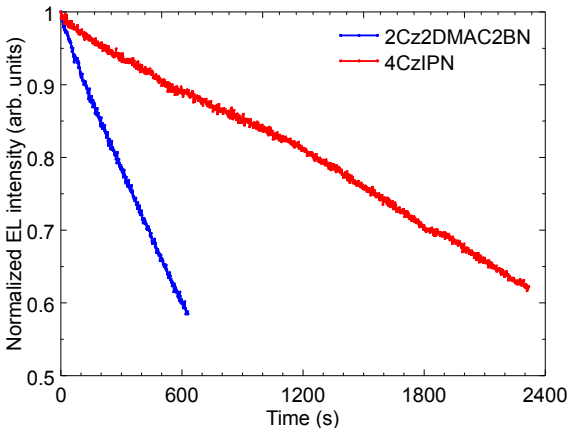

Figure 2.15: Photostability of TADF materials in the doped films for 2Cz2DMAC2BN and 4CzIPN. PL intensity change versus excitation time irradiated by continuous-wave laser light at 355 nm (excitation power of 2.7 W cm^{-2}).

Compound	λ_{PL} [nm]	S_1 [eV]	T_1 [eV]	ΔE_{ST} [eV]	Φ_{PL} [-][a)]	Φ_p/Φ_d [-][a)]	τ_p [ns][a)]	τ_d [μs][a)]	k_r [10^6 s^{-1}]	k_{ISC} [10^7 s^{-1}]	k_{RISC} [10^5 s^{-1}]
2Cz2DMAC2BN	498	2.76	2.71	0.05	0.95	0.28/0.67	34	3.6	8.2	2.1	9.4
4CzIPN	520	2.70	2.67	0.03	0.93	0.23/0.70	18	2.6	12.9	4.3	14.9

Table 2.6. Photophysical characteristics of the 6 wt%-doped films of 2Cz2DAMC2BN and 4CzIPN in mCBP.

[a)]Measured under Ar

According to the previous results, the device stability of the 2Cz2DMAC2BN emitter is poorer than its photostability. To confirm the real reason behind the low device stability. The photostability of the HOD device and the EOD devices is measured under constant current, UV irradiation, and both UV irradiation and constant current[37,38]. Here, the devices are fabricated with mCBP host and the doping concentration is 15 wt%. In both devices, the PL intensity of the doped films did not change before or after the current application. So, there is no degradation under constant current conditions. In the HOD device, the photodegradation rate under UV irradiation and applying both UV and current is the same (**Fig. 2.16 a)**. However, in the EOD device, the degradation rate in these conditions is not the same, and when applying both current and UV irradiation, the photodegradation rate increases (**Fig. 2.16 b**). Thus, it is clear that the degradation rate increased with the electron current.

The photostability of 2Cz2DMAC2BN is not unstable. However, according to the OLED results, the device stability of 2Cz2DMAC2BN is very low. Generally, Cz moiety is known to be stable, and the C-N bond might be weak because several papers pointed out the bond dissociation of C-N[34]. However, the chemical stability of the CN group would not be too low, since 4CzIPN also has C-N groups. According to the DFT calculations, since DMAC has a highly twisted angle, the low stability may attributed to the DMAC.

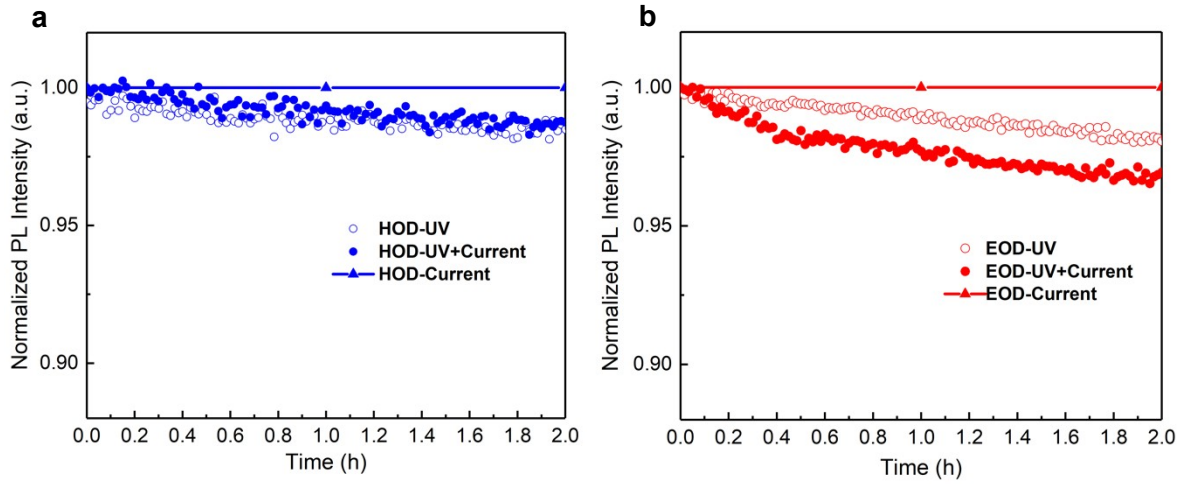

Figure 2.16: a) Photostability of TADF molecules in hole-only and (b) electron-only devices. The structures of the hole- and electron-only devices are ITO/HATCN (10 nm)/Tris-PCz (30 nm)/mCBP (5 nm)/2Cz2DMAC2BN: mCBP (30 nm, 15 wt%)/Tris-PCz (50 nm)/Al (100 nm) and ITO/ T2T (45 nm)/2Cz2DMAC2BN: mCBP (30 nm, 15 wt%)/T2T (10 nm)/ BPy-TP2 (40 nm)/Liq (2 nm)/ Al (100 nm), respectively. The devices applied with (1) 21.5 mW cm^{-2} illumination (404 nm); (2) a constant current density of 0.75 mA cm −2 ; (3) both 21.5 mW cm^{-2} illumination(404 nm) and 0.75 mA cm^{-2} current.

2.4. Conclusion

A multiple D–A type TADF compound was developed using hetero donors of Cz and DMAC moieties. The fundamental TADF properties were comparable to those of excellent green emitters such as 4CzIPN. In addition, high PLQY can be maintained in the polar solvents and films with high doping concentrations. The OLED performances were optimized by changing the doping concentrations of the emitters, demonstrating the reasonable EQE. The main motivation of the work was to offer a better understanding of the structure-stability relationship. Thus, we compared the stabilities of four different types of TADF materials. The multiple D–A type design seems to be valuable for increasing excited state stability. However, the device's operational stability is more complicated, and the polaron-related degradation might have a larger impact on the OLED durability. Since the carrier injection and transport properties in the EML are affected by TADF molecules even though their main function is to control the excitonic process, careful consideration of each donor-acceptor strength in the TADF molecule is necessary.

2.5. References

1. Uoyama, H., Goushi, K., Shizu, K., Nomura, H. & Adachi, C. Highly efficient organic light-emitting diodes from delayed fluorescence. *Nature* **492**, 234 (2012).
2. Hong, G., Gan, X., Leonhardt, C., Zhang, Z., Seibert, J., Busch, J. M. & Bräse,S. Brief history of OLEDs–Emitter development and industry milestones. *Adv. Mater.* **33**, 2005630 (2021).
3. Im, Y., Kim, M., Cho, Y. J., Seo, J. -A., Yook, K. S. & Lee. J. Y. Molecular design strategy of organic thermally activated delayed fluorescence emitters. *Chem. Mater.* **29**, 1946–1963 (2017).
4. Liu, Y., Li, C., Ren, Z., Yan, S. & Bryce, M. R. All-organic thermally activated delayed fluorescence materials for organic light-emitting diodes. *Nat. Rev. Mater.* **3**, 18020 (2018).
5. Imahori, H., Kobori, Y. & Kaji, H. Manipulation of charge transfer states by molecular design: Perspective from “dynamic exciton”. *Acc. Mater. Res.* **2**, 501–514 (2021).
6. Park, I. S., Matsuo, K., Aizawa, N. & Yasuda, T. High-performance Dibenzoheteraborin-based thermally activated delayed fluorescence emitters: Molecular architectonics for concurrently achieving narrowband emission and efficient triplet–singlet spin conversion. *Adv. Funct. Mater.* **28**, 1802031 (2018).

7. Liu, J. Li, Z., Hu, T., Wei, X., Wang, R., Hu, X., Liu, Y., Yi, Y., Takamura, Y. Y., Wang, Y. & Wang. P. Experimental evidence for “hot exciton” thermally activated delayed fluorescence emitters. *Adv. Opt. Mater.* **7**, 1801190 (2018).
8. Matsuo, K. & Yasuda, T. Boronate- and borinate-based π-systems for blue thermally activated delayed fluorescence materials. *Chem. Commun.* **55**, 2501–2504 (2019).
9. Wang, X., Wang, S., Lv, J., Shao, S., Wang, L., Jinga X. & Wang F. Through-space charge transfer hexaarylbenzene dendrimers with thermally activated delayed fluorescence and aggregation-induced emission for efficient solution-processed OLEDs. *Chem. Sci.* **10**, 2915–2923 (2019).
10. Wada, Y., Nakagawa, H., Matsumoto, S., Wakisaka, Y. & Kaji, H. Organic light emitters exhibiting very fast reverse intersystem crossing. *Nat. Photon.* **14**, 643–649 (2020).
11. Aizawa, N., Matsumoto, A. & Yasuda, T. Thermal equilibration between singlet and triplet excited states in organic fluorophore for submicrosecond delayed fluorescence. *Sci. Adv.* **7**, eabe5769 (2021).
12. Cui, L. -S., Gillett, A. J., Zhang, S. -F., Ye, H., Liu, Y., Chen, X. -K., Lin, Z. -S., Evans, E. W., Myers, W. K., Ronson, T. K., Nakanotani, H., Reineke, S., Bredas, J. -L., Adachi C. & Friend R. H. Fast spin-flip enables efficient and stable organic electroluminescence from charge-transfer states. *Nat. Photon.* **14**, 636 (2020).
13. Kim, J. U., Park, I. S., Chan, C. -Y., Tanaka, M., Tsuchiya, Y., Nakanotani H. & Adachi. C. Nanosecond-time-scale delayed fluorescence molecule for deep-blue OLEDs with small efficiency rolloff. *Nat. Commun.* **11**, 1765 (2020).
14. Ren, Y., Wada, Y., Suzuki, K., Kusakabe, Y., Geldsetzer J. & Kaji. H. Efficient blue thermally activated delayed fluorescence emitters showing very fast reverse intersystem crossing. *Appl. Phys. Express* **14**, 071003 (2021).
15. Hasan, M. Shukla, A., Ahmad, V., Sobus, J., Bencheikh, F., McGregor, S. K. M., Mamada, M., Adachi, C., Lo, S. -C. & Namdas. E. B. Exciton–exciton annihilation in thermally activated delayed fluorescence emitter. *Adv. Funct. Mater.* **30**, 2000580 (2020).
16. Hasan, M. Shukla, A., Mamada, M., Adachi, C., Lo, S, -C. & Namdas. E. B. Correlating exciton dynamics of thermally activated delayed-fluorescence emitters to efficiency roll-off in OLEDs. *Phys. Rev. Appl.* **18**, 054082 (2022).

17. Nakanotani, H., Masui, K., Nishide, J., Shibata, T. & Adachi, C. Promising operational stability of high-efficiency organic light-emitting diodes based on thermally activated delayed fluorescence. *Sci. Rep.* **3**, 2127 (2013).
18. Hosokai, T., Matsuzaki, H., Nakanotani, H., Tokumaru, K., Tsutsui, T., Furube, A., Nasu, K., Nomura, H., Yahiro, M. & Aadachi, C. Evidence and mechanism of efficient thermally activated delayed fluorescence promoted by delocalized excited states. *Sci. Adv.* **3**, e1603282 (2017).
19. Noda, H., Nakanotani, H. & Adachi, C. Excited state engineering for efficient reverse intersystem crossing. *Sci. Adv.* **4**, eaao6910 (2018).
20. Chan, C.-Y. Tanaka, M., Lee, Y. -T., Wong, Y. -W., Nakanotani, H., Hatakeyama T. & Adachi C. Stable pure-blue hyperfluorescence organic light-emitting diodes with high-efficiency and narrow emission. *Nat. Photon.* **15**, 203 (2021).
21. Cho, Y. J., Yook, K. S. & Lee, J. Y. High efficiency in a solution-processed thermally activated delayed-fluorescence device using a delayed-fluorescence emitting material with improved solubility. *Adv. Mater.* **26**, 6642–6646 (2014).
22. Zou, Y., Gong, S., Xie, G. & Yang, C. Design strategy for solution-processable thermally activated delayed fluorescence emitters and their applications in organic light-emitting diodes. *Adv. Opt. Mater.* **6**, 1800568 (2018).
23. Zhang, D., Song, X., Gillett, A. J., Drummond, B. H., Jones, S. T. E., Li, G., He, H., Cai, M., Credgington, D. & Duan. L. Efficient and stable deep-blue fluorescent organic light-emitting diodes employing a sensitizer with fast triplet upconversion. *Adv. Mater.* **32**, 1908355 (2020).
24. Yin, C., Zhang, D. & Duan, L. A perspective on blue TADF materials based on carbazole-benzonitrile derivatives for efficient and stable OLEDs. *Appl. Phys. Lett.* **116**, 120503 (2020).
25. Mamada, M., Katagiri, H., Chan, C. -Y., Lee, Y. -T., Goushi, K., Nakanotani, H., Hatakeyama, T. & Adachi C. Highly efficient deep-blue organic light-emitting diodes based on rational molecular design and device engineering. *Adv. Funct. Mater.* **32**, 2204352 (2022).
26. Wada, Y., Shizu, K. & Kaji, H. Molecular vibration accelerates charge transfer emission in a highly twisted blue thermally activated delayed fluorescence material. *J. Phys. Chem. A* **125**, 4534–4539 (2021).

27. Kim, Y.-H., Wolf, C., Cho, H., Jeong, S.-H. & Lee, T.-W. Highly Efficient, Simplified, Solution-Processed ThermallyActivated Delayed-Fluorescence Organic Light-Emitting Diodes. *Adv. Mater.* **28**, 736 (2016).

28. Lee, Y. H., Shin, Y.-S., Lee, T., Jung, J., Lee, J. -H. & Lee M. H. Managing local triplet excited states of boron-based TADF emitters for fast spin-flip process: Toward highly efficient TADF-OLEDs with low efficiency roll-off. *Chem. Eng. J.* **423**, 130224 (2021).

29. Li, N., Ni, F., Lv, X., Huang, Z., Cao, X., & Yang C. Host-dopant interaction between organic thermally activated delayed fluorescence emitter and host material: Insight into the excited state. *Adv. Opt. Mater.* **10**, 2101343 (2022).

30. Ihn, S.-G., Jeong, D., Kwon, E. S., Kim, S., Chung, Y. S., Sim, M., Chwae, J., Koishikawa, Y., Jeon, S. O., Kim, J. S., Kim, J., Nam, S., Kim, I., Park, S., Kim, D. S., Choi, H. Kim, S. Dipole moment- and molecular orbital-engineered phosphine oxide-free host materials for efficient and stable blue thermally activated delayed fluorescence. *Adv. Sci.* **9**, 2102141 (2022).

31. Lin, N., Qiao, J., Duan, L., Wang, L. & Qiu, Y. Molecular understanding of the chemical stability of organic materials for OLEDs: A comparative study on sulfonyl, phosphine-oxide, and carbonyl-containing host materials. *J. Phys. Chem. C* **118**, 7569–7578 (2014).

32. Nakanotani, H., Higuchi, T., Furukawa, T., Masui, K., Morimoto, K., Numata, M., Tanaka, H., Sagara, Y., Yasuda, T. & Adachi, C. High-efficiency organic light-emitting diodes with fluorescent emitters. *Nat. Commun.* **5**, 4016 (2014).

33. Kaji, H., Suzuki, H., Fukushima, T., Shizu, K., Suzuki, K., Kubo, S., Komino, T., Oiwa, H., Suzuki, F., Wakamiya, A., Murata Y. & Adachi C. Purely organic electroluminescent material realizing 100% conversion from electricity to light. *Nat. Commun.* **6**, 8476 (2015).

34. Ahmad, V., Sobus, J., Bencheikh, F., Mamada, M., Adachi, C., Lo, S. -C. & Namdas E. B. High EQE and high brightness solution-processed TADF light-emitting transistors and OLEDs. *Adv. Opt. Mater.* **8**, 2000554 (2020).

35. Sandanayaka, A. S. D., Matsushima, T. & Adachi, C. Degradation mechanisms of organic light-emitting diodes based on thermally activated delayed fluorescence molecules. *J. Phys. Chem.* C **119**, 23845 (2015).

36. Mamada, M. & Adachi, C. Unexpected role of hole and electron blocking interlayers controlling charge carrier injection and transport in TADF based blue organic light-emitting diodes. *Appl. Phys. Lett.* **121**, 131103 (2022).

37. Cui, L. -S., Deng, Y. -L., Tsang, D. P. -K., Jiang, Z. -Q., Zhang, Q., Liao, L. -S. & Adachi, C. Controlling Synergistic Oxidation Processes for Efficient and Stable Blue Thermally Activated Delayed Fluorescence Devices. *Adv. Mater.* **28,** 7620–7625 (2016).

38. Tanaka, M., Noda, H., Nakanotani, H. & Adachi, C. Effect of Carrier Balance on Device Degradation of Organic Light-Emitting Diodes Based on Thermally Activated Delayed Fluorescence Emitters. *Adv. Electron. Mater.* **5**, 1800708 (2019).

CHAPTER III. Hexacarbazolylbenzene: An excellent host molecule causing strong guest molecular orientation and the high-performance OLEDs

3.1. Introduction

The event of charge recombination in the EML, followed by singlet and triplet exciton generations, required multifunction materials, resulting in the great importance of the host materials having good charge carrier transport, exciton confinement, and annihilation alleviation[1,2,3,4,5]. In particular, triplet management to maximize the internal quantum efficiency (η_{int}) up to 100% via phosphorescence or TADF emitters demands the host materials with sufficiently high triplet energy. Therefore, the π-conjugation of the host materials needs to be restricted to keep high energies, while their molecular size and rigidity ought to be high for better thermal stability. In addition, it is essential to consider the HOMO and the LUMO levels to ease carrier injection, while minimizing undesirable situations such as exciplex formation with emitters[6,7,8,9].

Carbazole derivatives are frequently used as the host material because of facile preparation and modification of chemical structures, efficient hole transporting ability, relatively deep HOMO level, and high energy levels of both the singlet and triplet excited states (S_1 and T_1). In particular, 4,4'-bis(9-carbazolyl)-biphenyl (CBP) has a long history of green and red OLEDs[10,11,12,13,14]. Since the T_1 of CBP is relatively low (2.6 eV) caused by *para*-linked conjugation, *meta*-linked carbazole derivatives such as 3,5-bis(9-carbazolyl)benzene (mCP) and 3,3'-bis(9-carbazolyl)-biphenyl (mCBP) showing higher T_1 energies (~2.9 eV for mCP and 2.8 eV for mCBP) were often used in blue OLEDs[15,16,17,18,19]. The severe problem of mCP is poor morphological stability because of the low glass transition temperature (T_g = 60 °C). Although there are a lot of CBP analogs based on the different strategies for reducing conjugation, those compounds are not very useful because of low operational stabilities[20,21,22,23,24,25]. Thus, the traditional compound such as mCBP still has been the best choice. Under these circumstances, a simple compound with high energies and stabilities has a high potential to be widely used as the standard host material. Ideally, further advantages derived from new hosts are highly desired.

Herein, I demonstrate the attractive features of hexacarbazolylbenzene (6CzPh, **Scheme 3-1.**) as a host material. The material preparation is in a facile one-step reaction and possible on the gram scale. Because of the sterically twisted and crowded carbazoles, both S_1 and T_1 energies are high enough, whereas a relatively small energy gap facilitates the charge injections. In addition, this structural aspect reduces host aggregation, resulting in high-

quality amorphous film. Moreover, the large molecular weight leads to high morphological stability of the films. The devices using common TADF material, 4CzIPN, showed high efficiencies with a small rolloff in efficiencies[26]. Since the hole transport property of 6CzPh is much higher than its electron transport, causing charge recombination at the interface of the EML/hole blocking layer (HBL), I also introduced the mixed host with an electron-transporting material, validating good durability in the devices. Finally, the high efficiencies for 4CzIPN devices could be rationalized by the completely horizontal dipole orientation of the emitter despite the difficulty of realizing a high degree of horizontal molecular orientation except for linear shape molecules. Thus, this achievement is a significant milestone for the future development of OLEDs. Importantly, 6CzPh improved the horizontal orientation of several emitters including phosphorescence and MR materials.

3.2. Results and Discussion

3.2.1. Synthesis of 6CzPh

To a dispersion of sodium hydride (60% in mineral oil) (0.88 g, 22.0 mmol) in dry DMF (20 ml) was added carbazole (3.52 g, 21.0 mmol) in dry DMF (10 ml) at 0 °C under Ar. After stirring for 30 minutes, hexafluorobenzene (0.55 g, 3.0 mmol) in dry DMF (20 ml) was added. After stirring for 30 min, the reaction mixture was stirred for 12 h at 80 °C. After cooling, H_2O was added and the precipitates were filtered, and washed with H_2O and methanol. The crude product (3.50 g) was purified by sublimation at 400 °C under vacuum (~10^{-2} Pa) to give an almost pure product as a colorless solid (2.50 g, 78.9%). Note that the impurity of 1,2,4,5-tetra(*N*-carbazolyl)-3,6-difluorobenzene, which was sublimed at ~320 °C and showed sky blue emission in the solid state, partially overlapped with the target product showing deep blue emission. Thus, the sublimed compounds were triturated and washed with hot chloroform, and the sublimation was repeated until fluorine was not detected in the NMR for the whole area of the sublimed solid (**Fig. 3.1**). Because of the crystallization after the first sublimation, the sublimation temperature might be different in the second run.

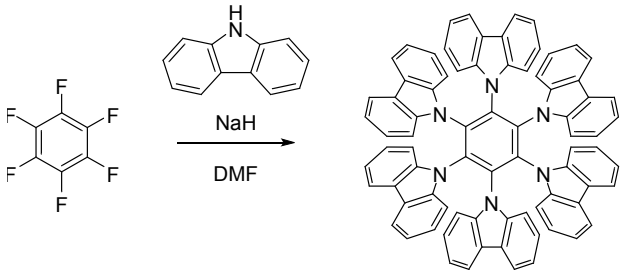

Scheme 3-1: Synthetic route to **6CzPh:** Compound **6CzPh** (1,2,3,4,5,6-hexa(9*H*-carbazol-9-yl)benzene).

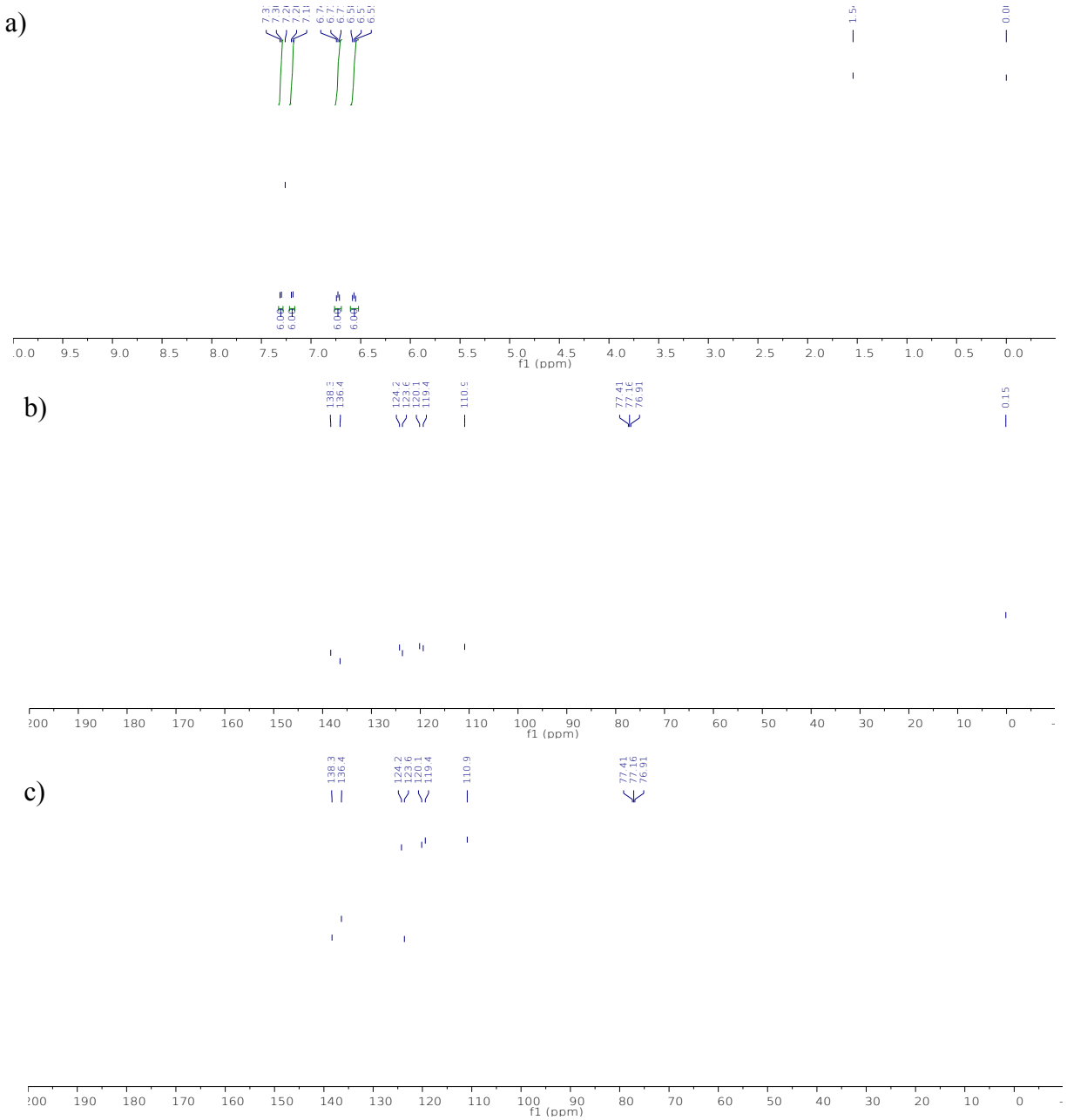

Figure 3.1: NMR spectra of 6CzPh compound. a) ^{1}H-NMR spectrum (500 MHz, $CDCl_3$, 300 K), b) ^{13}C-NMR spectra (125 MHz, $CDCl_3$, 300 K), and ^{13}C-NMR-APT spectra (125 MHz, $CDCl_3$, 300 K)

Although there is literature on the preparation of 6CzPh, the properties of the compound have not been investigated[27]. In addition, the reported synthesis procedure did not include the purification. Indeed, the purification of 6CzPh was necessary and found to be crucial aimed at OLED application. Although we used the excess amount of carbazole for the nucleophilic aromatic substitution, byproducts with unreacted fluorine atoms were detected. Note that both precursor materials are commercially available in large volumes at low cost, and the purification is possible on scalable vacuum sublimation; therefore, 6CzPh is potentially a practical material.

The melting point could not be observed in the standard apparatus. The thermogravimetry-differential thermal analysis (TG-DTA) measurement also did not show endothermic transitions until starting decomposition at 527 °C (**Fig. 3.2**). The single crystals were obtained by vacuum sublimation, which has a columnar structure with a relatively large void of Kitaigorodskii packing index (KPI) = 66.1% (**Fig. 3.3**). Thus, the neat film becomes amorphous to reduce the void, confirmed by the small anisotropy of the dipole orientation and well-fitted experimental data with the model in the variable angle spectroscopic ellipsometry measurements (**Fig. 3.4 and Table 3.1)**

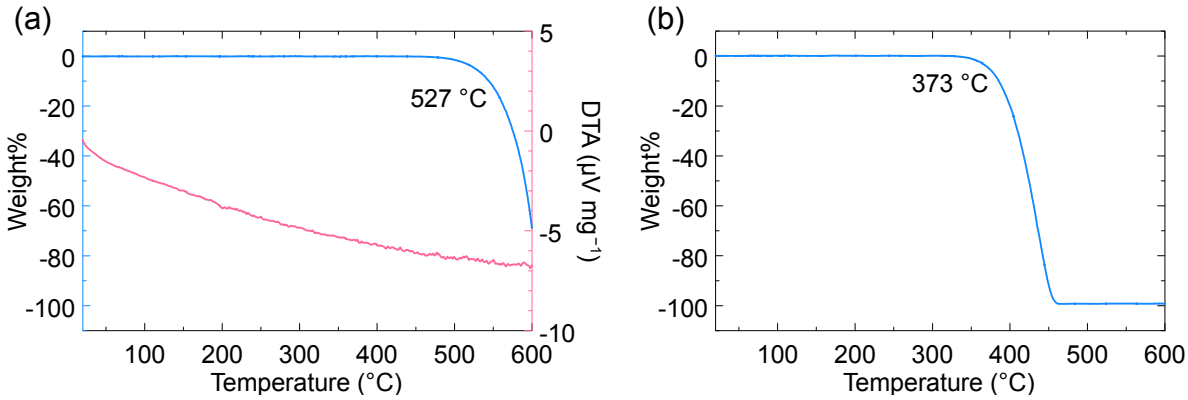

Figure 3.2: a) TG-DTA at 1 atm and b) TG at 1 Pa for 6CzPh.

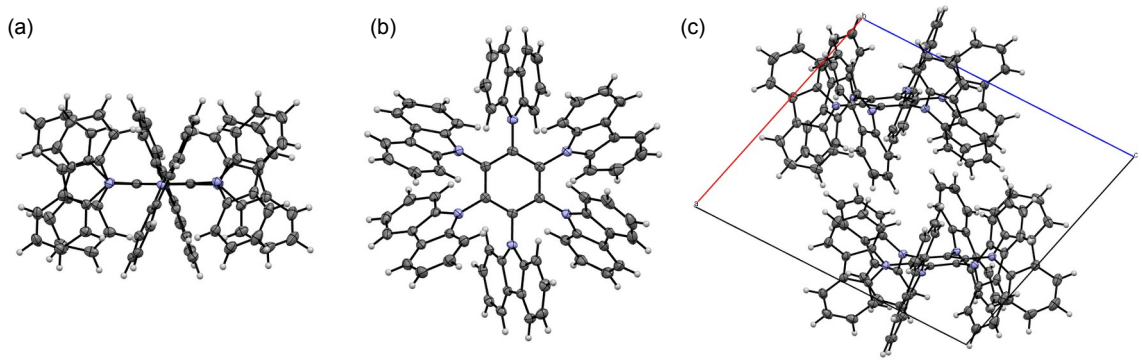

Figure 3.3: Crystal structure in the asymmetric unit, showing 50% probability displacement ellipsoids for 6CzPh. a) side view, b) top view, and c) packing arrangement along with the *b*-axis.

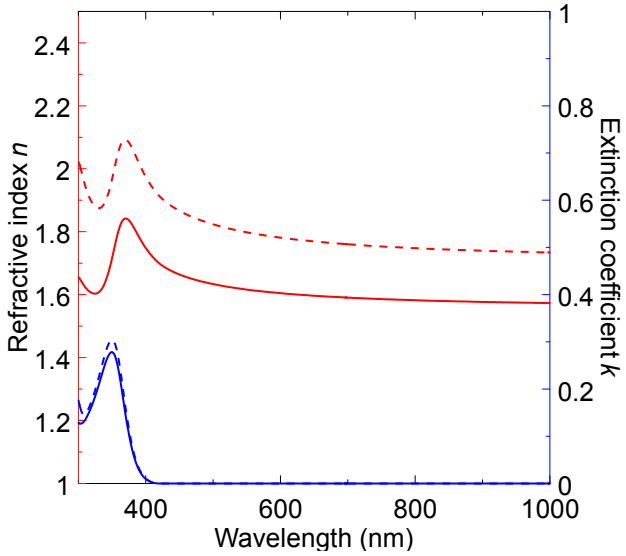

Figure 3.4: Variable angle spectroscopic ellipsometry measurements of neat-films of vacuum-deposited 6CzPh. Ordinary (solid lines) and extraordinary (dashed lines) refractive indices (red) and extinction coefficients (blue) are obtained from an analysis using homogeneous anisotropic optical constants of the films.

Table 3.1. Ordinary and extraordinary refractive indices and orientation order parameters of 6CzPh vacuum deposited neat films on Si substrates.

Sample	Ordinary refractive index n_o [a)]	Extraordinary refractive index n_e [a)]	Birefringence $\Delta n = n_o - n_e$	Orientation order parameter S [b)]
6CzPh	1.62	1.80	−0.18	0.03

[a)]At 550 nm. [b)]$S = (3\cos^2\theta - 1)/2 = (k_e - k_o)/(k_e + 2k_o)$, where k_o and k_e are the ordinary and extraordinary extinction coefficients at the peak wavelength.

The physical properties of 6CzPh were first investigated by the DFT calculations with references to common hosts of mCBP and mCP (**Fig. 3.5**). These materials showed relatively similar HOMO energies, while the LUMO is different. Compared to fragment moieties, biphenyl has nearly the same LUMO energies as carbazole, whereas benzene has a much shallower LUMO energy. Thus, the LUMO distributions are dominantly located on the center biphenyl unit with electron-withdrawing nitrogen atoms in mCBP and spread over the whole molecule in mCP. On the other hand, 6CzPh showed the LUMO distribution at the center benzene ring because of multiple substitutions of electron-withdrawing nitrogen atoms in the inductive effect. These results indicated the smaller energy gaps for 6CzPh compared to mCBP and mCP.

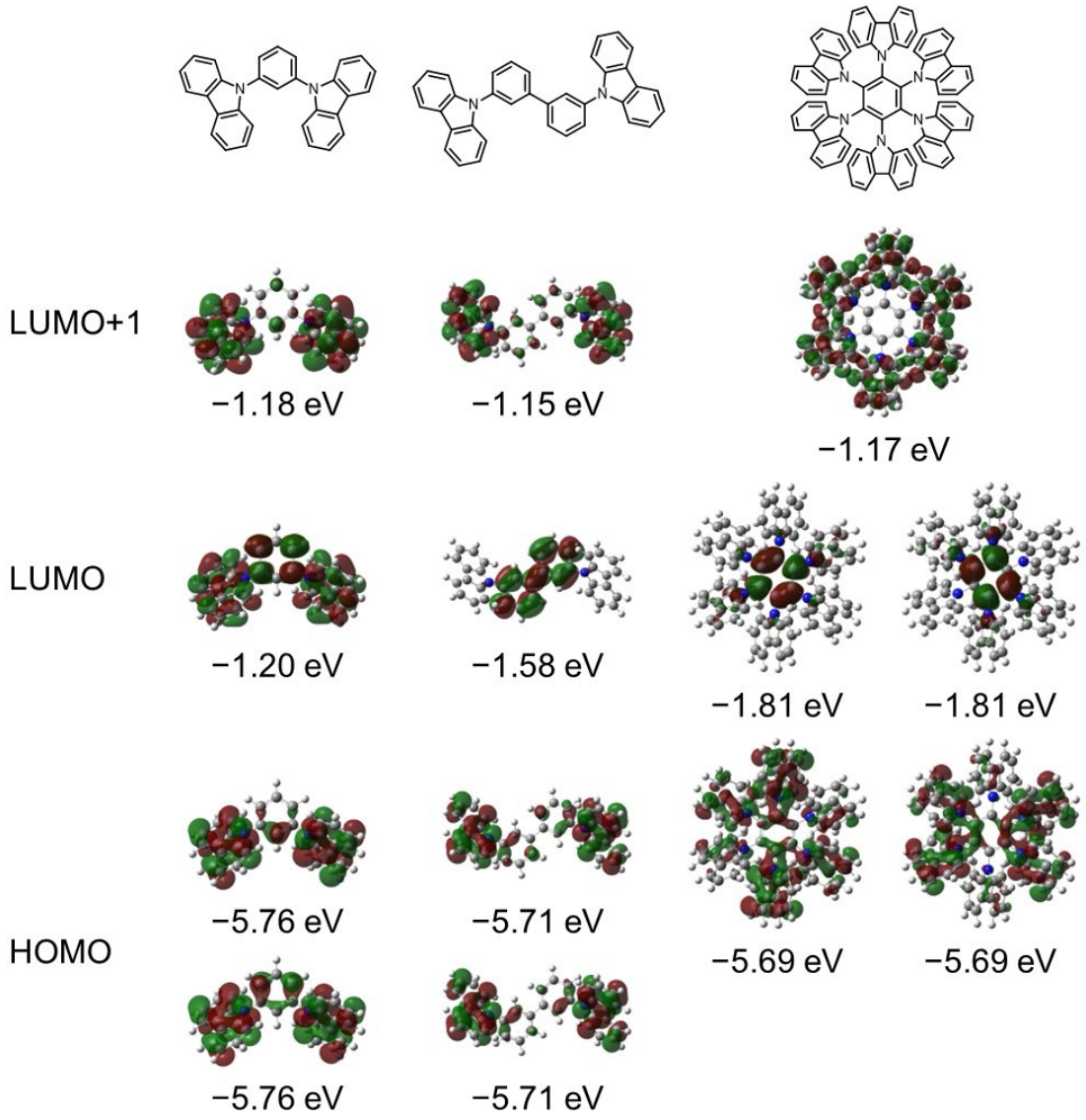

Figure 3.5: Molecular orbitals of 6CzPh and related molecules.

Indeed, the experimental results of 6CzPh appeared distinct from those of the other compounds. The absorption and PL spectra are shown in **Fig. 3.6** and summarized in **Table**

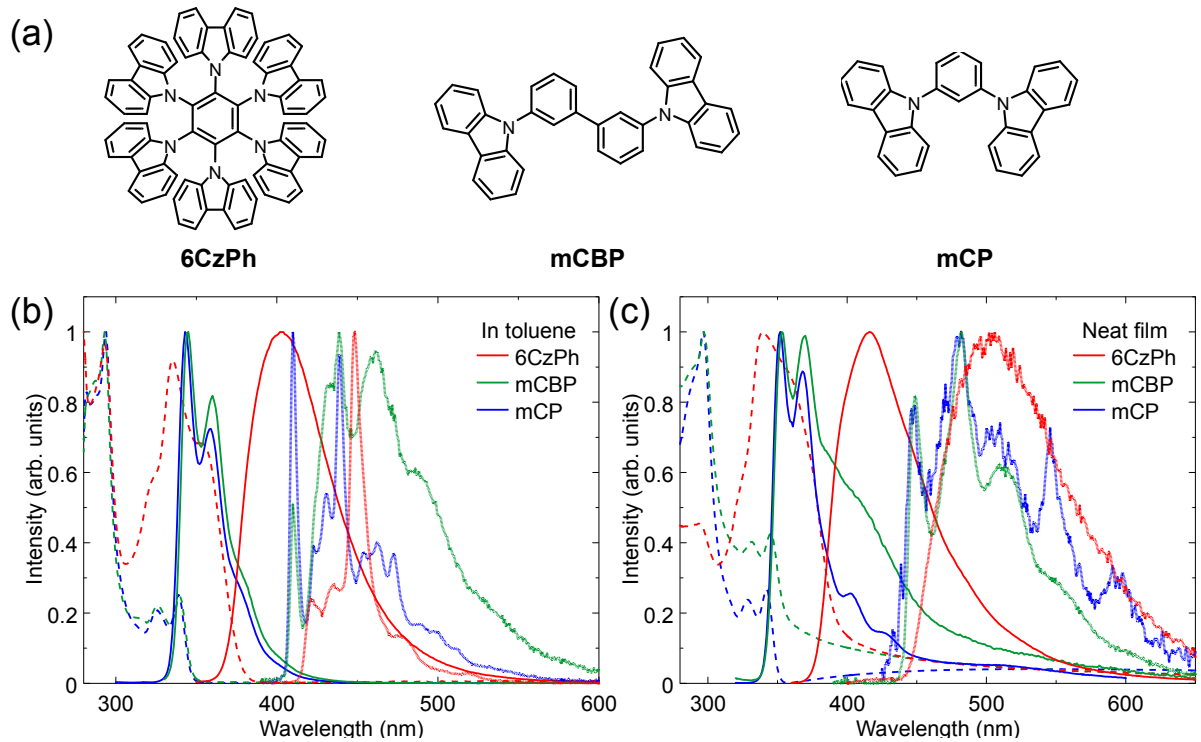

3.2-3.3. The onsets of the spectra for mCP and mCBP are nearly the same (**Fig. 3.6 b**), which is mainly assigned to the local excited states of the carbazole moiety. On the other hand, 6CzPh showed clear bathochromic shifts of absorption and PL spectra. The fluorescence spectrum is relatively broad and structureless, although the phosphorescence exhibited vibronic structures.

Figure 3.6: a) Chemical structures of 6CzPh, mCBP, and mCP. Absorption (dashed lines), fluorescence (solid lines), and phosphorescence (dotted lines) spectra for 6CzPh, mCBP, and mCP b) in toluene and c) in neat films.

Table 3.2 Photophysical characteristics for the host materials in solution.

Compound	Solvent	λ_{abs} [nm]	E_g^{opt} [eV]	λ_{PL} [nm]	S_1 [eV]	T_1 [eV]	ΔE_{ST} [eV]	Φ_{air} [-][a)]	Φ_{N2} [-][b)]	τ [ns][b)]
mCP	Toluene	294, 326, 339	3.57	343, 359	3.70	3.05	0.65	-	-	-
mCBP	Toluene	293, 326, 340	3.56	345, 360	3.69	3.05	0.64	-	-	-
6CzPh	Toluene	293, 335, 352	3.29	402	3.37	2.99	0.38	0.12	0.16	2.8
6CzPh	Chloroform	293, 336, 352	3.29	414	3.35	3.05	0.30	0.10	0.11	3.4
6CzPh	Benzonitrile	295, 336	3.29	419	3.37	3.05	0.32	0.17	0.19	5.7

[a)]Measured in ambient condition; [b)]Measured under N_2;

The natural transition orbitals indicated the hybridized local and charge transfer (HLCT) character for both S_1 and T_1 and more clear CT of nearly degenerated higher singlet levels. However, the solvatochromism of emission is not remarkable (**Fig. 3.7**), indicating the DFT might slightly underestimate the energies for CT characteristics. These features may also be related to the three-dimensional π-delocalization of multiple carbazole rings[28,29,30,31].

Table 3.3 Photophysical characteristics for the host materials in neat film.

Compound	Condition	λ_{abs} [nm]	E_g^{opt} [eV]	λ_{PL} [nm]	S_1 [eV]	T_1 [eV]	ΔE_{ST} [eV]	Φ_{air} [-][a)]	Φ_{N2} [-][b)]	τ [ns][b)]
mCP	Neat	297, 329, 342	3.53	352, 368	3.63	2.85	0.78	-	-	-
mCBP	Neat	296, 329, 343	3.51	350, 366	3.64	2.81	0.83	-	-	-
6CzPh	Neat	339, 357	3.14	416	3.28	2.80	0.48	0.12	0.14	2.6

[a)]Measured in ambient condition; [b)]Measured under N_2;

In toluene, the S_1 energy of 6CzPh is 3.37 eV, which is relatively lower than those (~3.7 eV) of mCP and mCBP. In contrast, the T_1 energies of 6CzPh in toluene (2.99 eV) and chloroform (3.05 eV) are similar to those (3.05 eV) of mCP and mCBP and kept at very high energy levels. Moreover, the T_1 energy of 6CzPh (2.80 eV) in the neat film is still comparable to those of mCP (2.85 eV) and mCBP (2.81 eV), suggesting a promising candidate as the host for OLEDs.

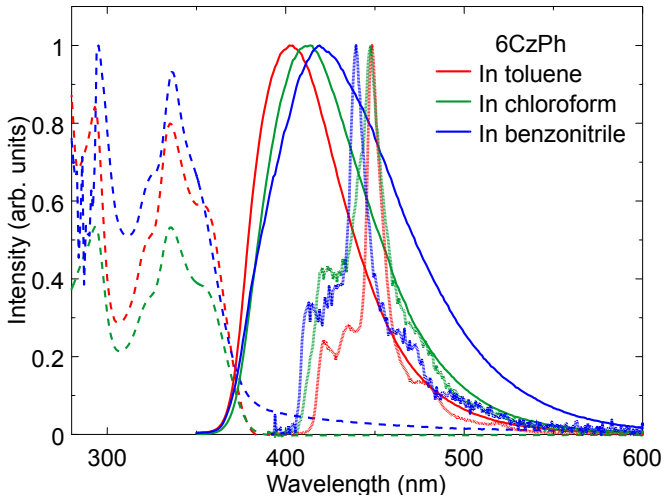

Figure 3.7: Absorption and emission spectra in solution. Absorption (dashed lines), fluorescence (solid lines), and phosphorescence (dotted lines) spectra for 6CzPh in toluene, chloroform, and acetonitrile.

The green TADF emitter 4CzIPN was used to check the host's performance. Then, we checked the PL properties of the doped films and compared the results with the mCBP host (**Fig. 3.8, Table 3.4**). Here, while the PLQY with 6 wt% 4CzIPN doped mCBP film is 93%, the 6 wt% 4CzIPN doped 6CzPh film showed an acceptable PLQY of 80%. We can observe a small delta ΔE_{ST} value and comparable k_{RISC} value with both host materials. When we increased the doping concentration, both films showed lower PLQY. This is because of the increase of the concentration quenching with the 4CzIPN doping.

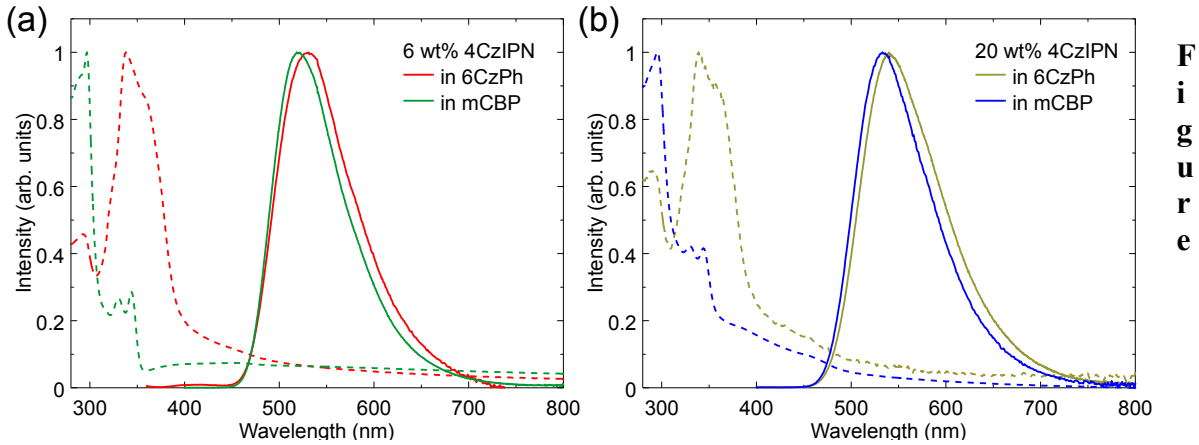

Figure 3.8: Absorption and emission spectra for the doped films. Absorption (dashed lines) and fluorescence (solid lines) spectra for the 4CzIPN-doped films of mCBP and 6CzPh.

Table 3.4. Photophysical characteristics for the 4CzIPN-doped films of mCBP and 6CzPh.

Host	Doping conc.	λ_{PL} [nm]	S_1 [eV]	T_1 [eV]	Φ_{PL} [-][a)]	ΔE_{ST} [eV]	τ_p [ns][a)]	τ_d [μs][a)]	k_r [10^7 s^{-1}]	k_{ISC} [10^7 s^{-1}]	k_{RISC} [10^6 s^{-1}]
mCBP	6 wt%	518	2.64	2.61	0.93	0.03	19.0	2.6	1.5	3.7	1.2
6CzPh	6 wt%	531	2.64	2.61	0.80	0.03	16.4	2.1	2.0	4.1	1.0
mCBP	20 wt%	533	2.60	2.56	0.87	0.04	23.9	3.0	1.2	3.0	1.0
6CzPh	20 wt%	540	2.58	2.52	0.63	0.06	22.2	2.0	1.5	3.0	0.69

[a)]Measured under Ar

I evaluated the host properties of 6CzPh in OLEDs using 4CzIPN, the typical benchmark TADF emitte[26,32]. The device structure follows the reported architecture for 4CzIPN-based device with an mCBP host, ITO/HAT-CN (10 nm)/tris-PCz (30 nm)/electron blocking layer (EBL) (5 nm)/6 or 20 wt%-4CzIPN: host (30 nm)/T2T (10 nm)/Bpy-TP2 (40 nm)/Liq (2 nm)/Al (100 nm) as shown in **Fig. 3.9**. Note that higher doping concentrations of 4CzIPN will improve electron injection, carrier balance, and device durability while reducing

the maximum external quantum efficiency (EQE) due to concentration quenching[32]. Firstly, mCBP as the EBL and host in Device A was replaced by 6CzPh in Device B. The HOMO and LUMO energies of 6CzPh estimated by photoelectron yield spectroscopy (PYS) and the optical energy gap for the neat film are −6.1 eV and −2.9 eV, respectively.

As discussed above, 6CzPh showed similar HOMO and deeper LUMO levels compared to those of mCBP. The cyclic voltammetry measurements also showed oxidation and reduction processes with a similar energy gap. In general, maximum efficiencies, rolloff characteristics, and device durability are the key parameters affected by the host properties. The devices using the 6CzPh host showed higher EQE and smaller rolloff (**Figs. 3.9 b and 3.10**, and **Table 3.5.**). Since the PL measurements for the 4CzIPN doped 6CzPh film (EML) revealed slightly poor performances relative to those of mCBP (**Fig. 3.8 and Table 3.4.**), the improvements of OLED characteristics might be fundamentally related to better carrier transport properties.

Although the fast RISC rate is considered favorable to reduce long-lived triplet excitons caused by annihilations, the rolloff could also be reduced by increasing the carrier transport and balance in the EML[33,34,35,36]. The annihilations of 4CzIPN in each host were also evaluated by the PL intensity dependence on laser fluence and confirmed similar results (**Fig. 3.9 c**), suggesting that small variations of the TADF properties negligibly affected the device performances. Despite the better EQE, the device durability was decreased in comparison to the corresponding mCBP devices (**Fig. 3.11**). To clarify this, we investigated carrier balance by fabricating hole-only and electron-only devices (HOD and EOD) (**Fig. 3.9 d**). These donor carbazole-based hosts normally exhibit higher hole currents than electron currents[1,2,3,4,5]. Although both hole and electron currents are higher for 6CzPh devices than mCBP devices, the ratio of_hole/electron was increased (110 for 6CzPh vs. 25 for mCBP at 6 V). Thus, 6CzPh-based devices have the recombination dominantly at the interface of EML/HBL, although the lower injection barrier of electrons to the EML might reduce rolloff[37,38,39]. Since the interfaces are known to be susceptible sites of degradation, Device B using 6CzPh would exhibit lower stability than Device A[40,41,42,43].

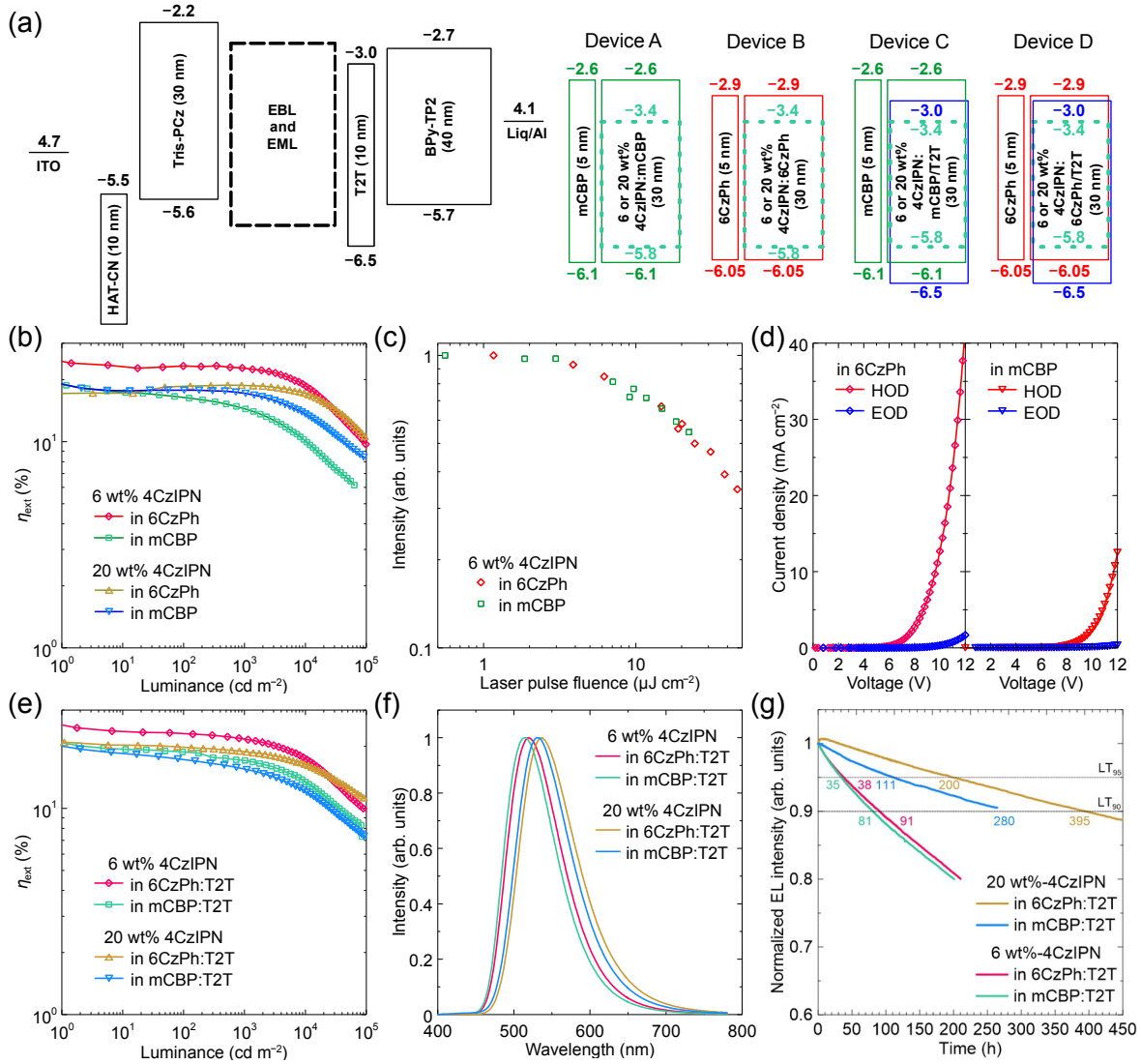

Figure 3.9: a) Optimized device structures of the 4CzIPN-based OLED, b) EQE-luminance characteristics for Devices A and B, c) PL intensity dependence on laser fluence for the 4CzIPN-doped films of mCBP and 6CzPh, d) current density-voltage characteristics for HODs and EODs, e) EQE-luminance characteristics for Devices C and D, f) EL spectra in the Devices C and D at 1000 cd m^{-2}, g) Luminance change versus operational time at an initial luminance of 1000 cd m^{-2}. The initial increase in luminance is sometimes observed for some reasons[47,48,49,50,51,52,53].

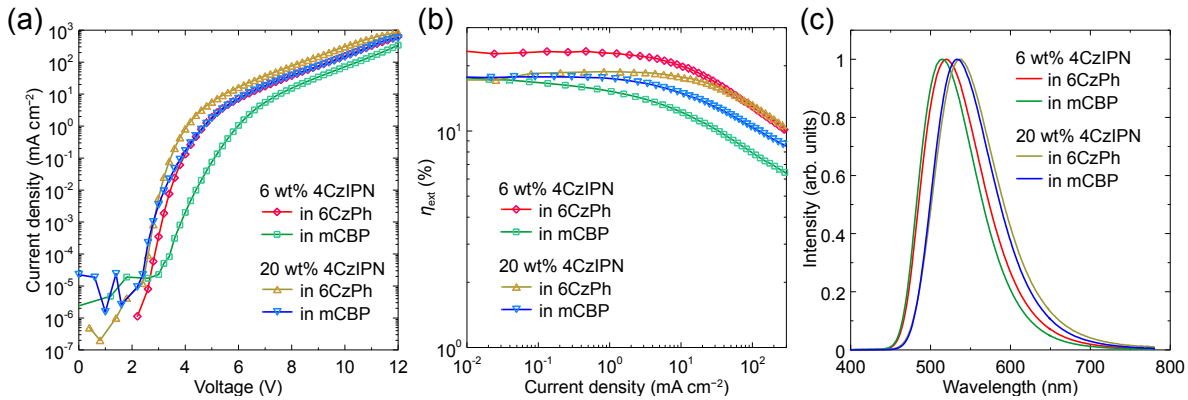

Figure 3.10: Device performances for Devices A and B. a) Current density-voltage characteristics, b) EQE-current density characteristics, and c) EL spectra at 1000 cd m^{-2}.

Table 3.5. Device performance of OLEDs.

Host	Doping conc. of 4CzIPN [wt%]	Voltage [V][a)]	EQE [%][b)]	Rolloff [%][c)]	*L*max [cd m^{-2}][d)]	λ_{EL} [nm][e)]
6CzPh	6	3.2/4.0/5.0/7.0	24.0/23.3/22.4/18.5	23	98500	520
mCBP	6	4.0/5.4/6.4/9.0	18.8/16.3/14.4/9.9	47	63400	514
6CzPh	20	3.0/3.6/4.4/6.2	18.8/18.6/18.7/16.9	10	124500	536
mCBP	20	3.0/4.0/5.0/7.2	18.2/17.8/17.1/13.6	25	90500	533
6CzPh:T2T	6	3.2/4.0/4.8/7.2	24.6/22.9/21.5/17.3	30	100200	520
mCBP:T2T	6	3.6/4.6/5.6/8.0	20.1/18.8/17.1/13.4	33	84200	515
6CzPh:T2T	20	2.6/3.6/4.8/7.4	20.9/19.7/18.8/16.2	23	127800	536
mCBP:T2T	20	2.8/3.8/4.6/6.8	19.4/17.0/15.4/12.0	38	100000	531

[a)]Voltage at 1 (turn-on voltage, V_{on}), 100, 1000, and 10000 cd m^{-2}, respectively. [b)]EQE for maximum, and at 100, 1000, and 10000 cd m^{-2}, respectively. [c)]EQE at 10000 cd m^{-2} against EQE for maximum. [d)]Maximum luminance. [e)]λ_{EL}: EL emission maximum at 1000 cd m^{-2}.

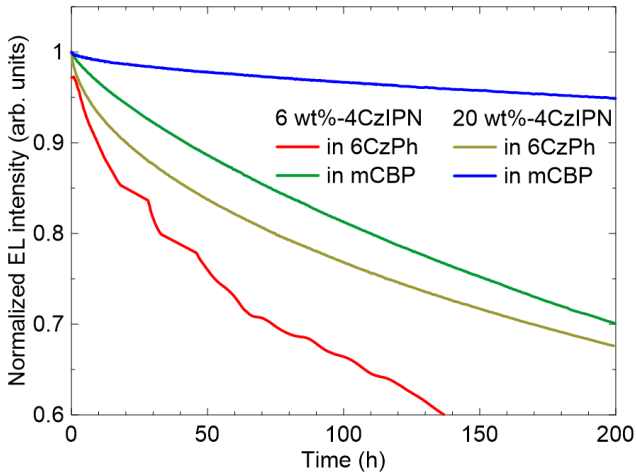

Figure 3.11: Luminance changes versus operational time for Devices A and B at an initial luminance of 1000 cd m^{-2}.

Therefore, I next fabricated the devices using the mixed hosts with n-type T2T (Devices C and D) to facilitate electron injection from the HBL, avoid hole accumulation at the interface, and broaden the recombination zone in the EML. The fluorescence of the blend film of 6CzPh: T2T in the ratio 1:1 appeared to be similar to that of the 6CzPh neat film because T2T has slightly higher S_1 energy with a fluorescence maximum of 400 nm in the neat film. However, the shoulder at around 480 nm was slightly increased (**Fig. 3.12**), which might be due to weak exciplex formation. However, the exciplex host is advantageous to saving energy by direct exciton formation[44,45]. The PL properties for the films doped with 4CzIPN showed improved quantum yields and RISC rates compared to those for the single host (**Fig. 3.13** and **Table 3.6.**). As a result, the device performances for the mixed hosts are similar or slightly improved (**Figs. 3.9 e and 3.14**, and **Table 3.5.**), although the rolloff was slightly increased because of the intrinsically large rolloff for the devices with T2T as the host[46]. The EL spectra showed a similar tendency as those in the single host and PL spectra (**Fig. 3.9 f**). Importantly, the device lifetime for the devices with 6CzPh: T2T host (LT_{95} = 200 h at 1000 cd m^{-2}) was longer than those with mCBP: T2T host (LT_{95} = 111 h), indicating great promise for OLED applications (**Fig. 3.9 g**).

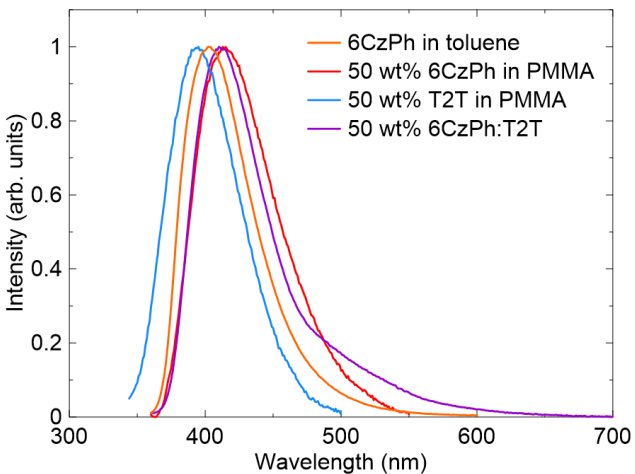

Figure 3.12: PL spectra for 6CzPh in toluene, 50-wt%-6CzPh doped film of PMMA, 50-wt %-doped film of T2T, and the blend film of 6CzPh: T2T in the ratio 1:1.

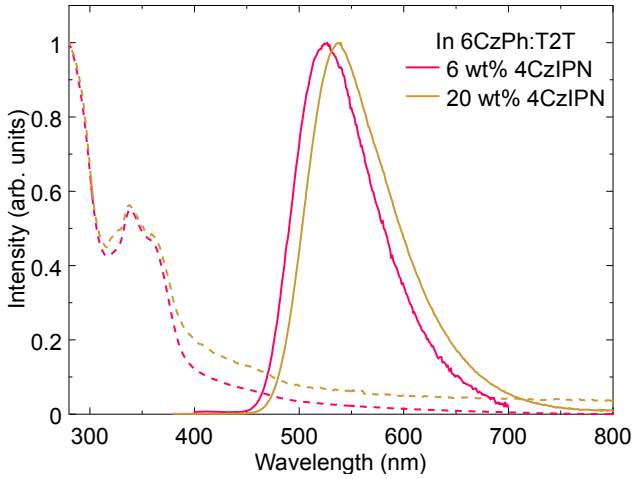

Figure 3.13: Absorption and emission spectra for the doped films. Absorption (dashed lines) and fluorescence (solid lines) spectra for the 4CzIPN-doped films of 6CzPh: T2T.

Table 3.6. Photophysical characteristics for the 4CzIPN-doped films of 6CzPh: T2T.

Host	Doping conc.	λ_{PL} [nm]	S_1 [eV]	T_1 [eV]	Φ_{PL} [-][a)]	ΔE_{ST} [eV]	τ_p [ns][a)]	τ_d [μs][a)]	k_r [10^7 s^{-1}]	k_{ISC} [10^7 s^{-1}]	k_{RISC} [10^6 s^{-1}]
6CzPh:T2T	6 wt%	527	2.65	2.58	0.85	0.07	18.3	2.4	1.5	4.0	1.2
6CzPh:T2T	20 wt%	538	2.59	2.53	0.69	0.06	22.1	2.3	1.3	3.2	0.84

[a)]Measured under Ar

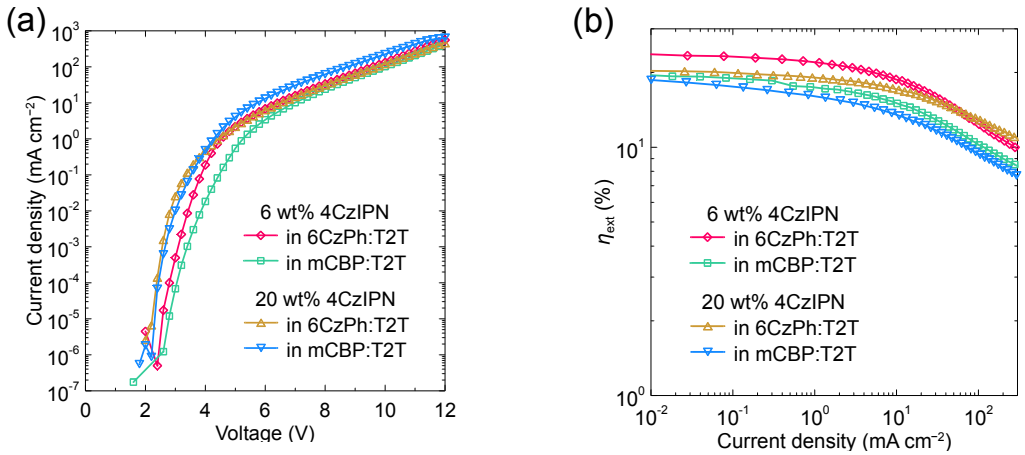

Figure 3.14: Device performances for Devices C and D. a) Current density-voltage characteristics, and b) EQE-current density characteristics.

Finally, the maximum η_{EQE} was discussed by the equation for EL efficiency comprising four factors, $\eta_{EQE} = \eta_{IQE} \times \eta_{out} = \gamma \times \eta_r \times \Phi_{PL} \times \eta_{out}$, where η_{IQE} is the internal quantum efficiency, γ is the carrier balance factor, η_r is the radiative-exciton production efficiency, Φ_{PL} is the PL quantum yield, and η_{out} is the light outcoupling efficiency. The values of γ and η_r could be 100% by utilizing TADF emitters which can harvest triplet excitons[7]. The Φ_{PL} values were experimentally determined for the corresponding doped films. Thus, the η_{out} values of about 30% are assumed to explain the experimental η_{EQE}. The η_{out} depends on not only the thicknesses and refractive indices of the materials but also the orientation of the transition dipole moment of the emitter in the amorphous host. In particular, horizontal molecular orientations to the substrate enhance the η_{out} and η_{EQE}. Thus, the engineering of molecular orientations has been an active topic of research in the last decade[54–70]. Nevertheless, the examples of high-order horizontal orientations ($\Theta_h > 90\%$, $S < -0.46$) are very limited, and complete horizontal orientation ($\Theta_h = 100\%$, $S = -0.50$) has been achieved by controlling kinetic relaxation and kinetic stability at the low substrate temperature[71-79]. It is generally accepted that a linear molecular geometry with a high aspect ratio is favorable to realizing horizontal orientation in vacuum-deposited amorphous films. Thus, the disk-shaped molecules, especially polar molecules with the permanent dipole moment, are disadvantageous regarding molecular orientations[80,81,82]. In fact, 4CzIPN in mCP: B3PyMPM showed only $\Theta_h = 73\%$ ($S = -0.18$), which is consistent with our result of angular-dependent PL measurements for 4CzIPN in mCBP ($\Theta_h = 72\%$, $S = -0.15$) (**Fig. 3.15**)[83]. In contrast, 4CzIPN in 6CzPh realized the ideal horizontal orientation ($\Theta_h = 100\%$, $S = -0.50$). The mixed host of 6CzPh and T2T also showed a high degree of horizontal orientations ($\Theta_h = 91\%$, $S =$

−0.47 for hosts in the ratio 1:1) with increasing 6CzPh concentrations (**Fig. 3.17**). These results fully rationalize the experimental EQE values because the simulated η_{out} using the orientation order parameter was >30% (**Fig. 3.18 and Table 3.7.**). These great improvements in the degree of molecular orientations may be attributed to the suppression of reorientation and randomization of emitters during deposition by 6CzPh with high rigidity and high evaporation temperature, although the effect of T_g on orientation order parameter was found to be unclear for polar emitters. The dipole-dipole interactions may also be an important factor in affecting molecular orientations, and thus, a polar host has good compatibility with polar emitters[84-87]. A high EQE value for 4CzIPN has been reported in a host molecule satisfying these criteria[88]. Here, 6CzPh should have a negligibly small permanent dipole moment even considering the fluctuations of the carbazole rings. To confirm the superiority and availability of 6CzPh, we also investigated several different types of TADF emitters, such as linear shape PXZ-TRZ, disk-shaped non-polar 2Cz2DAMC2BN, octahedral-shaped $Ir(ppy)_3$, and relatively planar DABNA-2 and *ν*-DABNA[89,90,91,92]. The slight vertical molecular orientation of PXZ-TRZ in mCBP in the literature (Θ_h = 65%, S = 0.05) was well reproduced (Θ_h = 61%, S = 0.17), while horizontal orientation is feasible in 6CzPh host (Θ_h = 77%, S = −0.27)[93]. The other emitters also showed the same tendency, indicating the generality of boosting horizontal orientation by utilizing 6CzPh as a host. The homoleptic iridium compound, $Ir(ppy)_3$, is known to show random orientations in many hosts (e.g., 69% in CBP),[79] while there are some examples of small orientation (Θ_h = 63% in UGH-2 to 77% in 2-phenyl-4,6-bis(12-phenylindolo[2,3-*a*] carbazole-11-yl)-1,3,5-triazine) [94,33]. Indeed, nearly random orientation was observed in mCBP, while 6CzPh leads to the increase of the horizontal orientation ratio to Θ_h = 86%. It may not be surprising because many iridium-based phosphors show a preference for horizontal orientation. Since $Ir(ppy)_3$ has a relatively high permanent dipole moment of 6.26 D, it tends to strongly aggregate owing to increased intermolecular forces by dipole-dipole interactions[95,96]. In contrast, the iridium complexes with horizontal alignment exhibit substantially small dipole-dipole potential. Thus, the interactions between $Ir(ppy)_3$ molecules might compete with the dipole interaction with the π-hole in_the center of the 6CzPh molecule (**Fig. 3.16**). This result seems to be consistent with the result of 4CzIPN, indicating the existence of dipole interactions between host and guest molecules. Although DABNA-2 of MR-TADF molecule was known to show only a small degree of horizontal orientations, it appears to have a clear predominance of horizontal orientation with 6CzPh (Θ_h = 87%, S = −0.44).

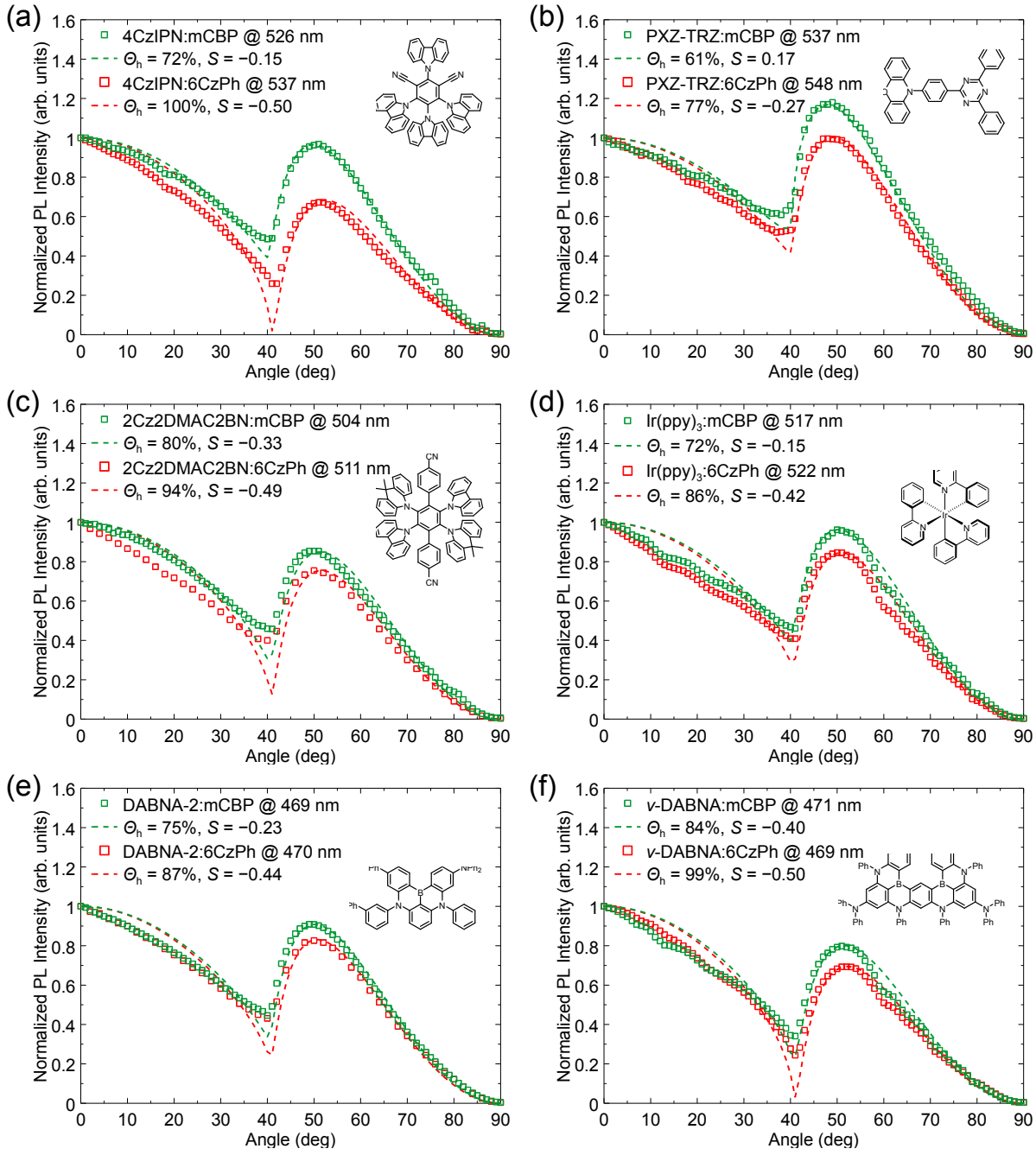

Figure 3.15: Radiation patterns of the *p*-polarized light from angular dependent PL measurements. a) 4CzIPN doped films, b) PXZ-TRZ doped films, c) 2Cz2DAMAC2BN doped films, d) $Ir(ppy)_3$, e) DABNA-2, and f) *ν*-DABNA doped films of mCBP and 6CzPh. The optical simulation was performed using simulation software (Setfos 4.6, Fluxim).

In addition, *ν*-DABNA with an increased aspect ratio shows nearly complete horizontal orientation in 6CzPh (Θ_h = 99%, S = −0.50) because of intrinsically better orientations in mCBP (Θ_h = 84%, S = −0.40). Since the MR molecules are normally used as a terminal emitter in TADF-assisted fluorescence (TAF, i.e., hyperfluorescence) or phosphor-sensitized

fluorescence (PSF) OLEDs, their molecular orientations would have a large impact on the efficiencies[97–101]. Thus, there has been some effort for modulating the orientations by increasing the aspect ratio of molecular shape and replacing substitution, while our result offers a more straightforward approach toward highly efficient OLEDs[102–105]. Note that the doping concentration of the film is 10wt% of 4CzIPN, PXZ-TRZ, and $Ir(ppy)_3$ in mCBP and 6CzPh hosts. The doping concentration of 15 wt% was used in the case of 2Cz2DMAC2BN in mCBP and 6CzPh hosts. Because of the rather rapid degradation of the MR-TADF molecules, the doping concentration of *v*-DABNA and DABNA-2 was kept as low as 5 wt% in the doped films for the angular-dependent PL measurements. I did not measure angular-dependent PL characteristics by changing the emitter concentration to check the molecular orientation in the doped films.

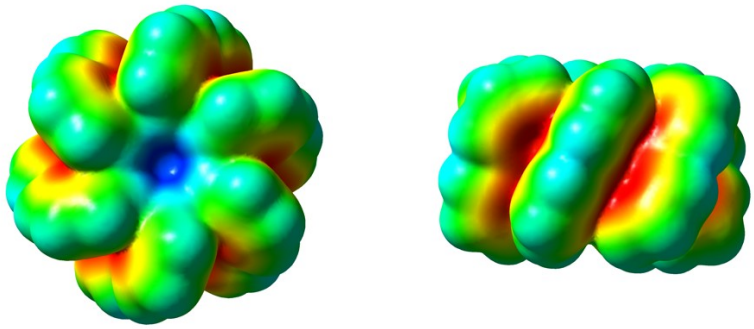

Figure 3.16: Electrostatic potential (ESP) of 6CzPh calculated at B3LYP/6-31+G(d,p).

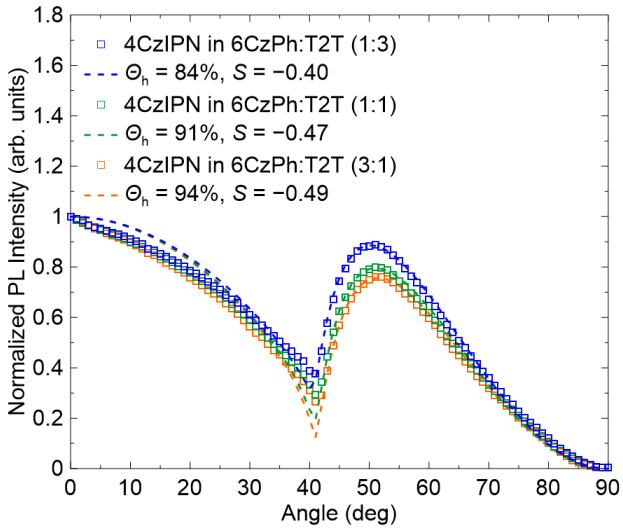

Figure 3.17: Angular-dependent PL measurements for 4CzIPN doped films of 6CzPh: T2T. The optical simulation was performed using simulation software (Setfos 4.6, Fluxim).

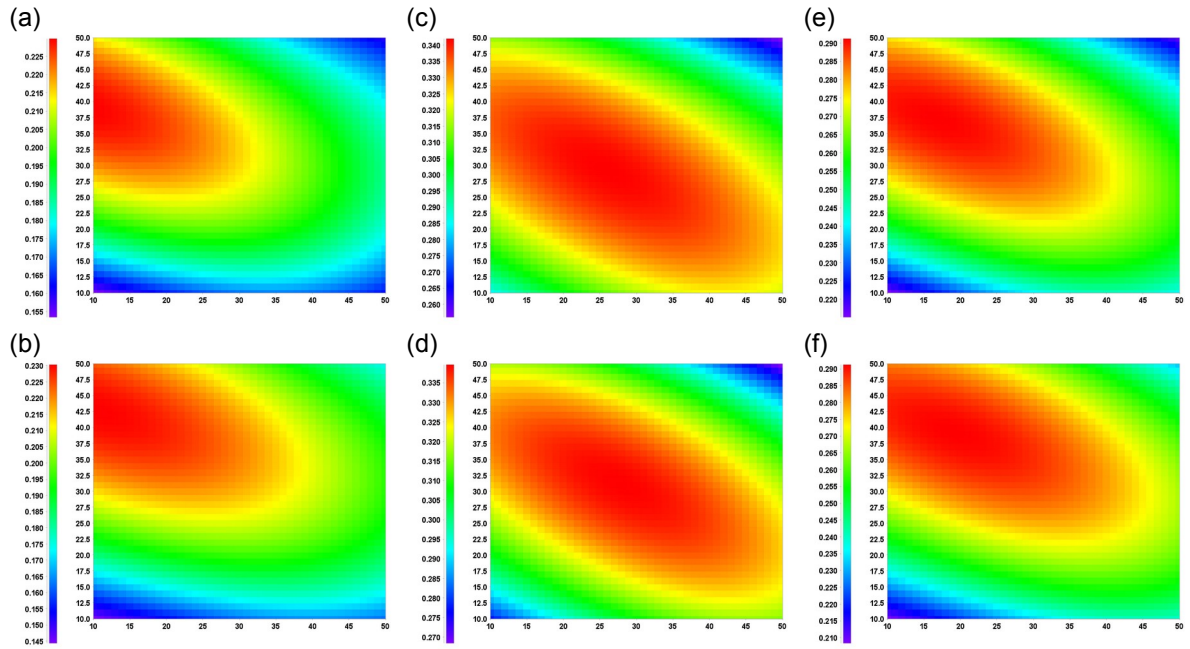

Figure 3.18: Light-outcoupling efficiency simulated with Setfos software. The efficiency as a function of HTL and ETL thickness. The *n* and *k* values for each layer were measured by variable-angle spectroscopic ellipsometry. a) 6 wt% 4CzIPN in mCBP, b) 20 wt% 4CzIPN in mCBP, c) 6 wt% 4CzIPN in 6CzPh, d) 20 wt% 4CzIPN in 6CzPh, e) 6 wt% 4CzIPN in 6CzPh:T2T, and f) 20 wt% 4CzIPN in 6CzPh:T2T.

Table 3.7. Theoretical EQE calculated from the Φ_{PL} and η_{out}.

Host	Doping conc.	Φ_{PL}	η_{out} [a)]	Theoretical η_{EQE} [b)]	Experimental η_{EQE}
mCBP	6 wt%	0.93	0.210	19.5	18.8
6CzPh	6 wt%	0.80	0.327	26.2	24.0
mCBP	20 wt%	0.87	0.219	19.1	18.2
6CzPh	20 wt%	0.63	0.331	20.8	18.8
6CzPh:T2T	6 wt%	0.85	0.280	23.8	24.6
6CzPh:T2T	20 wt%	0.69	0.286	19.7	20.9

[a)]Taken from Figure 3.18. [b)]Calculated with $\eta_{EQE} = \gamma \times \eta_r \times \Phi_{PL} \times \eta_{out}$, where γ and η_r were estimated to be 100%.

3.1. Conclusion

I revealed that hexacarbazolylbenzene, 6CzPh, is a highly efficient host material in OLEDs. With the facile and scalable synthesis, excellent thermal stability, and appropriate energy levels including high triplet energy, 6CzPh presents great promise for an OLED material. Accordingly, OLEDs using a 6CzPh host achieved superior performances of high efficiencies and high durability compared to the OLEDs using the standard host material of mCBP. Most importantly, 6CzPh significantly improved horizontal molecular orientations for the guest emitters having several types of structures. To the best of our knowledge, this is the first example of the complete horizontal orientation for disk-shaped polar molecules such as 4CzIPN. Since the internal quantum efficiency of OLEDs has already reached unity, light outcoupling has dominantly limited device efficiencies to a low level, while meaning much room for improvement. Thus, versatile host material that can enhance the molecular orientation of a wide variety of emitters would be enormously valuable in practical applications. Furthermore, instead of introducing T2T to enhance electron transport in the EML, it could be better to replace a carbazole group with a carboline group as the host molecule. Overall, this achievement can pave the way to ultimate OLED characteristics.

3.2. References

1. Xiao, L., Chen, Z., Qu, B., Luo, J., Kong, S., Gong, Q. & Kido, J. Recent Progresses on Materials for Electrophosphorescent Organic Light-Emitting Devices. *Adv. Mater*. **23**, 926–952 (2011).
2. Tao, Y., Yang, C. & Qin, J. Organic host materials for phosphorescent organic light-emitting diodes. *Chem. Soc. Rev.* **40**, 2943 (2011).
3. Sasabe, H. & Kido, J. Development of high performance OLEDs for general lighting. *J. Mater. Chem. C* **1**, 1699 (2013).
4. Yang, X., Zhou, G. & Wong, W.-Y. Functionalization of phosphorescent emitters and their host materials by main-group elements for phosphorescent organic light-emitting devices. *Chem. Soc. Rev.* **44**, 8484 (2015).
5. Wang, Y., Yun, J. H., Wang, L. & Lee, J. Y. High Triplet Energy Hosts for Blue Organic Light-Emitting Diodes. *Adv. Funct. Mater.* **31**, 2008332 (2021).
6. Osaheni, J. A. & Jenekhe, S. A. Efficient Blue Luminescence of a Conjugated Polymer Exciplex. *Macromolecules* **27**, 739 (1994).
7. Berggren, M., Gustafsson, G., Inganäs, O., Andersson, M. R., Hjertberg, T. & Wennerström, O. White light from an electroluminescent diode made from poly[3(4-octylphenyl)-2,2-bithiophene] and an oxadiazole derivative. *J. Appl. Phys.* **76**, 7530 (1994).
8. Tamoto, N., Adachi, C. & Nagai, K. Electroluminescence of 1,3,4-Oxadiazole and Triphenylamine-Containing Molecules as an Emitter in Organic Multilayer Light Emitting Diodes. *Chem. Mater.* **9**, 1077 (1997).
9. Gebler, D. D., Wang, Y. Z., Blatchford, J. W., Jessen, S. W., Fu, D. -K., Swager, T. M., MacDiarmid, A. G. & Epstein, A. J. Exciplex emission in bilayer polymer light-emitting devices. *Appl. Phys. Lett.* **70,** 1644 (1997).
10. Baldo, M. A., Lamansky, S., Burrows, P. E., Thompson, M. E. & Forrest, S. R. Very high-efficiency green organic light-emitting devices based on electrophosphorescence. *Appl. Phys. Lett.* **75**, 4 (1999).
11. O'Brien, D. F., Baldo, M. A., Thompson, M. E., Forrest, S. R. Improved energy transfer in electrophosphorescent devices. *Appl. Phys. Lett.* **74**, 442 (1999).

12. Adachi, C., Baldo, M. A., Forrest, S. R., Lamansky, S., Thompson, M. E. & Kwong, R. C. High-efficiency red electrophosphorescence devices. *Appl. Phys. Lett.* **78**, 1622 (2001).
13. Adachi, C., Baldo, M. A., Thompson, M. E. & Forrest, S. R. Nearly 100% internal phosphorescence efficiency in an organic light-emitting device. *J. Appl. Phys.* **90**, 5048 (2001).
14. Yang, C.-H., Tai, C.-C. & Sun, I.-W. Synthesis of a high-efficiency red phosphorescent emitter for organic light-emitting diodes. *J. Mater. Chem.* **14**, 947 (2004).
15. Adamovich, V., Brooks, J., Tamayo, A., Alexander, A. M., Djurovich, P., D'Andrade, B. W., Adachi, C., Forrest, S. R. & Thompson, M. E. High efficiency single dopant white electrophosphorescent light emitting diodes. *New J. Chem.* **26**, 1171 (2002).
16. Holmes, R. J., Forrest, S. R., Tung, Y. J., Kwong, R. C., Brown, J. J., Garon, S. & Thompson, M. E. Blue organic electrophosphorescence using exothermic host–guest energy transfer. *Appl. Phys. Lett.* **82**, 2422 (2003).
17. Kawamura, Y., Goushi, K., Brooks, J., Brown, J. J., Sasabe, H. & Adachi, C. 100% phosphorescence quantum efficiency of Ir (III) complexes in organic semiconductor films. *Appl. Phys. Lett.* **86**, 71104 (2005).
18. Schrögel, P., Langer, N., Schildknecht, C., Wagenblast, G., Lennartz, C. & Strohriegl, P. Meta-linked CBP-derivatives as host materials for a blue iridium carbene complex. *Org. Electron*. **12**, 2047 (2011).
19. Gong, S., He, X., Chen, Y., Jiang, Z., Zhong, C., Ma, D., Qin, J. & Yang, C. Simple CBP isomers with high triplet energies for highly efficient blue electrophosphorescence. *J. Mater. Chem*. **22**, 2894 (2012).
20. Tokito, S., Iijima, T., Suzuri, Y., Kita, H., Tsuzuki, T. & Sato, F. Confinement of triplet energy on phosphorescent molecules for highly-efficient organic blue-light-emitting devices. *Appl. Phys. Lett.* **82**, 569 (2003).
21. Tanaka, I., Tabata, Y. & Tokito, S. Energy-transfer and light-emission mechanism of blue phosphorescent molecules in guest-host systems. *Chem. Phys. Lett.* **400**, 86 (2004).
22. He, J., Liu, H., Dai, Y., Ou, X., Wang, J., Tao, S., Zhang, X., Wang, P. & Ma, D. Nonconjugated Carbazoles: A Series of Novel Host Materials for Highly Efficient Blue Electrophosphorescent OLEDs. *J. Phys. Chem. C* **113**, 6761 (2009).

23. Fukagawa, H., Watanabe, K., Tsuzuki, T. & Tokito, S. Highly efficient, deep-blue phosphorescent organic light emitting diodes with a double-emitting layer structure. *Appl. Phys. Lett.* **93**, 133312 (2008).
24. Tsai, M.-H., Lin, H.-W., Su, H.-C., Ke, T.-H., Wu, C.-C., Fang, F.-C., Liao, Y.-L., Wong, K.-T. & Wu, C.-L. Highly Efficient Organic Blue Electrophosphorescent DevicesBased on 3,6-Bis(triphenylsilyl)carbazole as the Host Material. *Adv. Mater.* **18**, 1216 (2006).
25. Wu, M.-F., Yeh, S.-J., Chen, C.-T., Murayama, H., Tsuboi, T., Li, W.-S., Chao, I., Liu, S.-W. & Wang, J.-K. The Quest for High-Performance Host Materials for Electrophosphorescent Blue Dopants. *Adv. Funct. Mater.* **17**, 1887 (2007).
26. Uoyama, H., Goushi, K., Shizu, K., Nomura, H. & Adachi, C. Highly efficient organic light-emitting diodes from delayed fluorescence. *Nature* **492**, 234 (2012).
27. Qiao, S., Huang, W., Wei, H., Wang, T. & Yang. R. Fine tailoring the steric configuration of initial building blocks to construct ultramicroporous polycarbazole networks with high CO_2 uptake and selectivity of CO_2 over N_2. *Polymer* **70**, 52 (2015).
28. Rosokha, S. V., Neretin, I. S., Sun, D. & Kochi, J. K. Very Fast Electron Migrations within p-Doped Aromatic Cofacial Arrays Leading to Three-Dimensional (Toroidal) π-Delocalization. *J. Am. Chem. Soc.* **128**, 9394 (2006).
29. Nishiuchi, T., Takeuchi, S., Makihara, Y., Kimura, R., Saito, S., Sato, H. & Kubo. T. Synthesis, Properties, and Intermolecular Interactions in the Solid States of π-Congested X-Shaped 1,2,4,5-Tetra(9-anthryl)benzenes. *Bull. Chem. Soc. Jpn.* **95**, 1591 (2022).
30. Nishiuchi, T., Sotome, H., Shimizu, K., Miyasaka, H. & Kubo, T. 1,2,3-Tri(9-anthryl)benzene: Photophysical Properties and Solid-State Intermolecular Interactions of Radially Arranged, Congested Aromatic π-Planes. *Chem. Eur. J.* **28**, e202104245 (2022).
31. Furukawa, S., Fujita, M., Kanatomi, Y., Minoura, M., Hatanaka, M., Morokuma, K., Ishimura, K. & Saito, M. Double aromaticity arising from σ- and π-rings. *Commun. Chem.* **1**, 60 (2018).
32. Nakanotani, H., Masui, K., Nishide, J., Shibata, T. & Adachi, C. Promising operational stability of high-efficiency organic light-emitting diodes based on thermally activated delayed fluorescence. *Sci. Rep.* **3**, 2127 (2013).
33. Wada, Y., Nakagawa, H., Matsumoto, S., Wakisaka, Y. & Kaji, H. Organic light emitters exhibiting very fast reverse intersystem crossing. *Nat. Photon.* **14**, 643 (2020).

34. Aizawa, N., Matsumoto, A. & Yasuda, T. Thermal equilibration between singlet and triplet excited states in organic fluorophore for submicrosecond delayed fluorescence. *Sci. Adv.* **7**, eabe5769 (2021).
35. Cui, L.-S., Gillett, A. J., Zhang, S.-F., Ye, H., Liu, Y., Chen, X.-K., Lin, Z.-S., Evans, E. W., Myers, W. K., Ronson, T. K., Nakanotani, H., Reineke, S., Bredas, J.-L., Adachi, C. & Friend, R. H. Fast spin-flip enables efficient and stable organic electroluminescence from charge-transfer states. *Nat. Photon.* **14**, 636 (2020).
36. Mamada, M., Katagiri, H., Chan, C.-Y., Lee, Y.-T., Goushi, K., Nakanotani, H., Hatakeyama, T. & Adachi, C. Highly Efficient Deep-Blue Organic Light-Emitting Diodes Based on Rational Molecular Design and Device Engineering. *Adv. Funct. Mater.* **32**, 2204352 (2022).
37. Chwang, A. B., Kwong, R. C. & Brown, J. J. Graded mixed-layer organic light-emitting devices. *Appl. Phys. Lett.* **80**, 725 (2002).
38. Luo, Y., Aziz, H. Space charge effects on the electroluminescence efficiency and stability of organic light-emitting devices with mixed emitting layers. *Appl. Phys. Lett.* **95**, 073304 (2009).
39. Song, W., Lee, J. Y., Kim, T., Lee, Y. & Jeong, H. Comprehensive understanding of degradation mechanism of high efficiency blue organic light-emitting diodes at the interface by hole and electron transport layer. *Org. Electron.* **57**, 158 (2018).
40. Scholz, S. Kondakov, D. Lüssem, B. & Leo, K. Degradation Mechanisms and Reactions in Organic Light-Emitting Devices. *Chem. Rev*. **115**, 8449 (2015).
41. Zhao, C. & Duan, L. Review on photo- and electrical aging mechanisms for neutral excitons and ions in organic light-emitting diodes. *J. Mater. Chem. C*, **8**, 803 (2020).
42. Mamada, M. & Adachi, C. Unexpected role of hole and electron blocking interlayers controlling charge carrier injection and transport in TADF based blue organic light-emitting diodes. *Appl. Phys. Lett*. **121**, 131103 (2022).
43. Kiriyama, S. Mamada, M. Goushi, K. Madushani, B. Hatakeyama, T. & Adachi, C. Effect of Multiple Acceptor Structures in Electron Transport Materials on Operational Lifetime of Blue Thermally Activated Delayed Fluorescence Organic Light-Emitting Diodes. *Adv. Funct. Mater*. 2402287 (2024).
44. Wang, Q., Tian, Q.-S., Zhang, Y.-L., Tanga, X. & Liao, L.-S. High-efficiency organic light-emitting diodes with exciplex hosts. *J. Mater. Chem. C* **7**, 11329 (2019).

45. Zhang, B. & Xie, Z. Recent Applications of Interfacial Exciplex as Ideal Host of Power-Efficient OLEDs. *Front. Chem.* **7**, 306 (2019).
46. Chen, H.-F. Yang, S.-J. Tsai, Z.-H. Hung, W.-Y. Wang, T.-C. & Wong, K.-T. 1,3,5-Triazine derivatives as new electron transport–type host materials for highly efficient green phosphorescent OLEDs. *J. Mater. Chem.* **19**, 8112 (2009).
47. a) Aziz, H. & Popovic, Z. D. Degradation Phenomena in Small-Molecule Organic Light-Emitting Devices. *Chem. Mater*. **16**, 4522 (2004).
48. Perumal, A. Lüssem, B. & Leo, K. Ultra-bright alternating current organic electroluminescence. *Org. Electron*. **13**, 1589 (2012).
49. Tsang, D. P.-K. Matsushima, T. & Adachi, C. Operational stability enhancement in organic light-emitting diodes with ultrathin Liq interlayers. *Sci. Rep*. **6**, 22463 (2016).
50. Acharya, K. P. Titov, A. Hyvonen, J. Wang, C. Tokarz, J. & Holloway, P. H. High efficiency quantum dot light emitting diodes from positive aging. *Nanoscale* **9**, 14451 (2017).
51. Cho, H. Kim, Y.-H. Wolf, C. Lee, H.-D. & Lee, T.-W. Improving the Stability of Metal Halide Perovskite Materials and Light-Emitting Diodes. *Adv. Mater*. **30**, 1704587 (2018).
52. Sun, L. Uemura, K. Takahashi, T. Yoshida, T. & Suzuri, Y. Interfacial Engineering in Solution Processing of Silicon-Based Hybrid Multilayer for High Performance Thin Film Encapsulation. *ACS Appl. Mater. Interfaces* **11**, 43425 (2019).
53. S. Hillebrandt, S. Keum, C. Deng, Y. Chavas, J. Galle, C. Hardin, T. Galluppi, F. Gather, M. C. High Brightness, Highly Directional Organic Light-Emitting Diodes as Light Sources for Future Light-Amplifying Prosthetics in the Optogenetic Management of Vision Loss. *Adv. Opt. Mater*. **11**, 2200877 (2023).
54. Yokoyama, D., Sakaguchi, A., Suzuki, M. & Adachi, C. Horizontal orientation of linear-shaped organic molecules having bulky substituents in neat and doped vacuum-deposited amorphous films. *Org. Electron*. **10**, 127 (2009).
55. Frischeisen, J., Yokoyama, D., Adachi, C. & Brütting, W. Determination of molecular dipole orientation in doped fluorescent organic thin films by photoluminescence measurements. *Appl. Phys. Lett*. **96**, 073302 (2010).
56. Yokoyama, D., Setoguchi, Y., Sakaguchi, A., Suzuki, M. & Adachi, C. Orientation Control of Linear-Shaped Molecules in Vacuum-Deposited Organic Amorphous Films and Its Effect on Carrier Mobilities. *Adv. Funct. Mater*. **20**, 386 (2010).

57. Yokoyama, D. Molecular orientation in small-molecule organic light-emitting diodes. *J. Mater. Chem*. **21**, 19187 (2011).
58. Brütting, W., Frischeisen, J., Schmidt, T. D., Scholz, B. J. & Mayr, C. Device efficiency of organic light-emitting diodes: Progress by improved light outcoupling. *Phys. Status Solidi A* **210**, 44 (2013).
59. Kim, K.-H. Lee, S. Moon, C.-K. Kim, S.-Y. Park, Y.-S. Lee, J.-H. Lee, J. W. Huh, J. You & Y. Kim. J.-J. Phosphorescent dye- based supramolecules for high-efficiency organic light-emitting diodes, *Nat. Commun*. **5**, 4769 (2014).
60. Kaji, H., Suzuki, H., Fukushima, T., Shizu, K., Suzuki, K., Kubo, S., Komino, T., Oiwa, H., Suzuki, F., Wakamiya, A., Murata, Y. & Adachi, C. Purely organic electroluminescent material realizing 100% conversion from electricity to light. *Nat. Commun*. **6**, 8476 (2015).
61. Jurow, M. J., Mayr, C., Schmidt, T. D., Lampe, T., Djurovich, P. I., Brütting, W. & Thompson, M. E. Understanding and predicting the orientation of heteroleptic phosphors in organic light-emitting materials. *Nat. Mater*. **15**, 85 (2016).
62. Lin, T.-A., Chatterjee, T., Tsai, W.-L., Lee, W.-K., Wu, M.-J., Jiao, M., Pan, K.-C., Yi, C.-L., Chung, C.-L., Wong, K.-T. & Wu, C.-C. Sky- Blue Organic Light Emitting Diode with 37% External Quantum Efficiency Using Thermally Activated Delayed Fluorescence from Spiroacridine-Triazine Hybrid. *Adv. Mater*. **28**, 6976 (2016).
63. Komino, T., Oki, Y. & Adachi, C. Dipole orientation analysis without optical simulation: application to thermally activated delayed fluorescence emitters doped in host matrix. *Sci. Rep*. **7**, 8405 (2017).
64. Kim, K.-H. & Kim, J.-J. Origin and Control of Orientation of Phosphorescent and TADF Dyes for High-Efficiency OLEDs. *Adv. Mater*. **30**, 1705600 (2018).
65. Wu, T.-L., Huang, M.-J., Lin, C.-C., Huang, P.-Y., Chou, T.-Y., Chen-Cheng, R.-W., Lin, H.-W., Liu, R.-S. & Cheng, C.-H. Diboron compound-based organic light-emitting diodes with high efficiency and reduced efficiency. roll-off. *Nat. Photon*. **12**, 235 (2018).
66. Watanabe, Y., Sasabe, H. & Kido, J. Review of Molecular Engineering for Horizontal Molecular Orientation in Organic Light-Emitting Devices. *Bull. Chem. Soc. Jpn*. **92**, 716 (2019).

67. Ahn, D. H., Kim, S. W., Lee, H., Ko, I. J., Karthik, D., Lee, J. Y. & Kwon, J. H. Highly efficient blue thermally activated delayed fluorescence emitters based on symmetrical and rigid oxygen-bridged boron acceptors. *Nat. Photon*. **24**, 540 (2019).
68. Hofmann, A. Schmid, M. & Brütting, W. The Many Facets of Molecular Orientation in Organic Optoelectronics. *Adv. Opt. Mater*. **9**, 2101004 (2021).
69. Lee, Y. H. Lee, W. Lee, T. Jung, J. Yoo, S. & Lee, M. H. Achieving over 36% EQE in blue OLEDs using rigid TADF emitters based on spiro-donor and spiro-B-heterotriangulene acceptors. *Chem. Eng. J.* **452**, 139387 (2023).
70. Arai, H., Yoshida, N., Sasabe, H., Sagae, Y., Hoshi, K., Yokoyama, D. & Kido, J. Fundamental guidelines for the active control of the molecular orientation of heteroleptic iridium complexes enabled by carbazole- based host materials. *J. Mater. Chem. C* **12**, 2772–2779 (2024).
71. Mayr, C., Lee, S. Y., Schmidt, T. D., Yasuda, T., Adachi, C. & Brütting, W. Efficiency Enhancement of Organic Light-Emitting Diodes Incorporating a Highly Oriented Thermally Activated Delayed Fluorescence Emitter. *Adv. Funct. Mater.* **24**, 5232 (2014).
72. Kim, D. H., Inada, K., Zhao, L., Komino, T., Matsumoto, N., Ribierre, J. C. & Adachi, C. Organic light emitting diodes with horizontally oriented thermally activated delayed fluorescence emitters. *J. Mater. Chem. C* **5**, 1216 (2017).
73. Liu, M., Komatsu, R., Cai, X., Hotta, K., Sato, S., Liu, K., Chen, D., Kato, Y., Sasabe, H., Ohisa, S., Suzuri, Y., Yokoyama, D., Su, S.-J. & Kido, J. Horizontally Orientated Sticklike Emitters: Enhancement of Intrinsic Out-Coupling Factor and Electroluminescence Performance. *Chem. Mater.* **29**, 8630 (2017).
74. Lee, Y.-T., Tseng, P.-C., Komino, T., Mamada, M., Ortiz, R. J., Leung, M., Chiu, T.-L., Lin, C.-F., Lee, J.-H., Adachi, C., Chen C.-T. & Chen. C.-T. A Chemical Structure Approach Enhancing Light Outcoupling of Dopant OLEDs and Internal Quantum Efficiency of Non-Dopant OLEDs Having Bluish TADF Emitters. *ACS Appl. Mater. Interfaces* **10**, 43842 (2018).
75. Byeon, S. Y., Kim, J., Lee, D. R., Han, S. H., Forrest, S. R. & Lee, J. Y. Nearly 100% Horizontal Dipole Orientation and Upconversion Efficiency in Blue Thermally Activated Delayed Fluorescent Emitters. *Adv. Opt. Mater.* **6**, 1701340 (2018).
76. Oda, S., Kawakami, B., Kawasumi, R., Okita, R. & Hatakeyama, T. Multiple Resonance Effect-Induced Sky-Blue Thermally Activated Delayed Fluorescence with a Narrow Emission Band. *Org. Lett.* **21**, 9311 (2019).

77. Lee, Y., Woo, S.-J., Kim, J.-J. & Hong, J.-I. Linear-shaped thermally activated delayed fluorescence emitter using 1,5-naphthyridine as an electron acceptor for efficient light extraction. *Org. Electron.* **78**, 105600 (2020).
78. Balijapalli, U., Lee, Y.-T., Karunathilaka, B. S. B., Tumen-Ulzii, G., Auffray, M., Tsuchiya, Y., Nakanotani, H. & Adachi, C. Tetrabenzo[a,c]phenazine Backbone for Highly Efficient Orange–Red Thermally Activated Delayed Fluorescence with Completely Horizontal Molecular Orientation. *Angew. Chem. Int. Ed.* **60**, 19364 (2021).
79. Komino, T., Sagara, Y., Tanaka, H., Oki, Y., Nakamura, N., Fujimoto, H. & Adachi, C. Electroluminescence from completely horizontally oriented dye molecules. *Appl. Phys. Lett.* **108**, 241106 (2016).
80. Moon, C.-K., Kim, K.-H., Lee, J. W. & Kim, J.-J. Influence of Host Molecules on Emitting Dipole Orientation of Phosphorescent Iridium Complexes. *Chem. Mater.* **27**, 2767 (2015).
81. Mamada, M., Inada, K., Komino, T., Potscavage, W. J., Jr., Nakanotani, H. & Adachi, C. Highly Efficient Thermally Activated Delayed Fluorescence from an Excited-State Intramolecular Proton Transfer System. *ACS Cent. Sci.* **3**, 769 (2017).
82. Zeng, X., Pan, K.-C., Lee, W.-K., Gong, S., Ni, F., Xiao, X., Zeng, W., Xiang, Y., Zhan, L., Zhang, Y., Wu, C. -C. & Yang, C. High-efficiency pure blue thermally activated delayed fluorescence emitters with a preferentially horizontal emitting dipole orientation via a spiro-linked double D–A molecular architecture. *J. Mater. Chem. C* **7**, 10851 (2019).
83. Sun, J. W., Lee, J.-H., Moon, C.-K., Kim, K.-H., Shin, H. & Kim, J.-J. A fluorescent organic light-emitting diode with 30% external quantum efficiency. *Adv. Mater.* **26**, 5684 (2014).
84. Mayr, C. & Brütting, W. Control of Molecular Dye Orientation in Organic Luminescent Films by the Glass Transition Temperature of the Host Material. *Chem. Mater*. **27**, 2759 (2015).
85. Jiang, J., Walters, D. M., Zhou, D. & Ediger, M. D. Substrate temperature controls molecular orientation in two-component vapor-deposited glasses. soft *Matter* **12**, 3265 (2016).
86. Esaki, Y. Komino, T. Matsushima, T. & Adachi, C. Enhanced Electrical Properties and Air Stability of Amorphous Organic Thin Films by Engineering Film Density. *J. Phys. Chem. Lett*. **8**, 5891 (2017).

87. Tanaka, M., Noda, H., Nakanotani, H. & Adachi, C. Molecular orientation of disk-shaped small molecules exhibiting thermally activated delayed fluorescence in host-guest films, *Appl. Phys. Lett.* **116**, 023302 (2020).
88. Chen, C.-H. Ding, W.-C. Lin, B.-Y. Huang, J.-J. Leung, M.-k. Lee, J.-H. & Chiu, T.-L. Long-Distance Triplet Diffusion and Well-Packing Hosts with Ultralow Dopant Concentration for Achieving High-Efficiency TADF OLED. *Adv. Opt. Mater.* **9**, 2100857 (2021).
89. Tanaka, H., Shizu, K., Miyazaki, H. & Adachi, C. Efficient green thermally activated delayed fluorescence (TADF) from a phenoxazine–triphenyltriazine (PXZ–TRZ) derivative. *Chem. Commun.* **48**, 11392 (2012).
90. Madushani, B., Mamada, M., Goushi, K., Nguyen, T. B., Nakanotani, H., Kaji, H. & Adachi, C. Multiple donor-acceptor design for highly luminescent and stable thermally activated delayed fluorescence emitters. *Sci. Rep.* **13**, 7644 (2023).
91. Kawamura, Y., Goushi, K., Brooks, J., Brown, J. J., Sasabe, H. & Adachi, C. 100% phosphorescence quantum efficiency of Ir (III) complexes in organic semiconductor films. *Appl. Phys. Lett.* **86**, 071104 (2005).
92. Hatakeyama, T., Shiren, K., Nakajima, K., Nomura, S., Nakatsuka, S., Kinoshita, K., Ni, J., Ono, Y. & Ikuta, T. Ultrapure Blue Thermally Activated Delayed Fluorescence Molecules: Efficient HOMO-LUMO Separation by the Multiple Resonance Effect. *Adv. Mater.* **28**, 2777 (2016).
93. Komino, T., Tanaka, H. & Adachi, C. Selectively Controlled Orientational Order in Linear-Shaped Thermally Activated Delayed Fluorescent Dopants. *Chem. Mater.* **26**, 3665 (2014).
94. Graf, A., Liehm, P., Murawski, C., Hofmann, S., Leo, K. & Gather, M. C. Correlating the transition dipole moment orientation of phosphorescent emitter molecules in OLEDs with basic material properties. *J. Mater. Chem. C* **2**, 10298 (2014).
95. Kim, J.-M., Hwang, K. Y., Kim, S., Lim, J., Kang, B., Lee, K. H., Choi, B., Kwak, S.-Y. & Lee, J. Y. Enhancing Horizontal Ratio of Transition Dipole Moment in Homoleptic Ir Complexes for High Outcoupling Efficiency of Organic Light-Emitting Diodes. *Adv. Sci.* **9**, 2203903 (2022).
96. Reineke, S., Rosenow, T. C., Lüssem, B. & Leo, K. Improved High-Brightness Efficiency of Phosphorescent Organic LEDs Comprising Emitter Molecules with Small Permanent Dipole Moments. *Adv. Mater.* **22**, 3189 (2010).

97. Nakanotani, H., Higuchi, T., Furukawa, T., Masui, K., Morimoto, K., Numata, M., Tanaka, H., Sagara, Y., Yasuda, T. & Adachi, C. High-efficiency organic light-emitting diodes with fluorescent emitters. *Nat. Commun.* **5**, 4016 (2014).

98. Chan, C. -Y., Tanaka, M., Lee, Y. -T., Wong, Y. -W., Nakanotani, H., Hatakeyama, T. & Adachi, C. Stable pure-blue hyperfluorescence organic light-emitting diodes with high-efficiency and narrow emission. *Nat. Photon.* **15**, 203 (2021).

99. Jeon, S. O., Lee, K. H., Kim, J. S., Ihn, S.-G., Chung, Y. S., Kim, J. W., Lee, H., Kim, S., Choi, H. & Lee, J. Y. High-efficiency, long-lifetime deep-blue organic light-emitting diodes. *Nat. Photon.* **15**, 208 (2021).

100. Heimel, P., Mondal, A., May, F., Kowalsky, W., Lennartz, C., Andrienko, D. & Lovrincic, R. Unicolored phosphor-sensitized fluorescence for efficient and stable blue OLEDs. *Nat. Commun.* **9**, 4990 (2018).

101. Kim, E., Park, J., Jun, M., Shin, H., Baek, J., Kim, T., Kim, S., Lee, J., Ahn, H. & Kim. S. Highly efficient and stable deep-blue organic light-emitting diode using phosphor-sensitized thermally activated delayed fluorescence. *Sci. Adv.* **8**, eabq1641 (2022).

102. Kondo, Y., Yoshiura, K., Kitera, S., Nishi, H., Oda, S., Gotoh, H., Sasada, Y., Yanai, M. & Hatakeyama, T. Narrowband deep-blue organic light-emitting diode featuring an organoboron-based emitter. *Nat. Photon.* **13**, 678 (2019).

103. Naveen, K. R., Lee, H., Braveenth, R., Karthik, D., Yang, K. J., Hwang, S. J. & Kwon, J. H. Achieving High Efficiency and Pure Blue Color in Hyperfluorescence Organic Light Emitting Diodes using Organo-Boron Based Emitters. *Adv. Funct. Mater.* **32**, 2110356 (2021).

104. Kim, H. S., Cheon, H. J., Lee, D., Lee, W., Kim, J., Kim, Y. -H. & Yoo, S. Toward highly efficient deep-blue OLEDs: Tailoring the multiresonance-induced TADF molecules for suppressed excimer formation and near-unity horizontal dipole ratio. *Sci. Adv.* **9**, eadf1388 (2023).

105. Mamada, M., Hayakawa, M., Ochi, J. & Hatakeyama. T. Organoboron-based multiple-resonance emitters: synthesis, structure–property correlations, and prospects. *Chem. Soc. Rev.* **10**. 1039/d3cs00837a (2024).

Chapter IV. Summary and Future Perspective

4.1. Summary

This thesis presented TADF emitter and host materials to boost the efficiency and stability of TADF OLEDs. Because of their high stability and efficiency, D-A-type compounds are one of the most promising TADF material families. We explored the relationship between molecular architectures and photophysical parameters including k_{RISC} and device durability. By comparing the stabilities of different TADF molecules, we unlocked the potential for generating new TADF materials. Additionally, the outcoupling efficiency lowers the EQE to 20–30% even if the IQE of OLEDs may approach 100% by using both singlets and triplets in TADF OLEDs. In the EML, the host molecule is essential for improving the guest molecule's molecular orientation. We introduced a host material with great thermal stability and triplet energy, which leads to better orientation of diverse guest materials.

In Chapter 2, I designed a new TADF material with multiple D-A type structures and a hetero-donor design that uses two different donor units, DMAC and Cz. The newly designed emitter showed high PLQY under different circumstances, including polar media and high doping concentrations. The EQE of OLEDs was rather high in p-type hosts mCBP, CCP, and n-type host PPT. Furthermore, I determined that multiple D-A-type molecules have higher photostability than single D-A-type molecules. However, additional critical factors might have an impact on OLED operating stability. While many researchers use DMAC moiety, the stability was not carefully investigated. Even with better optical properties, the stability is the most important issue. Our results revealed the problem of a DMAC moiety, which is useful information for future OLED development.

In Chapter 3, I presented a new molecule, 6CzPh, as a host. Compared to typical host materials, 6CzPh, an undiscovered carbazole derivative in OLEDs, has exceptional qualities as a host. According to our research, 6CzPh is a viable option for OLED applications. The new host's high triplet energy and robust structure help to achieve high EQE and device stability. The host material enhanced the horizontal molecular orientation of several guest emitter types, in addition to their intrinsic properties. Notably, the disk-shaped 4CzIPN emitter showed a fully horizontal molecular orientation with the new host 6CzPh.

4.2. Future Perspective

I have already experimented with PPT, CCP, and mCBP hosts for device fabrication. Despite being a bipolar emitter, 2Cz2DMAC2BN mostly transports holes rather than electrons. Because of that, according to Chapter 3, it showed stable performance with the PPT host. The HOD and EOD photostability studies demonstrated that the DMAC moiety's radical anion was unstable. Consequently, the flow of electrons within the emitter is incompatible with device stability. To decrease electron transport via the emitter, it is preferable to examine the emitter's performance with bipolar hosts. In addition, alternative exciplex host systems with the emitter would increase the OLEDs' EQE and device stability.

4.2.1. Bipolar hosts

Bipolar host materials are composed of electron transport and hole transport materials that can be linked directly or via a spacer (**Fig. 4.1**). Bipolar materials significantly enhance the charge balance in the device by facilitating the transport of both electrons and holes. Because the HOMO, and LUMO levels in the host, are determined by the donor and acceptor moieties, the driving voltage is decreased due to the lower energy barrier. Additionally, the recombination zone broadened due to enhanced carrier balance, and roll-off improved because charge balance is not disrupted at high driving voltage[1,2]. Therefore, a bipolar host is a better choice for improving the performance of the 2Cz2DMAC2BN.

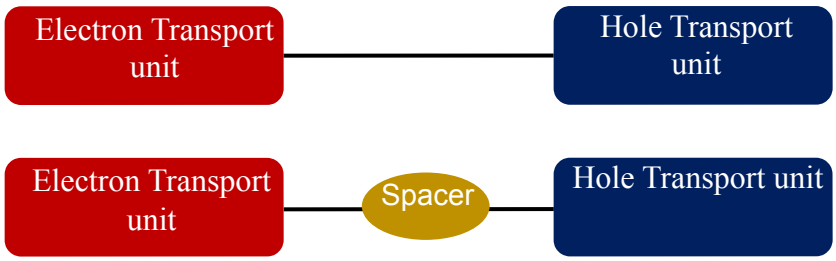

Figure 4.1: Schematic diagram of the molecular structure of bipolar host materials.

4.2.2. Exciplex hosts

An exciplex host consists of at least one p-type host and one n-type host, which facilitates the charge injection and transport in the EML compared to the single hosts. The simultaneous operation of the ISC and RISC within the host (Fig. 4.2 b) reduces the driving

voltage in the OLEDs[3]. The balanced electrons and holes in the EML may increase the efficiency of the OLEDs. The recombination zone is broadened because of the characteristics mentioned above. (a) (b) 2Cz2DMAC2BN is a green emitter with relatively high triplet energy. When selecting an exciplex host for the emitter, it is preferable to utilize one with a weak acceptor, and a weak donor to produce a high triplet level while preventing back energy transfer.

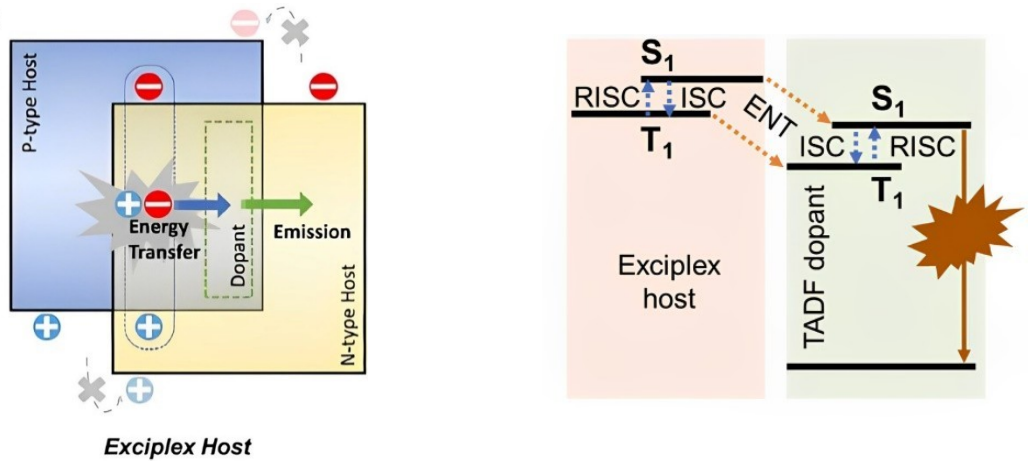

Figure 4.2: a) The working process of the exciplex as a host[4]. b) Energy transfer mechanisms in exciplex-hosted OLEDs for TADF dopants[3]. The broken arrows indicate nonradiative processes.

4.2.3. TAF OLEDs

A TAF system consists of a host, a TADF emitter, and a fluorescent emitter. Using this system, we can achieve a high EQE and narrow band emission while maintaining color purity[5]. To reduce charge carrier trapping in hyperfluorescence (HF, TAF)-OLEDs, emitter molecules are doped at a low concentration (~1 wt%). Also, because the TADF assistance dopant is the primary recombination source in the EML, the doping concentration ranges between 15% to 50%[6]. Further, the horizontally oriented emitter molecules will enhance the EQE of the HF OLEDs. Because 6CzPh improved the outcoupling efficiency in OLEDs, it will be a better option for use as a host in the TAF system. One requirement as the host in HF OLEDs is that the triplet energy of the host should be higher than that of the two dopant materials to prevent the back energy transfer.

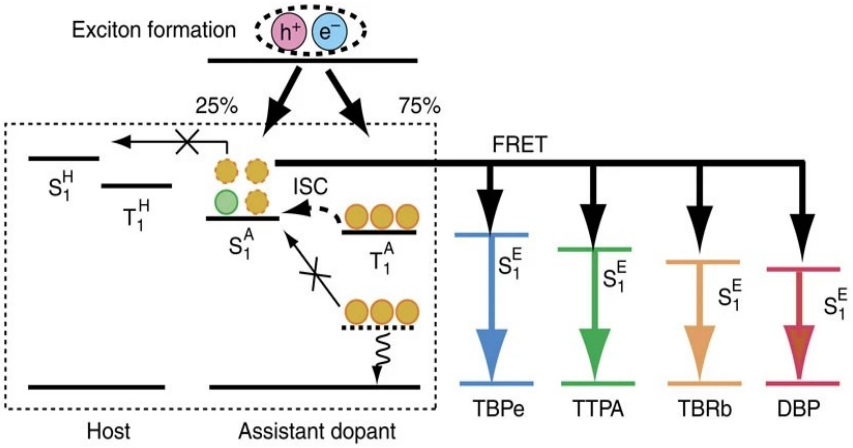

Figure 4.3: Energy transfer mechanisms in the TAF system[5].

.

4.3. References

1. Liu, X. K., Zheng, C. J., Xiao, J., Ye, J., Liu, C. L., Wang, S. D., Zhao, W. M. & Zhang, X. H. Novel bipolar host materials based on 1,3,5-triazine derivatives for highly efficient phosphorescent OLEDs with extremely low efficiency roll-off. *Phys. Chem. Chem. Phys*. **14**, 14255–14261 (2012).
2. Zhao, X.-H., Zhang, Z.-S., Qian, Y., Yi, M.-D., Xie, L.-H., Hu, C.-P., Xie, G.-H., Xu, H., Han, C.-M., Zhao, Y. & Huang, W. A. bulky pyridinylfluorene-fuctionalizing approach to synthesize diarylfluorene-based bipolar host materials for efficient red, green, blue and white electrophosphorescent devices. *J. Mater. Chem. C* **1**, 3482-3490 (2013).
3. Sarma, M., Chen, L.-M., Chen, Y.-S. & Wong, K.-T. Exciplexes in OLEDs: Principles and promises. *Mater. Sci. Eng. R* **150**, 100689 (2022).
4. Jung, M. & Lee, J. Y. Exciplex hosts for blue phosphorescent organic light-emitting diodes. *J. Inf. Disp*. **21**, 12 (2020).
5. Nakanotani, H., Higuchi, T., Furukawa, T., Masui, K., Morimoto, K., Numata, M., Tanaka, H., Sagara, Y., Yasuda, T. & Adachi, C. High-efficiency organic light-emitting diodes with fluorescent emitters. *Nat. Commun*. **5**, 4016 (2014).

List of Acronyms

Keywords

Charge transfer (CT)

Cyclic voltammetry (CV)

Differential pulse voltammetry (DPV)

Electroluminescence (EL)

Electron affinity (EA)

Electron-blocking layer (EBL)

Electron-injection layer (EIL)

Electron-only device (EOD)

Electron-transporting layer (ETL)

Emission layer (EML)

Electron-only devices (EOD)

Electrostatic potential (ESP)

External quantum efficiency (EQE)

Förster resonance energy transfer (FRET)

Highest occupied molecular orbital (HOMO)

Hole-blocking layer (HBL)

Hole-injection layer (HIL)

Hole-only devices (HOD)

Hole-transporting layer (HTL)

Hybridized local and charge transfer (HLCT)

Internal quantum efficiency (IQE)

Intersystem crossing (ISC)

Ionization potential (IP)

Kitaigorodskii packing index (KPI)

Lifetime (LT)

Locally excited state (LE)

Lowest singlet excited state (S_1)

Lowest triplet excited state (T_1)

Lowest unoccupied molecular orbital (LUMO)

Organic light-emitting diode (OLED)

Permanent dipole moment (PDM)

Photoluminescence (PL)

Photoluminescence quantum yield (PLQY)

Phosphor-sensitized fluorescence (PSF)

Polaron (P)

Reverse intersystem crossing (RISC)

Room temperature (RT)

Singlet ground state (S_0)

Spontaneous orientation polarization (SOP)

TADF-assisted fluorescence (TAF)

Thermally-activated delayed fluorescence (TADF)

Thermogravimetry-differential thermal analysis (TG-DTA)

Time-dependent density functional theory (TD-DFT)

Transition dipole moment (TDM)

Materials

10-[4-(4,6-Diphenyl-1,3,5-triazin-2-yl)phenyl]-10H-phenoxazine (ACRXTN)

Tris(8-hydroxyquinolinato)aluminium (Alq_3)

2,7-Bis(2,20-bipyridine-5-yl)triphenylene (BPy-TP2)

4,4'-Di(9H-carbazol-9-yl)-1,1'-biphenyl (CBP)

9-phenyl-9*H*-3,9′-bicarbazole (CCP)

N,*N*-Dimethylformamide (DMF)

1,4,5,8,9,11-Hexaazatriohenyleane hexacarbonitrile (HAT-CN)

Indium-tin-oxide (ITO)

8-Hydroxyquinolinolato-lithium (Liq)

Tris(2-phenylpyridine)iridium(III) ($Ir(ppy)_3$)

3,3'-Di(9*H*-carbazol-9-yl)-1,1'-biphenyl (mCBP)

1,3-Bis(N-carbazolyl)benzene (mCP)

2,8-bis(diphenyl-phosphoryl)-dibenzo[*b,d*]thiophene (PPT)

3-(9,9-Dimethylacridin-10(9H)-yl)-9H-xanthen-9-one (PXZ-TRZ)

2-(9,9'-Spirobi[fluoren]-3-yl)-4,6-diphenyl-1,3,5-triazine (SF3-TRZ)

9,9'-Diphenyl-6-(9-phenyl-9H-carbazol-3-yl)-9H,9'H-3,3'-bicarbazole (Tris-Pcz)

2,4,6-Tris(biphenyl-3-yl)-1,3,5-triazine (T2T)

2,4,5,6-Tetra(9H-carbazol-9-yl)isophthalonitrile (4CzIPN)

Physical symbol

Boltzmann constant (k_b)

Carrier balance ratio (γ)

Change in driving voltage (ΔV)

Current density (J)

Delayed lifetime (τ_d)

Distance between the electrons 1 and 2 (r_{12})

Energy gap between the lowest singlet and triplet excited energy levels (ΔE_{ST})

Exciton generation efficiency (η_{ST})

Exciton generation factor (β)

Existence probability of a dipole parallel to the substrate (p_x, p_y)

Existence probability of a dipole orthogonal to the substrate (p_z)

Extraordinary extinction coefficient (k_e)

Glass transition temperature (T_g)

Initial luminance (L_0)

Initial voltage (V_0)

Internal quantum efficiency (η_{int})

Inter system crossing efficiency (Φ_d)

Light-outcoupling efficiency (η_{out})

Luminance (L)

Order parameter (S)

Ordinary extinction coefficients (k_o)

Oscillator strength (f)

Permanent dipole moment (p)

Photoluminescence quantum yield (Φ_{PL})

Rate constant of the intersystem crossing of excitonic state (k_{ISC})

Rate constant of radiative decay from singlet excited state (k_r^S)

Rate constant of the reverse intersystem crossing of excitonic state (k_{RISC})

Ratio between horizontally oriented dipoles and total dipoles (Θ_h)

Refractive index of the organic layer relative to the air (n)

Separation between the substrate normal and the transition dipole (θ)

Singlet exciton generation rate (η_S)

Thickness (d)

Triplet exciton generation rate (η_T)

Voltage (V)

Wavefunction of the HOMO (ϕ_{HOMO})

Wavefunction of the LUMO (ϕ_{LUMO})

List of Publication

1. **B. Madushani**, M. Mamada, K. Goushi, T. B. Nguyen, H. Nakanotani, H. Kaji, C. Adachi, Sci. Rep. **2023**, 13, 7644.
2. **B. Madushani**, M. Mamada, K. Goushi, H. Katagiri, H. Nakanotani, T. Hatakeyama, C. Adachi, Hexacarbazolylbenzene: An excellent host molecule causing strong guest molecular orientation and the high-performance OLEDs. Adv. Mater. **2024**, 36**,** 2402275.
3. S. Kiriyama, M. Mamada, K. Goushi. **B. Madushani**, T. Hatakeyama, C. Adachi, Adv. Funct. Mater. **2024**, 34, 2402287.

List of Conference

1. **Madushani, B.**, Mamada, M., Goushi, K., Katagiri, H., Nakanotani, H., Hatakeyama T. & Adachi C., Japan Society of Applied Physics (JSAP Spring meeting-2024), Tokyo, Japan. (March 22 nd, 2024). (Oral presentation).

2. **Madushani, B**., Mamada, M., Goushi, K., Nguyen, T. B., Nakanotani, H., Kaji, H. & Adachi, C. Multiple donor-acceptor design for highly luminescent and stable thermally activated delayed fluorescence emitters, The 15th Asian Conference on Organic Electronics (A-COE, 2023), Taipei, Taiwan. (November 1st, 2023). (Poster presentation).

3. **Madushani, B.,** Mamada, M., Goushi, K., Nguyen, T. B., Nakanotani, H., Kaji, H. & Adachi, 2023 KJF-International Conference on Organic Materials for Electronics and Photonics (KJF-ICOMEP 2023), Fukuoka, Japan. (September 1st, 2023). (Poster presentation).

Acknowledgment

The studies in this thesis were carried out at Adachi Laboratory, Department of Chemistry and Biochemistry, Graduate School of Kyushu University from 2021-2024.

I am grateful to Professor Chihaya Adachi for supervising this thesis, excellent experimental environment, for helpful discussion, and the insightful feedback and advice for all my works. I am also deeply grateful to Associate Professor Masashi Mamada for encouraging me, believing in me, providing me with all the necessary guidance, and for constant support from his side through the years as the co-supervisor of this thesis. I would also like to thank Assistant Professor Kenichi Goushi for the valuable comments, and the support for my research work. In addition, I would like to thank Associate Professor Hajime Nakanotani, Associate Professor Yoichi Tsuchiya, and Professor Atula Sandanayaka. They also gave me useful advice and helped in my research work. Further, I would like to acknowledge Ms. Keiko Kusuhara, and Ms. Nozomi Nakamura for providing me with the materials, and Ms. Chihiro Nakanotani, and Ms. Sachiko Higashikawa for helping me with the document work.

I want to thank my parents, husband, aunt, and sisters for helping, understanding, and encouraging me during my studies. I'm thankful to them for the love, and care they provide me in my life.

I also acknowledge all the members of Adachi Laboratory for their support not only for my work but also for my daily life. Especially, I would like to thank the Japanese government for providing me with the MEXT scholarship support in my higher education, which made it possible to complete this study.